1-1-2005

Gas holdup in a 32 cm bubble column

Philip D. Hol
Iowa State University

Gas holdup in a 32 cm bubble column

by

Philip D. Hol

A thesis submitted to the graduate faculty

in partial fulfillment of the requirements for the degree of

MASTER OF SCIENCE

Major: Mechanical Engineering

Program of Study Committee:
Theodore J. Heindel, Major Professor
Francine Battaglia
R. Dennis Vigil

Iowa State University

Ames, Iowa

2005

Graduate College

Iowa State University

This is to certify that the master's thesis of

Philip D. Hol

has met the thesis requirements of Iowa State University

TABLE OF CONTENTS

LIST OF TABLES

LIST OF FIGURES

NOMENCLATURE

A	distributor open area
C	fiber mass fraction
C_0	drift-flux model constant
D	bubble column diameter
d_o	perforated plate orifice diameter
g	acceleration due to gravity
GL	gas-liquid
GLF	gas-liquid-fiber
GLS	gas-liquid-solid
H	unaerated axial height within bubble column
H_c	height of circulation cell
Δh	height difference between pressure transducers
i	index counter
L	fiber length
m_f	dry fiber mass
m_l	liquid mass
N	number of orifices in perforated plate
ΔP	pressure difference between pressure transducers
U_g	superficial gas velocity
U_t	drift-flux velocity
V_c	initial slurry volume
V_f	fiber volume
V_l	liquid volume

Symbols

ϵ_f	volumetric fiber phase holdup
ϵ, ϵ_g	volumetric gas phase holdup
ϵ_l	volumetric liquid phase holdup
ρ_{eff}	effective slurry density
ρ_f	fiber phase density
ρ_g	gas phase density
ρ_l	liquid phase density
Φ_f	fiber volume fraction
Φ_l	liquid volume fraction

ACKNOWLEDGEMENTS

I would like to take the opportunity to thank the people who have helped me through the course of this program.

First of all, I would like to thank Dr. Ted Heindel for providing the opportunity to further my education and for all the instruction throughout the course of my research.

Thanks to my family their encouragement, support, and especially for listening to me explain my research project.

This research was supported by the National Science Foundation under Grant Number CTS-0209928. The cellulose fiber supply and characterization was provided by Kimberly-Clark Corporation. Their support is greatly appreciated.

ABSTRACT

Air-water-fiber flows are found in the pulp and paper industry in a variety of unit operations such as flotation deinking of recycled paper and fiber bleaching. Vertical bubble column reactors are often used for these operations due to low cost, ease of operation, and high interfacial areas. The complex hydrodynamics of bubble columns are difficult to understand due to the presence of many different phenomena occurring in the flow. Therefore, it is difficult to scale up the information gathered from research for industrial sized applications.

The current study experimentally investigates the effects of fiber mass fraction, superficial gas velocity, fiber type, fiber length, and distributor plate open area on gas flow regime, and overall and local gas holdup in a 32.1 cm diameter semi-batch bubble column. Three different Rayon fiber lengths (L = 3, 6, 12 mm) and three different cellulose (natural) fiber types are experimentally studied over a range of superficial gas velocities ($U_g \leq 20$ cm/s), fiber mass fractions ($0 \leq C \leq 1.8\%$), and distributor open areas (A = 0.49, 0.95, and 2.03%). Local gas holdup is determined by pressure drop measurements at several axial locations spanning a height of ten column diameters (H = 321 cm). Overall gas holdup is determined from the pressure difference between the top and bottom pressure transducers. The Zuber and Findlay drift flux model is used to determine the gas flow regime.

Fiber mass fraction had the most significant influence on overall and local gas holdup, where increasing fiber mass fraction decreased gas holdup. Superficial gas velocity has different effects on gas holdup for flows that demonstrate three regimes (homogeneous, transitional, and heterogeneous) and flows that were heterogeneous for all superficial gas velocities (pure heterogeneous). Local gas holdup trends showed two local maximum gas holdup values and the existence of recirculation cells within the flow. Their location and size depends on fiber type and distributor plate open area.

CHAPTER 1: INTRODUCTION

1.1 Motivation

Gas-liquid (GL) and gas-liquid-solid (GLS) multiphase flow systems are applied in a broad range of industries such as petroleum fuel conversion, biological waste water treatment, flue gas desulphurization, and chemical and pharmaceutical production. These multiphase flow reactors are desired to promote interphase transport of species and energy and to enhance heat and/or mass transfer. The hydrodynamics of multiphase reactors are very complex and although much research has been completed on such systems, more research is needed to fully understand the hydrodynamics and to validate hydrodynamic models (Sundaresan, 2000).

A gas-liquid-fiber (GLF) multiphase flow system is a subset of a GLS system where fibers form the solid phase. These systems are used extensively in the pulp and paper industry for applications such as flotation deinking of recycled paper and fiber bleaching. The fiber phase differs greatly from the typical solid phase of a multiphase system due to the fact that the typical solid phases have high densities and a fiber phase has a relatively low density. GLF systems are extremely complex because the fibers tend to be flexible, absorb water and swell, and have a density comparable to that of water. Cellulose fibers also tend to flocculate at mass fractions as low as 0.3% and continuous fiber networks form for consistencies greater than 1% (Bennington et al., 1989). Even though three phase fluidization has been used since the 1940's (Reese et al., 1999), more research is necessary to understand and qualify the flow characteristics of multiphase flows (Heindel, 2003).

Bubble column reactors are commonly used for GL, GLS, and GLF multiphase flow systems because of low operating and maintenance costs, simplicity of operation, high interfacial area, high mass transfer coefficients, and high heat transfer coefficients (Shah et al., 1982). A bubble column reactor is a device in which a gas phase is bubbled through a

column of liquid or liquid-solid slurry to promote a chemical or biochemical reaction (Sarrafi et al., 1999). General bubble column systems have been extensively researched, but the complex hydrodynamics of GLF bubble columns are far from being completely understood (Lindsay et al., 1995; Reese et al., 1996). Additionally, limited knowledge of complex flow patterns and design parameters hinder the scale-up of general bubble column reactors (Gandhi et al., 1999; Moustiri et al., 2001).

Gas holdup, defined as the volumetric gas fraction, is a vital parameter in understanding the flow characteristics of a typical bubble column. Gas holdup has a significant impact on heat and mass transfer rates in gas-liquid or gas-liquid-solid bubble column applications.

1.2 Thesis Goal

The objectives of this research are to determine the effects of various parameters on overall and local gas holdup in a bubble column. The specific goal of this study is to explore the hydrodynamic characteristics of an air-water-fiber suspension in a large diameter semi-batch bubble column. This study will focus on gas holdup measurements with respect to the following parameters:

- Superficial Gas Velocity
- Fiber Mass Fraction
- Fiber Type
- Distributor Open Area

CHAPTER 2: LITERATURE REVIEW

This chapter is divided into six subsections. The first discusses general bubble column characteristics. The second, third, and fourth sections discuss gas holdup and other properties of gas-liquid, gas-liquid-solid, and gas-liquid-fiber multiphase flow systems, respectively. The fifth section reviews different measuring techniques that are commonly used to obtain gas holdup information. The final section summarizes the literature review.

2.1 Bubble Column Characteristics

The hydrodynamics of bubble columns are incredibly complex due to the presence of many different phenomena occurring in the multiphase flow. The hydrodynamics of each phase are interdependent, thus studying their interaction is important (Lefebvre and Guy, 1999). It is the gas phase superficial velocity that dominates the fluid dynamics of the entire system (Dudukovic et al., 1999). Bubble rise velocity, bubble size distribution, gas holdup, and flow regime are important in understanding the hydrodynamics in bubble columns (Lain et al., 1999; Heindel, 2003). This section summarizes general bubble column characteristics and multiphase flow hydrodynamics. Gas holdup in GL, GLS, and GLF systems will be discussed in Sections 2.2 – 2.4.

A general characteristic of bubble column flows is the different flow regimes that can be observed over a range of superficial gas velocities. The flow regimes observed in slurry bubble columns are analogous to those in fluidized bed reactors, except that the minimum fluidization velocity of a slurry bubble column is zero. The homogeneous and heterogeneous regimes are the two common flow regimes found in large diameter ($D > 15$ cm) bubble columns (Heindel, 2003). The homogeneous (bubbly) flow regime is observed first as the gas velocity is increased beyond the minimum fluidization velocity (Fig. 2.1a). (All figures and tables in this thesis are located at the end of the respective chapter.) Bubbles are

generally uniform in size and are uniformly distributed as the gas velocity increases up to a transitional gas velocity, where the bubbles are observed to begin coalescing to form larger and faster rising bubbles. A further increase in superficial gas velocity produces the heterogeneous (churn-turbulent) regime (Krishna et al., 1993), as represented in Fig. 2.1d. The heterogeneous flow regime is characterized by the irregular shaped gas pockets near the column center, which carry smaller bubbles in their wake and continuously coalesce to cause an oscillatory and unstable flow field (Xie et al., 2003). Chen et al. (1994) characterized the transition from homogeneous to heterogeneous flow in three-dimensional bubble columns as vortical-spiral flow. Increasing bubble column dimensions (height and diameter) were shown to decrease the stability of the homogeneous flow regime and lower the transitional gas velocity (Ruzicka et al., 2001a). Turbulence in the column is a result of large-scale flow structures, bubble shear, bubble oscillation, and bubble wake phenomena (Lain et al., 1999). Pure heterogeneous flow is identified as the flow conditions for which the heterogeneous flow regime is observed for all gas flow rates (Ruzicka et al., 2001b). Ruzicka et al. (2001b) also state that pure heterogeneous flow can be the result of non-uniform gas distribution due to distributor plate design.

The transition regime that exists between the homogeneous and heterogeneous flow regimes is characterized by the onset and complete development of liquid circulation patterns within the flow (Zahradnik et al., 1997). Figure 2.1b-c schematically represents the onset and complete development of the transitional regime. Bubble coalescence occurs but the central bubble plume is not completely developed during the onset of the transitional regime. The completely developed transitional regime displays the central plume up to the liquid dispersion height (Olmos et al., 2003). A maximum in the overall gas holdup may also be observed in the transitional regime and is attributed to the increasingly negative effect of the developing liquid circulation. The superficial gas velocity at which the local maximum gas holdup is observed corresponds to the complete development of the transitional regime. A

generic representation of three regime flow with and without the observation of the local maximum, as well as pure heterogeneous flow is shown in Figure 2.2.

Bubble size is also an important parameter in characterizing gas flow in a bubble column. Smaller bubbles that are uniformly dispersed within the column are preferred for a fiber bleaching process to maximize the gas-liquid mass transfer surface area. A distribution of bubble sizes is preferred in flotation deinking to provide a bubble size range to which contaminant can interact to form bubble-particle aggregates (Heindel, 2003). According to Lehr et al. (2002), the flow field and bubble size distribution are interdependent. In other words, the local flow field controls bubble coalescence, which controls the bubble size distribution, which in turn affects the local flow field.

Understanding gas bubble and solid particle distributions in three-phase reactors is critical in analyzing such systems. Solids particles are observed to be concentrated in an area near the column wall and the bubbles are observed to be concentrated near the center of the column (Warsito et al., 1997). Lefebvre and Guy (1999) observed that the local liquid velocity distributions in gas-liquid flows were more uniform in the homogeneous regime than in churn-turbulent flow. They also observed that the liquid flow mechanism depended on the superficial gas velocity.

One of the common features of bubble column hydrodynamics is the intense back mixing and liquid phase circulation resulting from the rising bubble swarm through the liquid medium (Walter and Blanch, 1983). The random displacement of liquid is a result of the fluid being carried along within the bubble wake and then randomly released (Lubbert et al., 1996). High superficial gas velocities show intense back mixing, where low superficial gas velocities display very little back mixing (Schulz and Heindel, 2000). Bubble columns typically have a high height-to-diameter ratio and therefore axial mixing is more important than radial mixing (Walter and Blanch, 1983). Zahradnik and Fialova (1996) showed that the extent of axial gas mixing was much higher in the heterogeneous regime than in the

homogeneous regime and axial liquid mixing was independent of the flow regime. Becker et al. (1999) concluded that flow behavior in cylindrical bubble columns is unpredictable and chaotic.

Grevskott et al. (1996) observed the existence of two circulation cells within a three phase (air-water-glass bead) system. Millies and Mewes (1995a, b) also showed the existence of liquid circulation cells. Liquid circulation arose from a disturbance in the gas distribution. The radial gas holdup profile at the top of the circulation cell caused a disturbance that created consecutive circulation cells (Millies and Mewes, 1995b). They also observed that gas holdup was a maximum in the center of the circulation cell. Millies and Mewes (1995a) observed that circulation cells were on the order of one column diameter, all circulation cells circulated in the same direction, and there existed an axial liquid velocity between two adjacent circulation cells to transport liquid from one cell to another.

Gas holdup, which is defined as the volumetric gas fraction, is an important parameter in bubble column operation. Gas holdup has a large influence on the mass transfer coefficient, and although many correlations have been proposed, they seldom agree (Walter and Blanch, 1983). Gas holdup characteristics in gas-liquid, gas-liquid-solid, and gas-liquid-fiber bubble column flows will now be discussed Sections 2.2-2.4, respectively.

2.2 Gas-Liquid Bubble Columns

Gas-liquid flows in bubble columns have been extensively researched due to their application to a variety of process industries and their inherent high heat and mass transfer characteristics (Dudukovic et al., 1999). Since GL systems are extensively studied, and several reviews are available (Bennett et al., 1999; Buwa and Ranade, 2004; Dudukovic et al., 1999; Moustiri et al., 2001; Shah et al., 1982; Sundaresan, 2000; Tsuchiya and Nakanishi, 1992; Zahradnik and Fialova, 1996), only a few selected studies are presented below.

Went et al. (1993) studied gas holdup in a 10.5 cm diameter, 180 cm tall bubble column. Superficial gas velocities were varied in the range 2 – 10 cm/s. The distributor plate consisted of 0.1 cm diameter orifices on a 1.8 cm triangular pitch. Using air and water, it was determined that three flow regimes occurred with increasing gas flow rate. The homogeneous regime was observed for $U_g \leq 5$ cm/s, with bubble coalesce and the transition regime being observed around 4 – 5 cm/s. The heterogeneous regime was found to occur for $5 \leq U_g \leq 10$ cm/s.

Su and Heindel (2003) studied gas holdup in a 15.24 cm internal diameter, 4 m tall cast acrylic, semi-batch bubble column. Compressed air made up the gas phase and was introduced into the system through a perforated plate with an open area of 0.57%. Gas holdup was determined from the pressure drop measured in the upper column section, $1 \leq H \leq 2$ m. All experiments were performed with an initial GL system volume corresponding to a height of 2.13 m, or 14 column diameters. The homogeneous, transitional, and heterogeneous flow regimes were observed for superficial gas velocities up to $U_g = 18$ cm/s. Homogeneous flow was observed for low superficial gas velocities, where bubbles were small and uniformly distributed. Gas holdup also increased linearly with increasing superficial gas velocity in this regime. The transitional flow regime was observed when the bubbles began to coalesce and gas holdup was no longer a linear function of superficial gas velocity. Gas holdup increased to a maximum value in the transitional regime, and then began to decrease to a minimum value as a result of bubble coalescence. Gas holdup once again began to increase with increasing superficial gas velocity, indicating the onset of the heterogeneous flow regime.

2.3 Gas-Liquid-Solid Bubble Columns

Gas-liquid-solid systems are simply gas-liquid systems with added solid particles that are typically spherical. Solid particles are often added to gas-liquid systems to simulate catalyst

particles. The addition of solid particles results in an overall decrease in gas holdup from that of a GL system. Particles tend to increase bubble coalescence and decrease bubble breakup by either increasing the apparent slurry viscosity or dampening the turbulence within the column (Li and Prakash, 1997). Chen et al. (1994) determined that the only difference between the GL and GLS systems was the size of the various flow structures, which can be attributed in part to the additional interphase interactions due to the introduction of the solid particles.

Jianping and Shonglin (1998) predicted local axial liquid velocities and local gas holdup values for a cocurrent gas-liquid-solid three-phase bubble column reactor by using a two-dimensional pseudo-two-phase fluid model with included turbulence. The bubble column reactor studied had an inner diameter of 0.29 m and was 3.0 m in height. The local gas holdup was found by using a five-point conductivity probe and a hot film anemometer was used to determine the local axial liquid velocity. Compressed air comprised the gas phase, tap water was the liquid phase, and 0.3 – 0.5 mm resin particles with an average density of 1346 kg/m^3 made up the solid phase. They found that the local gas holdup and axial liquid velocity increased with increasing superficial gas velocity (0 – 8 cm/s) and decreased with solids loading (0 – 6% by volume) relative to a two-phase system. The model accurately predicted the experimental results. Unusual results were noticed under certain operating conditions where local gas holdup decreased and axial liquid velocity increased with increasing superficial gas velocity.

Schweitzer et al. (2001) studied local radial gas holdup in a 5 cm inner diameter slurry bubble column with heptane, 50 μm particles, and nitrogen. The local radial gas holdup was measured at a height of 1 m above the distributor by using an optical probe. Studies were performed using a gas-liquid system and a gas-liquid-solid system with 10% solid fraction by volume. Gas holdup was determined to be low near the wall and reach a maximum near the center of the column. Gas holdup was also found to decrease with an increase in the solid

concentration. The presence of solids in the system did not seem to affect the radial flow structure.

Warsito et al. (1997) studied gas holdup in a 14 cm internal diameter, 140 cm tall semi-batch bubble column. Air, tap water, and glass beads with particle diameters of 100 and 260 μm were used for the three phases. The radial gas holdup profiles for the air-water only system and the air-water-solid system with 100 μm glass beads at 1% by volume solids loading were similar and nearly symmetrical. The radial gas holdup for a solids loading of 2% and 260 μm glass beads was drastically different, with the gas bubbles observed to be concentrated near the center of the column. The bubbles were also observed to be traveling in a zig-zag motion due to increased bubble coalescence at the column bottom where solids were settling.

Grevskott et al. (1996) observed two solid circulation cells in three phase experiments in two different bubble columns. The columns were 14 cm and 26 cm in internal diameter and 99 cm and 134 cm in height, respectively. The three phase system consisted of air, water, and 110-180 μm glass beads varied from 7 wt-% to 20 wt-%. The lower cell was on the order of one column diameter and the other cell extended to the top of the column. Therefore, the upper circulation cell was much larger than the lower cell. The solid circulation within the lower cell was observed to be upward along the column wall and downward in the center of the column. The circulation in the upper cell was the opposite.

2.4 Gas-Liquid-Fiber Bubble Columns

Gas-liquid-fiber (GLF) systems are a special version of GLS systems where some type of fiber makes up the solid phase. The solid phase is comprised of individual particles that have a large aspect ratio and, for the fiber systems discussed below, a specific gravity typically on the order of one. The fibers are also flexible, causing this type of system to be very complex. Fibers tend to flocculate and form fiber networks that alter gas flow patterns and air/slurry

interaction within the bubble column. Flocculation occurs in cellulose fiber suspensions with fiber mass fractions above C = 0.5%, and fiber network strength increases with increasing mass fraction (Bennington et al., 1989). Bubbles must gain the necessary buoyant force to break through the fiber network (Pelton and Piette, 1992).

Gas-liquid-fiber systems are used extensively in the pulp and paper industry for such applications as flotation deinking and fiber bleaching. Flotation deinking is a process in which hydrophobic ink particles are separated from waste paper by attaching to air bubbles traveling towards the surface of a water-fiber slurry. Ink particles are then removed from the top of the slurry and the paper fibers remain in the system. Bubble columns commonly used for flotation deinking are most effective when operated at fiber mass fractions of 0.8 to 1.3% (Walmsley, 1992). Flotation columns are typically continuously operated using an air flow rate that is approximately 20% of the slurry flow rate. The process is then repeated for up to six different stages to completely remove the hydrophobic ink particles (Seifert, 1994).

Fiber bleaching requires the fine mixing of an oxidizing gas and the pulp slurry. The oxidizing gas must be dissolved in water in order to chemically react with the lignin. The oxidizing gas has traditionally been chlorine due to its high solubility in water, but oxygen and ozone are becoming increasingly popular due to the environmental concerns with chlorine. Understanding the mixing process with oxygen and ozone is more important since these substances have a lower solubility in water than chlorine (Xie et al., 2003). Bubble coalescence causes a reduced reaction rate due to a decrease in the gas-liquid interfacial area and an increase in channeling, which decreases the gas residence time in the bubble column (Reese et al., 1999).

Went et al. (1993) studied gas holdup in the bubble column described in Section 2.2 with wood pulp fiber mass fractions up to 1.5%. Gas holdup was found to decrease significantly with increasing fiber mass fraction up to 1%. Gas holdup remained constant with increasing fiber mass fraction above 1%, at which fibers were noticed to collect in a large mass at the

column bottom. For mass fractions less than 0.3%, it was observed that the fibers moved freely throughout the slurry. Flocculation and bubble coalescence were noticed to occur at mass fractions above 0.3%. It was also observed that flow regime transitions occurred at lower superficial gas velocities for GLF systems than for GL systems.

Su and Heindel (2003) studied three lengths (L = 3, 6, 12 mm) of 20.6 μm diameter Rayon fiber in the bubble column described in Section 2.2. Gas holdup was observed to decrease with increasing fiber mass fraction, which was attributed to an increase in bubble coalescence and/or a decrease in bubble breakup. Homogeneous, transitional, and heterogeneous flow regimes were observed for low fiber mass fractions (C < 0.6%). Flocculation was observed at C = 0.25% for L = 6 and 12 mm, and at C = 0.4% for L = 3 mm. Distinct fiber networks were formed for $0.6\% \leq C \leq 1.8\%$, which resulted in pure heterogeneous flow for all superficial gas velocities. Fiber settling for $U_g \leq 9$ cm/s was also observed at higher fiber mass fractions, resulting in channeling in the lower column region. It was also observed that the fiber length had a greater effect on gas holdup at lower fiber mass fractions, while its influence decreased with increasing fiber mass fraction. Fiber mass fraction was noted to have a greater impact on gas holdup than fiber length, with fiber length having a negligible influence on gas holdup for $C \geq 0.4\%$.

Su and Heindel (2004) studied gas holdup in Nylon fiber suspensions (L = 2, 3, and 6 mm) in the same 15.24 cm diameter semi-batch bubble column described in Section 2.2. Nylon fiber was noted to have a time dependency on gas holdup due to the fact that the Nylon fiber had a surface additive that leached into the water to change the flow hydrodynamics, and therefore was recommended not to be used in future studies. The first day gas holdup results showed that gas holdup decreased as the Nylon fiber mass fraction increased; and fiber length did not influence gas holdup.

Heindel (2000) used flash X-ray radiography to observe gas flow characteristics in a 20 cm x 2 cm rectangular cross section, 1 m tall GLF bubble column with 6.35 mm thick clear

acrylic walls. Filtered compressed air entered the bottom of the column through a 40 μm diameter sintered bronze sparger. The superficial gas velocity was fixed at 0.83 cm/s. The liquid phase was deionized water. The initial liquid height was 80 cm. X-ray images were taken of the entire column width and a height of 20 cm, beginning at a column height of 25 cm. Cellulose fiber with a length-weighted average length of 1.3 mm and a coarseness of 0.13 mg/m was used. Fiber mass fractions were varied $0.5\% \leq C \leq 5\%$. The hydrodynamics for C = 0.5% were observed to be considerably different from that of the air-water system. Small bubbles were less numerous and spherical-capped large bubbles greater than 2 cm in diameter were observed. The bubbles were observed to coalesce and breakup as they rose in a serpentine pattern, entraining smaller bubbles in their wake. Back mixing was also visually observed. A fiber network began to form at C = 1%, which led to more bubble coalescence and larger bubbles near the column center. As the fiber mass fraction increased beyond C = 1%, channeling near the central column region became more obvious as bubble size increased due to increased fiber network strength. The flow regime was noted to change from churn-turbulent to surge churn-turbulent at C = 3% and to discrete channel flow at C = 5%. Gas holdup was not measured, but generally gas holdup for C = 0.5% was similar to C = 0%, decreased at C = 3.5%, and reduced further at C = 5%.

Schulz and Heindel (2000) measured gas holdup in a cocurrent, 12.7 cm diameter bubble column using gamma-ray densitometry. Gas holdup data was acquired at differing column heights (30 -132 cm) while varying the superficial liquid velocity (2.5 – 7.5 cm/s), superficial gas velocity (0.5 – 4 cm/s), and unprinted old newsprint fiber mass fraction (0, 0.8, and 1.2%). Gas holdup was observed to increase with increasing superficial liquid velocity, superficial gas velocity, and column height for the three fiber mass fractions studied. Maximum gas holdup for the entire column was found to occur at a concentration of 0.8%, while a minimum occurred at 1.2%. Fiber mass fraction had the same general effect on the

cross-sectional average gas holdup, although some deviations were observed and attributed to bubble coalescence and channeling.

Xie et al. (2003) studied flow regimes and gas holdup in a test loop consisting of a 5.08 m diameter, 1.8 m tall PVC bubble column using a gamma-ray densitometer at a height of 1.45 m from the column bottom. Data were recorded over a range of superficial liquid velocities (21 – 51 cm/s), superficial gas velocities (0 – 26 cm/s), and fiber mass fractions (0 – 1.5%). Five distinct flow regimes were visually observed with increasing superficial gas velocity: dispersed bubbly, layered bubbly, plug, churn-turbulent, and slug flow. The dispersed bubble regime was observed at low superficial gas velocities and consisted of very small, non-uniformly distributed bubbles that did not coalesce or breakup. The layered bubbly regime consisted of a flocculated core and a fiber-free annulus with no bubble coalescence. Plug flow was characterized by small bubble clusters and large gas plugs that moved in a swirling spiral pattern and entrained small bubbles in its wake. Large irregular-shaped gas pockets near the column center were observed in the churn-turbulent flow regime. Further bubble coalescence led to the observation of the slug flow regime, which was characterized by the presence of large bullet-shaped bubbles. Cross-sectional gas holdup was uniform for dispersed bubbly and layered bubbly flows due to the lack of mixing. The remaining flow regimes all showed the same parabolic gas holdup trend, with the highest gas holdup measured in the center of the column. The drift flux model (Zuber and Findlay, 1965) was used to correlate the gas holdup, with the drift flux parameters being a function of the fiber mass fraction.

Walmsley (1992) studied gas holdup in a 75 mm and a 150 cm diameter bubble column by measuring bed expansion. Tests were run with various initial slurry heights (H/D ratios). The distributor plates consisted of 0.5 mm, 1.0 mm, or 1.5 mm holes drilled on a 20 mm triangular pitch. The fibers studied were bleached Kraft pine, bleached Kraft eucalypt, and recycle yellow pages. The hydrodynamics of the column were noticed to change

considerably from that of an air-water system with the introduction of only 0.1% cellulose fiber. Flocculation was observed to begin at 0.3% and continuous fiber networks formed at 0.8%. Bubbles were observed to be trapped in the fiber flocs until enough bubble coalescence resulted in the bubble breaking through the flocs. The flow regime was observed to change from bubbly flow to churn-turbulent flow at $U_g = 10$ cm/s. The H/D ratio was observed to not affect gas holdup in the bubbly regime, but decreased gas holdup in the churn-turbulent regime due to significant back mixing. Fiber mass fractions beyond 0.6% significantly decreased gas holdup.

Lindsay et al. (1995) examined the flow structure in cellulose fiber flows using two different bubble column reactors. The first bubble column was a semi-batch transparent acrylic cylinder with a 12.7 cm inner diameter and was 66 cm in height. The distributor plate used in this column was a perforated rubber plate with approximately 230 holes drilled with a 2.4 mm drill bit on a square lattice with 0.7 cm pitch. The second bubble column was a transparent acrylic cylinder with a 12.7 cm inner diameter, 1.5 m in height, and was a component of a cocurrent flow loop. Superficial slurry velocities ranged from 2.5 to 7.5 cm/s for the cocurrent system. Superficial gas velocities ranged from 0 to 4.2 cm/s for both systems. Gamma ray densitometry was used to determine the time-averaged gas holdup. The fiber phase of the study consisted of 1% and 2% mass fractions of commercial unprinted newsprint. In the semi-batch bubble column, gas holdup for the fiber system was observed to be lower than for a pure air-water system due to fiber flocculation and network formation leading to bubble coalescence and gas channeling. In the cocurrent system, gas holdup was observed to be higher in the fiber slurry than in the GL system when the superficial liquid velocity was higher than the superficial gas velocity, and was attributed to the bulk flow of the slurry reducing bubble coalescence. Gas-liquid-solid hydrodynamic flow models and correlations were shown to not be applicable to gas-liquid-fiber flows.

Janse et al. (1999) studied the effects of gas flow rate, accept flow rate, bubble size distribution, and fiber mass fraction on gas holdup in a 10.2 cm diameter, 4.65 m high Plexiglas bubble column. Four pressure transducers at different axial locations were used to estimate gas holdup. Air entered the column through a porous, stainless steel sparger, and fiber consisting of 70% ONP/30% OMG (old newspaper/old magazine) was continuously fed into the system from a plant flotation deinking circuit. Process water, which came from the plant thickener overflow, was used to dilute and keep the pulp at the desired chemical composition. Process water was selected over tap water due to the presence of surfactants which act as frothing agents to create smaller bubbles and to retain bubble size, thus resulting in higher gas holdup. Gas holdup was found to decrease with increasing fiber mass fraction; while increasing with increasing superficial accept velocity. Gas holdup was also higher for a finer pore diameter sparger (1 μm) when compared to the results using a coarse diameter sparger (20 μm).

Reese et al. (1996) studied the hydrodynamic and gas holdup behavior of three-phase fiber slurries in a cylindrical bubble column. The cylindrical bubble column had a 10.2 inner diameter and was 2.2 m in height. Gas (air) was injected into the base of the bubble column through a perforated plate distributor. The slurry was created from water and commercially bleached southern softwood fiber. Fiber mass fractions ranged from 0.1 to 1.0%. The column was operated in semi-batch mode with an initial slurry height of 1.38 m. Superficial gas velocities were studied in the range of 0.1 to 5.0 cm/s. Bubble passing frequency was measured by an intrusive light transmittance probe assembly. Gas holdup in fiber slurries was lower than that of air-water systems, even at low fiber mass fractions, and was attributed to increased coalescence near the column bottom. The effects of fiber on gas holdup increased as the fiber mass fraction increased. Increased bubble coalescence resulted in increased bubble size, increasing turbulence and back mixing, as well as a decreasing the homogeneous flow regime superficial gas velocity operating conditions. Fibers were

uniformly distributed at lower mass fractions (0.1 and 0.25%) but fiber settling was observed at higher mass fractions (0.75 and 1.0%). The fiber was also observed to have an increased tendency to flocculate at high gas velocities and mass fractions. The dispersed bubble regime and coalesced bubble regime were the two regimes generally observed in their GL study. In the GLF system, the coalesced bubble regime was divided into the vortical-spiral regime and the turbulent flow regime. The vortical-spiral regime was observable in lower fiber mass fractions (0.1 and 0.25%) but was not observable for the higher fiber mass fractions (0.75 and 1.0%). The higher fiber mass fractions also led to fiber settling, gas channeling, and large bubble formation in the lower column section. The application of the light transmittance probe showed that bubble passing frequency decreased and bubble passing period increased with increasing fiber mass fraction, indicating that bubbles became larger and less numerous with increasing fiber mass fraction.

2.5 Gas Holdup Measuring Techniques

Many techniques to measure gas holdup have been discussed in the previous sections, both invasive and non-invasive to the system. Boyer et al. (2002) provided an excellent review of various techniques to measure gas holdup in bubble columns that will be summarized below.

Time-averaged pressure drop between two different levels within a bubble column can be used to determine the gas phase holdup. Piezoelectric pressure sensors can be flush-mounted to the column wall. The frictional pressure drop within slurry bubble columns is often negligible compared to the static pressure drop. The Zuber and Findlay (1965) drift flux model can be applied to the time-averaged pressure drop data over a range of superficial gas velocities to determine gas flow regime transitions (Hol and Heindel, 2005; Ruzicka et al., 2001b; Su and Heindel, 2003; Zahradnik et al., 1997).

Dynamic gas disengagement is a technique used in bubble columns to determine the global gas holdup, solid holdup, or the structure of the gas holdup. The aeration in the bubble column is stopped and either the liquid level or pressure is measured as a function of time.

Radiation attenuation techniques can also be applied to bubble columns. Gases, liquids, and solids all have different absorption coefficients. The attenuation is a function of density along the radiation path. X-ray, gamma-ray, and neutron beams are often used to show the local mass density along the path between the source and the detector. Light attenuation is also used if the liquid is clean and transparent and contains bubbles or drops. The light attenuation is a function of the specific interfacial area of the dispersed phase. Ultrasound techniques can also be used with the main benefit that the liquid phase does not need to be transparent.

2.6 Literature Review Summary

Numerous gas holdup studies have been completed in gas-liquid, gas-liquid-solid, and gas-liquid-fiber systems. The hydrodynamics of bubble columns are difficult to understand and more research must be done to completely understand the phenomenon for industrial scale up purposes. The work of this thesis will be another step in an attempt to determine the critical parameters that influence overall and local gas holdup in large diameter GLF bubble columns.

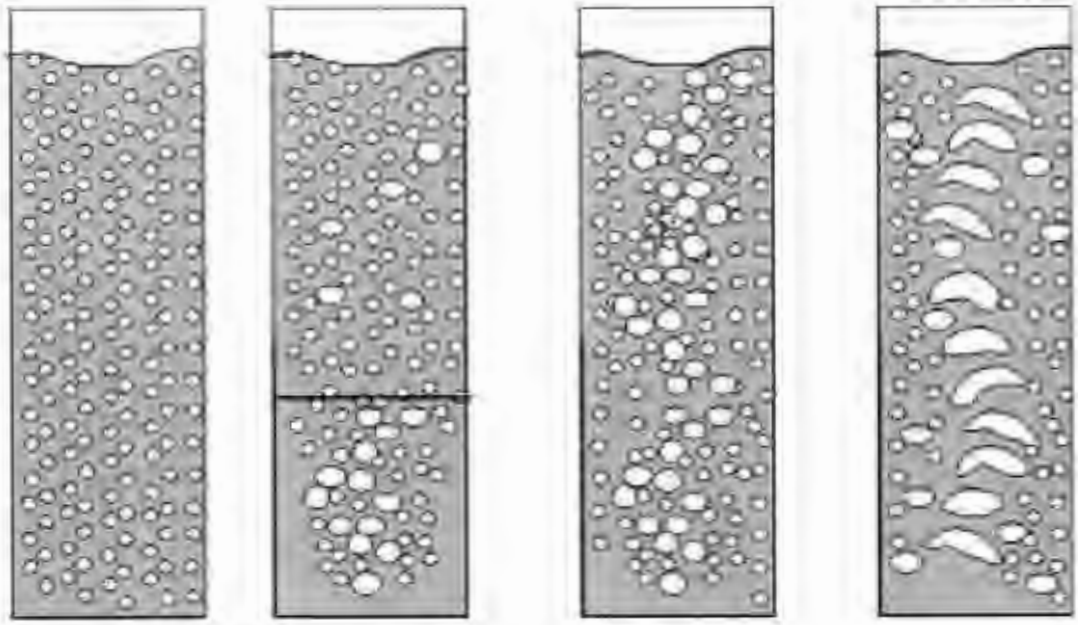

Figure 2.1: Schematic representation of the flow regimes: (a) homogeneous regime, (b) transitional regime 1, (c) transitional regime 2, (d) heterogeneous regime (Olmos et al., 2003). (Note, the black lines in some of the figures are found in the original paper.)

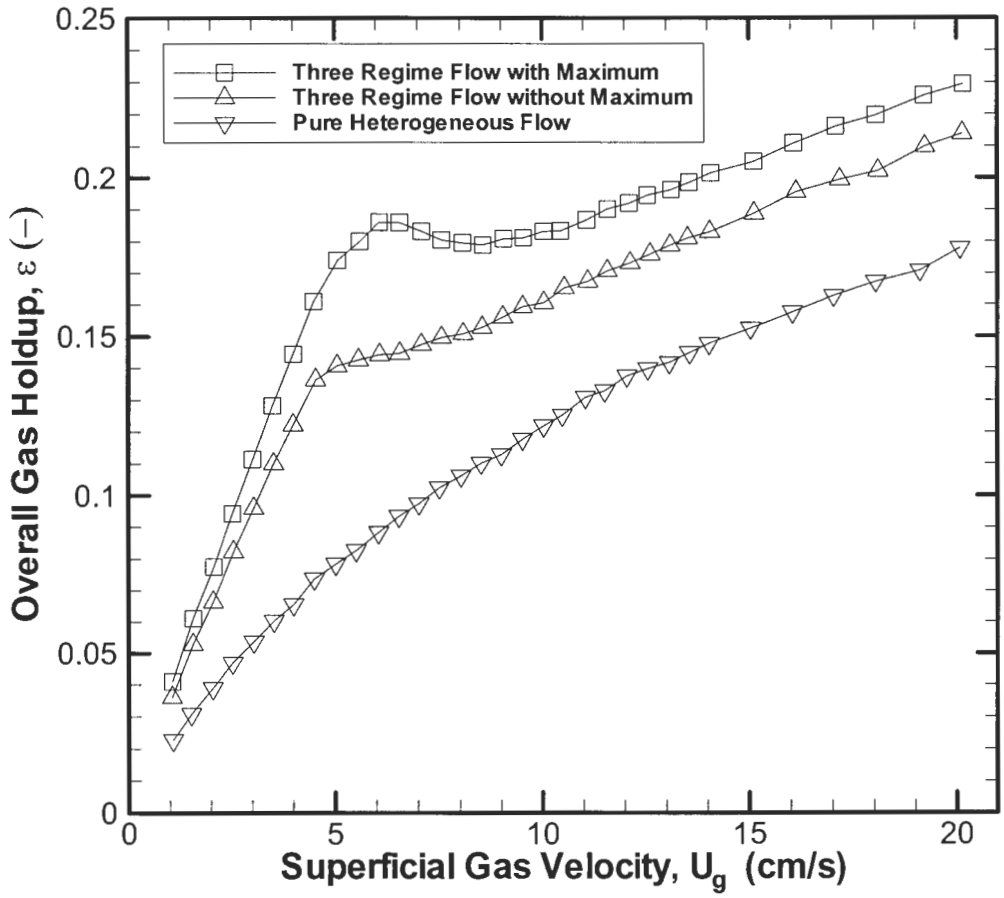

Figure 2.2: Generic overall gas holdup curves.

CHAPTER 3: MATERIALS AND METHODS

This chapter covers four subsections. The first section describes the experimental setup. The second section explains the data collection process. The third section discusses the data analysis. The last subsection will discuss the repeatability of the tests performed, as well as the uncertainty of the measurements, in this research.

3.1 Experimental Setup

This section is divided into four subsections. The first describes the bubble column facility. The second section summarizes the experimental conditions. The third section explains the fiber preparation process. The fourth section outlines the bubble column operation.

3.1.1 Bubble Column Facility

A schematic representation of the bubble column experimental facility used in this research is shown in Fig. 3.1. Figure 3.2 shows an actual picture of the lower column section and identifies several key features of the bubble column. The bubble column consists of four cast acrylic sections 122 cm in height, 32.1 cm internal diameter, and 1.25 cm thick walls. Compressed air travels through an air diffuser to provide a uniform pressure profile on the underside of a stainless steel perforated plate, where the air is introduced at the base of the bubble column. The air diffuser is a 33 cm section of the column located directly below the perforated plate that contains three 1.2 cm thick acrylic plates. The plates are separated by 6.5 cm and have an increasing number of smaller holes as the air travels towards the perforated plate. Air enters through the bottom of the diffuser, where there is also a drain to remove water that may seep through the distributor plate.

The air flow rate is controlled by a gas regulator and measured by one of three mass flow meters, covering a low, medium, and high gas flow rate range. The low range flow meter is an Aalborg GFM571 mass flow meter that covers a flow range of 0 – 200 L/min. The medium flow meter is an Aalborg GFM671 mass flow meter that covers a flow range of 0 – 500 L/min, and is specifically used in this research for the flow range of 200 – 500 L/min. The high flow meter is an Aalborg GFM771 mass flow meter that covers a flow range of 0 – 1000 L/min, and is specifically used for the flow range of 500 – 1000 L/min.

Eleven flush mounted pressure transducers are located on the side of the column. The first, or lowest, is located 15.2 cm from the bottom of the column and the remaining ten are separated axially by $\Delta h = 30.5$ cm, therefore the top pressure transducer is located 320 cm from the column base. The lowest pressure transducer is an Omega PX541-015GI, which covers a pressure range of 0 – 15 psi. The next eight pressure transducers are Omega PX540-7.5GI and cover the pressure range of 0 – 7.5 psi. The top two pressure transducers are Omega PX541-003GI and cover the pressure range of 0 – 3 psi.

Two T-type thermocouples are located on the side of the column; one near the bottom pressure transducer and another near the top pressure transducer.

The mass flow meters, pressure transducers, and thermocouples are connected to a computer controlled data acquisition system. The instruments are connected to a National Instruments SCB-100 DAQ connector block which interfaces with the computer via a National Instruments PCI-6031E DAQ card. Power is supplied to the connector block by a Pyramid PS-3KX regulated power supply, which supplies a 13.8 DC voltage and a constant 2.5 amps.

3.1.2 Experimental Conditions

All experiments in this study are conducted at atmospheric pressure and ambient temperature. The gas phase consists of filtered compressed air. Filtered tap water is used as

the liquid phase. The fiber phase in the gas-liquid-fiber (GLF) system consists of Rayon or cellulose fibers. Three different lengths of 20.6 μm diameter Rayon fiber (L = 3, 6, and 12 mm) and three different kinds of cellulose fiber, including bleached hardwood chemical pulped fiber (hardwood), bleached softwood chemical pulped fiber (softwood), and bleached softwood chemithermomechanical pulped fiber (BCTMP), are used to form the fiber slurries. These will be the six different fiber types studied in this research. Table 3.1 summarizes the characteristics of the cellulose fiber types.

Fiber mass fractions are varied from $0 \leq C \leq 1.8\%$, with Table 3.2 summarizing the specific fiber mass fractions. Superficial gas velocities, which are defined by the volumetric gas flow rate divided by the column cross sectional area, are studied over the range $U_g \leq 20$ cm/s. Nominal superficial gas velocities studied in this research are every 0.5 cm/s over the range $1 \leq U_g \leq 14$ cm/s and every 1 cm/s over the range $14 < U_g \leq 20$ cm/s.

Three different perforated plates (Fig. 3.3) are used for the column aerator; each with a different open area ratio (A = 0.49%, 0.95%, and 2.03%). The distributor plate open area ratio is determined by

$$A = N\left(\frac{d_o}{D}\right)^2 \tag{3.1}$$

where A is the distributor open area ratio, N is the number of uniformly distributed holes, d_o is the orifice diameter, and D is the bubble column inner diameter. The orifice diameter is constant at d_o = 1 mm for all three plates. The number of holes on each plate are N = 486, 953, and 2030 for A = 0.49%, 0.95%, and 2.03%, respectively. Table 3.3 shows the fiber types and lengths studied for each plate.

All experiments are performed using an initial slurry height of H = 321 cm, which corresponds to ten column diameters. The column is operated in semi-batch mode; hence the superficial liquid velocity is zero.

3.1.3 Fiber Preparation

The fiber mass fraction, C, is the ratio of the fiber mass to the total slurry mass within the bubble column. The total slurry volume within the bubble column for all the experiments is fixed at $V_c = 0.26$ cubic meters, which corresponds to the initial slurry height of H = 321 cm. The dry fiber mass, m_f, required for a specific fiber mass fraction is determined by

$$m_f = \frac{V_c \rho_l \rho_f C}{\rho_f + C(\rho_l - \rho_f)} \qquad (3.2)$$

The dry density of the fiber phase, ρ_f, is assumed to be 1500 kg/m^3 for both Rayon and cellulose fiber. The liquid density, ρ_l, is assumed to be 1000 kg/m^3 for all experiments. The derivation of this equation is shown in Appendix A. The required dry fiber mass for each mass fraction is shown in Table 3.2.

Since the fiber absorbs moisture from the air, the water contained within the fiber must be removed to obtain an accurate dry fiber mass. The moisture is removed by using a Sharp R-215EW carousel microwave. Softwood and hardwood cellulose fiber sheets, which arrive in the lab in a bale of 65 cm by 91 cm dry lap pulp sheets, are torn into approximately 10 cm by 10 cm pieces, placed on a paper towel in a single layer within the microwave, and then heated for approximately 30 - 40 seconds. BCTMP cellulose fiber sheets, which arrive in the lab as a fiber block, are broken up into smaller 2 cm by 3 cm pieces, placed on paper towel in the microwave, heated for approximately 40 – 45 seconds, rearranged, and heated for another 40 – 45 seconds. Moisture is removed from Rayon fiber by placing approximately 100 grams of fiber onto a paper towel in the microwave, heated for approximately 45 seconds, rearranged, and heated for another 45 seconds. Once the fiber has been heated it is immediately place on a Fisher Scientific XL-3000 digital scale to measure the dry fiber mass before the fiber begins to reabsorb moisture. The reading is recorded and the fiber is placed into a bucket. This process is repeated until the appropriate dry fiber mass is accumulated.

For higher mass fractions ($C \geq 0.40\%$), a difference in fiber mass is often used and added to the previous set to achieve the desired mass fraction.

After the correct dry fiber mass is measured, the fiber is prepared for evaluation within in the column. Different preparation methods are used for Rayon and cellulose fibers. Cellulose fiber is prepared by first soaking the measured fiber set in water for a minimum of twelve hours. Then the fiber is disintegrated for about ten minutes within a Black Clawson laboratory hydrapulper to break the fiber sheet pieces into individual fibers.

Rayon fiber preparation is different because a significant amount of foam was generated during initial Rayon fiber testing. The foam was determined to be a result of a coating placed on the fiber surface during the manufacturing process. The coating leached into the water during bubble column operation and was found to decrease the surface tension of the water in the fiber slurry and create large amounts of foam. Therefore, the fiber must be washed to remove the coating before being placed in the column. The fiber washing process is performed by continually rinsing and periodically agitating a concentrated slurry of Rayon fiber until the surface tension of the water exiting the fiber slurry stabilizes to around 55 – 60 dynes/cm to significantly reduce the amount of foam generated. The surface tension of the water in the lab before being mixed with the fiber is approximately 70 dynes/cm. The surface tension is measured by a KSV Sigma 703 digital tensiometer. A Cole Parmer Stir-pak 50002-30 variable speed laboratory mixer with an attached propeller blade is used at low speeds to agitate the L = 3 mm and L = 6 mm Rayon fibers. L = 12 mm Rayon fibers are agitated manually since the long fibers wrap around the mixer shaft and propeller. The Rayon fibers are washed and agitated the day prior to being placed into the column until the surface tension rises to approximately 50 dynes/cm. The fibers are then washed and agitated again the day of operation until the surface tension is at least 55 – 60 dynes/cm before being placed into the column. Figure 3.4 illustrates the surface tension measurements involved in

the fiber preparation process for L = 3 mm Rayon fiber at C = 0.16%. Once the fiber is prepared, the fiber is ready to be used within the column.

3.1.4 Bubble Column Operation

A number of steps are completed before placing a fiber set into the column. The water is run for about ten minutes to remove any impurities that may have settled in the water line. The column is then filled with water approximately half the initial slurry height. The prepared fiber slurry is then added to the column from the top. The sides of the column are then rinsed with water to wash all the fiber down into the water/fiber slurry. Water is again added to the slurry to raise the slurry height to the initial level of ten column diameters (H = 321 cm). The gas flow is then turned up to a moderate flow rate (200 – 300 L/min) and the column is allowed to mix for approximately ten minutes to ensure the slurry is well mixed. Water that seeps into the air diffuser during the filling process is removed at this time. Once the column is well mixed, the gas flow rate is reduced to the lowest gas flow rate of interest (U_g = 1 cm/s) to begin data collection. The column is allowed to operate for five minutes, not including data collection time, between data points. After a data point is taken the gas flow is increased sequentially.

3.2 Data Collection

A data point consists of pressure readings for each of the eleven pressure transducers, temperature readings for the two thermocouples, and superficial gas velocity readings for the one selected mass flow meter. A data point is an average of 4500 readings taken from each instrument at a sampling frequency of 100 Hz. LabVIEW is the data acquisition program used to control and display the process of acquiring data. This program creates a data file, whose file name contains the date and time it was created, and places each data point taken for a complete data set within this file.

3.3 Data Analysis

This section contains two subsections. The first subsection discusses the gas holdup analysis. The second subsection discusses the application of the drift flux model.

3.3.1 Gas Holdup

After data are acquired for a specific fiber type and fiber mass fraction, the information is analyzed to obtain gas holdup. Microsoft Excel is used to analyze the raw data from the LabVIEW data file. This file calculates local and overall gas holdup and plots gas holdup versus superficial gas velocity.

Local gas holdup between any two successive pressure transducers is determined from

$$\varepsilon = 1 - \frac{\Delta P}{[\rho_l + \Phi_f(\rho_f - \rho_l)]g\Delta h} \tag{3.3}$$

where ΔP refers to the pressure difference between two successive pressure transducers and Δh refers to the corresponding separation distance. The fiber volume fraction within the bubble column, Φ_f, is determined from the known slurry volume and the volume of fiber within the column which can be determined from the fiber mass and density. The derivation of the above gas holdup equation is in Appendix B. Note that for the mass fraction range in this study, $\Phi_f(\rho_f - \rho_l) << \rho_l$.

The local gas holdup in this study corresponding to the location of pressure transducer i is defined as the average of the gas holdup obtained using pressure transducers i and i + 1 and that of pressure transducers i – 1 and i. This definition minimizes large swings in the gas holdup resulting from a small change in the guage pressure readings. Therefore, local gas holdup values are defined at axial locations every 30.5 cm over the range $40 \leq H \leq 290$ cm, where H is the height from the column bottom.

The overall gas holdup is calculated according to Equation 3.3, where ΔP is the pressure difference between the top and bottom pressure transducers and Δh is the corresponding separation distance.

Tecplot is used to visualize various plots to determine the effects of fiber mass fraction, superficial gas velocity, fiber type, fiber length, and aeration method on overall and local gas holdup.

3.3.2 Application of the Drift Flux Model

Zahradnik et al. (1997) and Su and Heindel (2003) showed that the Zuber-Findlay drift flux model (Zuber and Findlay, 1965) could be used to identify the homogeneous and heterogeneous flow transitions when three regimes are observed over a range of superficial gas velocities. The drift flux model can be described by

$$\frac{U_g}{\varepsilon} = C_0 U_g + U_t \qquad (3.4)$$

where C_0 is a parameter that gauges the radial flow and gas holdup uniformity and U_t describes the drift flux velocity. Zahradnik et al. (1997) plotted U_g/ϵ as a function of U_g to determine the superficial gas velocity at which transition occurs, where changes in the slope signify a flow regime transition. The first change is the slope of the U_g/ϵ versus U_g plot identifies the transition from homogeneous to transitional flow. The last change in the slope represents the transition from the transitional regime to the heterogeneous regime. Two different slopes appear in the transitional flow regime when a local maximum gas holdup is observed; the change in slope in this region corresponds to the maximum gas holdup. The slope of the U_g/ϵ versus U_g plot is constant for pure heterogeneous flow. Figure 3.5 shows a sample of the drift flux plot for L = 3 mm Rayon fiber at two different mass fractions. When C = 0.10%, the location of the regime changes are clearly identifiable by the changes in the slope of the drift-flux plot; position 1 corresponds to the onset of the transitional regime,

position 2 correlates to the maximum gas holdup location, and position 3 marks the end of the transitional regime and the onset of heterogeneous flow. When C = 0.60%, the drift flux model indicates the flow is heterogeneous over the entire superficial gas velocity range because the slope is constant (i.e., the flow is pure heterogeneous).

3.4 Data Repeatability and Uncertainty

At least two data sets were taken for at least two different fiber mass fractions for all fiber types and distributor plate open areas. Figure 3.6 shows an example of the repeatability of the overall gas holdup data obtained for C = 0.10%, A = 0.95% and C = 0.25%, A = 2.03% softwood cellulose fiber. This figure shows that data is repeatable for flows that demonstrate homogeneous, transitional, and heterogeneous flow regimes, as well as flows that are pure heterogeneous. Figure 3.7 shows the repeatability of three different sets of C = 0.40% BCTMP cellulose fiber for A = 0.49%. The sudden increase in overall gas holdup at $U_g \approx$ 15 cm/s is due to the fiber slurry overcoming the foam at the top of the slurry and entraining that foam back into the slurry; thus creating a higher gas holdup. This trend was repeated three times at the same superficial gas velocity. The uncertainty of the superficial gas velocity was estimated to be approximately 1.5 – 6.0%. The absolute uncertainty in gas holdup was estimated to be $\Delta\epsilon \approx$ 0.005 to 0.01.

Table 3.1: Cellulose fiber properties.

Fiber Type / Properties	Hardwood	Softwood	BCTMP
Wood Species	Eucalyptus	65-75% Northern Black Spruce 20-25% Jackpine 5-10% Balsam Fir	Softwood (Northern Pine)
Length – PAFL (mm)	0.69	1.2	0.8
Length – LWAFL (mm)	0.78	2.31	1.91
Coarseness (mg/100m)	6.9	13.08	29.5
Number of Fibers per gram (millions)	21.4	6.37	4.25

PAFL – particle average fiber length
LWAFL – length weighted average fiber length

Table 3.2: Fiber mass fractions and corresponding dry fiber mass.

Fiber Mass Fraction (%)	**Fiber Mass (g)**
0.05	130
0.10	260
0.16	416
0.25	650
0.40	1040
0.60	1560
0.80	2080
1.00	2610
1.20	3130
1.40	3650
1.80	4700

Table 3.3: Fiber types studied for each distributor plate.

A / Fiber Type	0.49%	0.95%	2.03%
Hardwood	X	X	X
BCTMP	X	X	X
Softwood	X	X	X
L = 3 mm Rayon	X	X	X
L = 6 mm Rayon	X		
L = 12 mm Rayon	X		

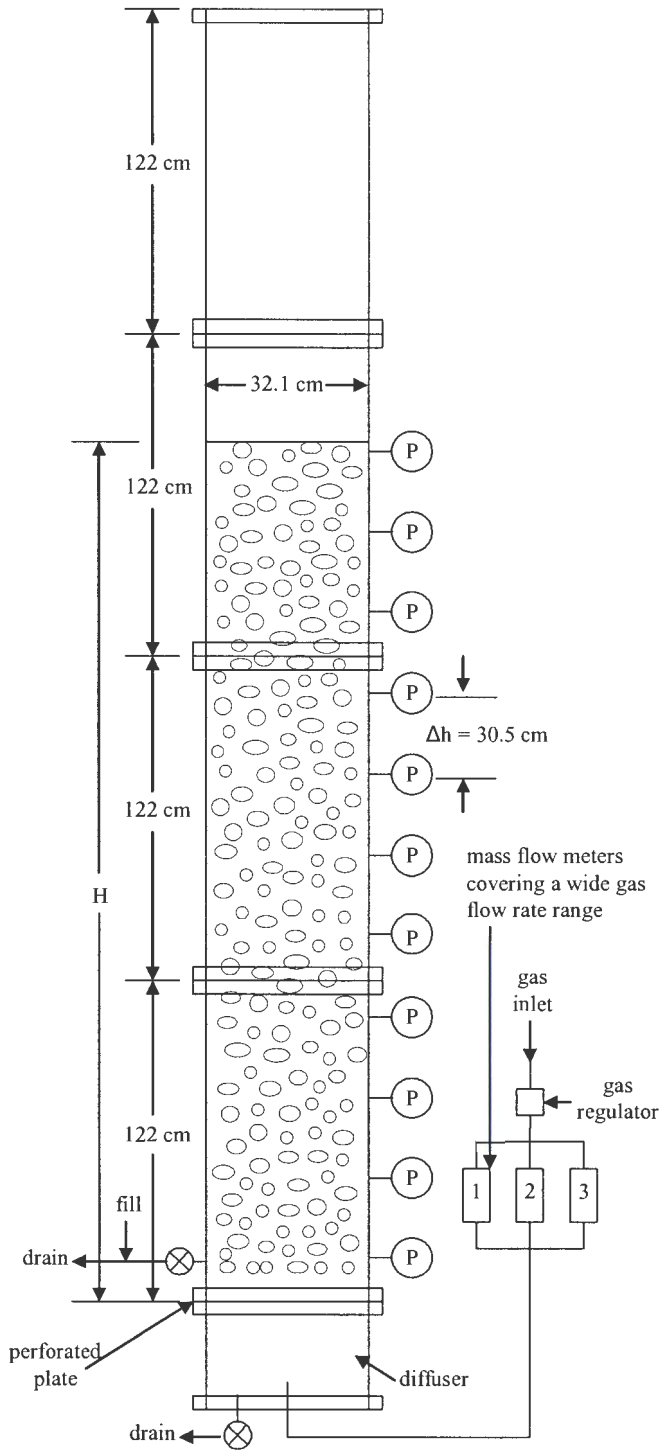

Figure 3.1: Experimental bubble column schematic.

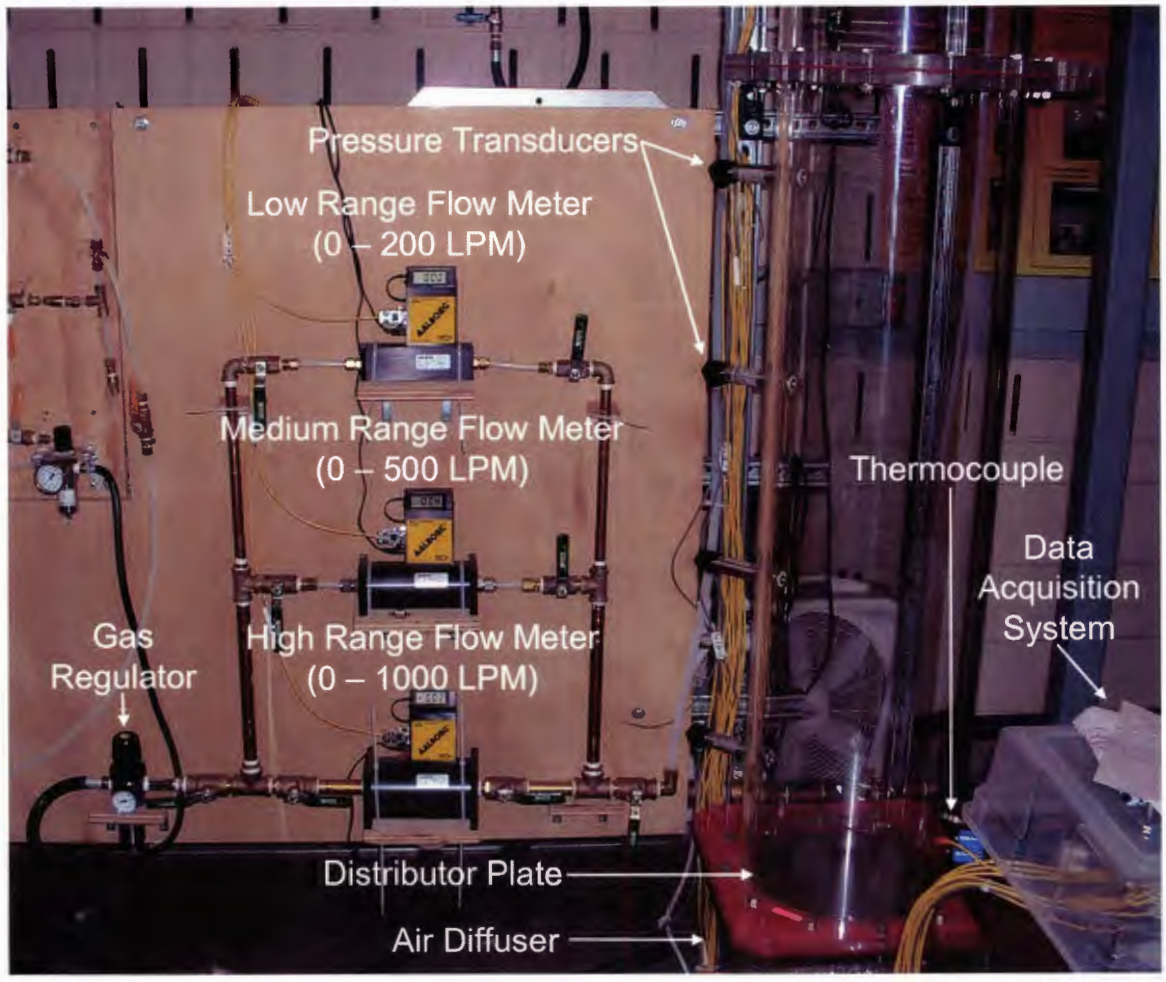

Figure 3.2: Lower column section.

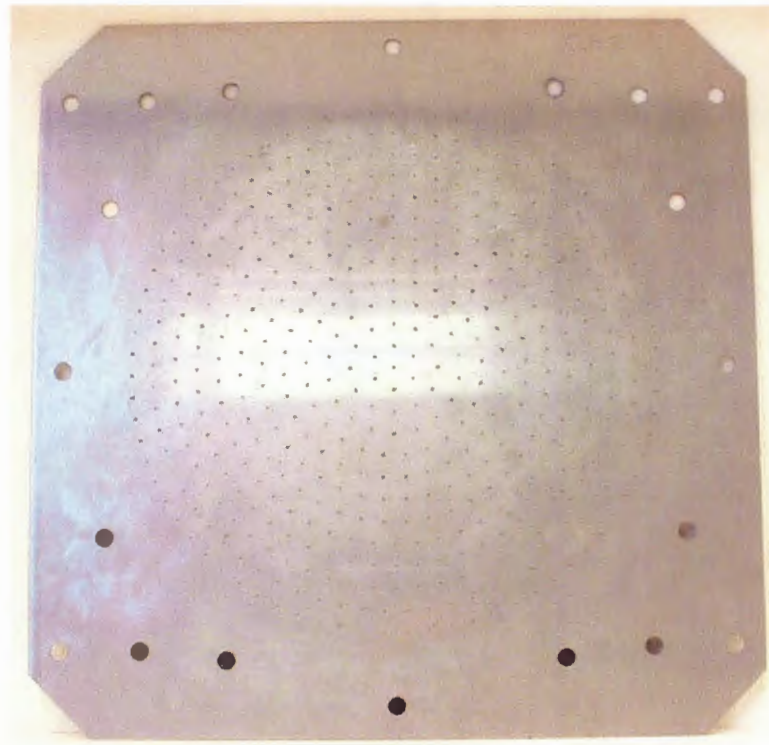

(a)

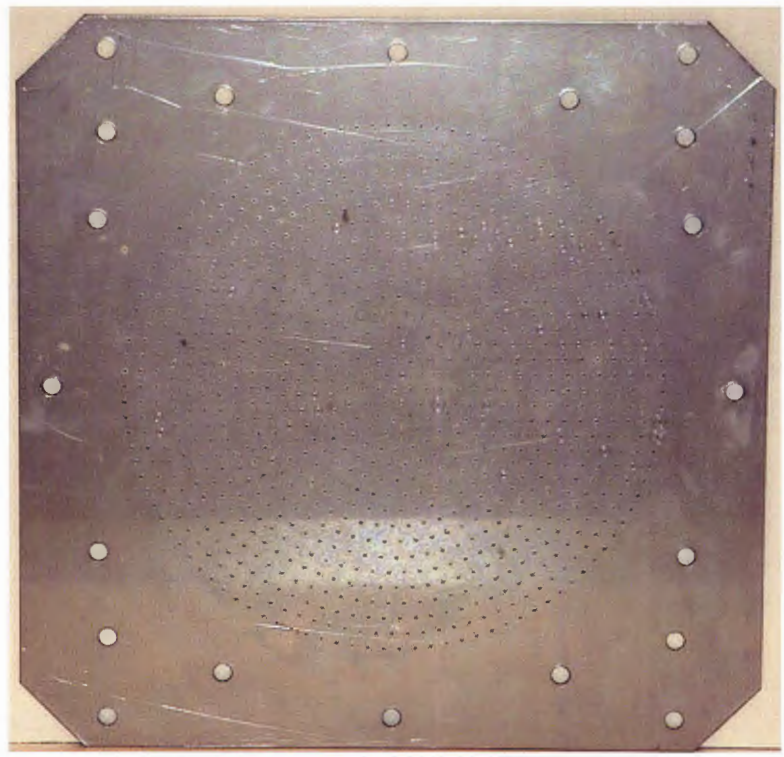

(b)

Figure 3.3: Perforated distributor plates: (a) A = 0.49%, (b) A = 0.95%, (c) A = 2.03%.

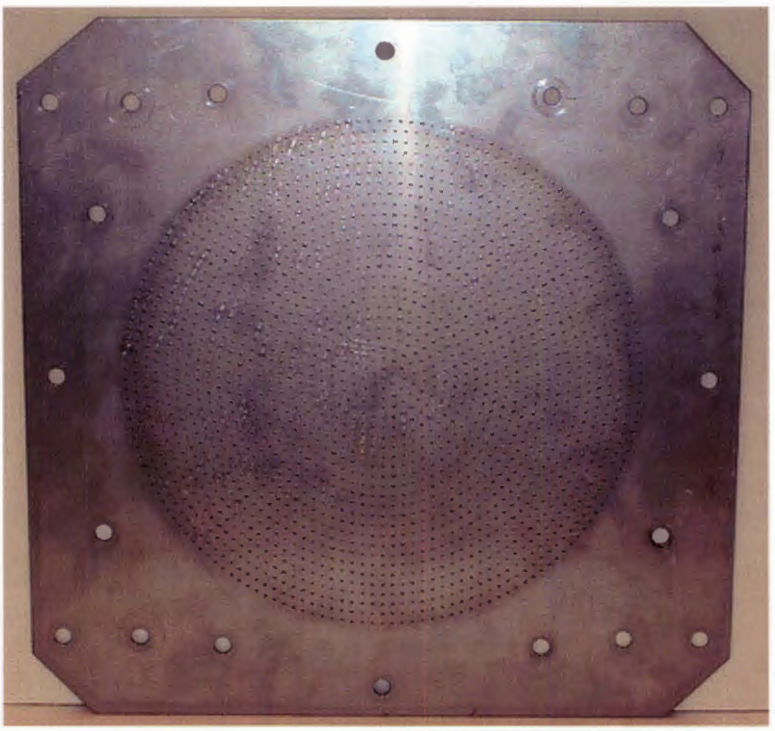

(c)

Figure 3.3: Continued.

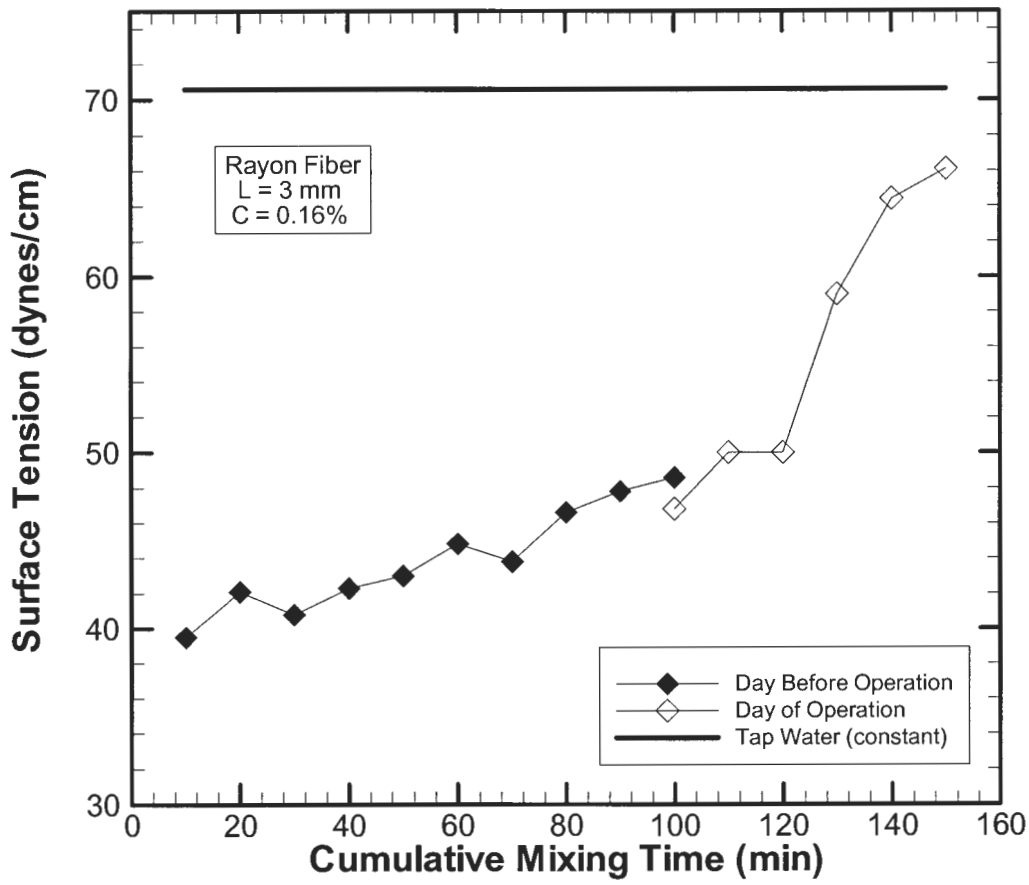

Figure 3.4: Fiber preparation surface tension measurements.

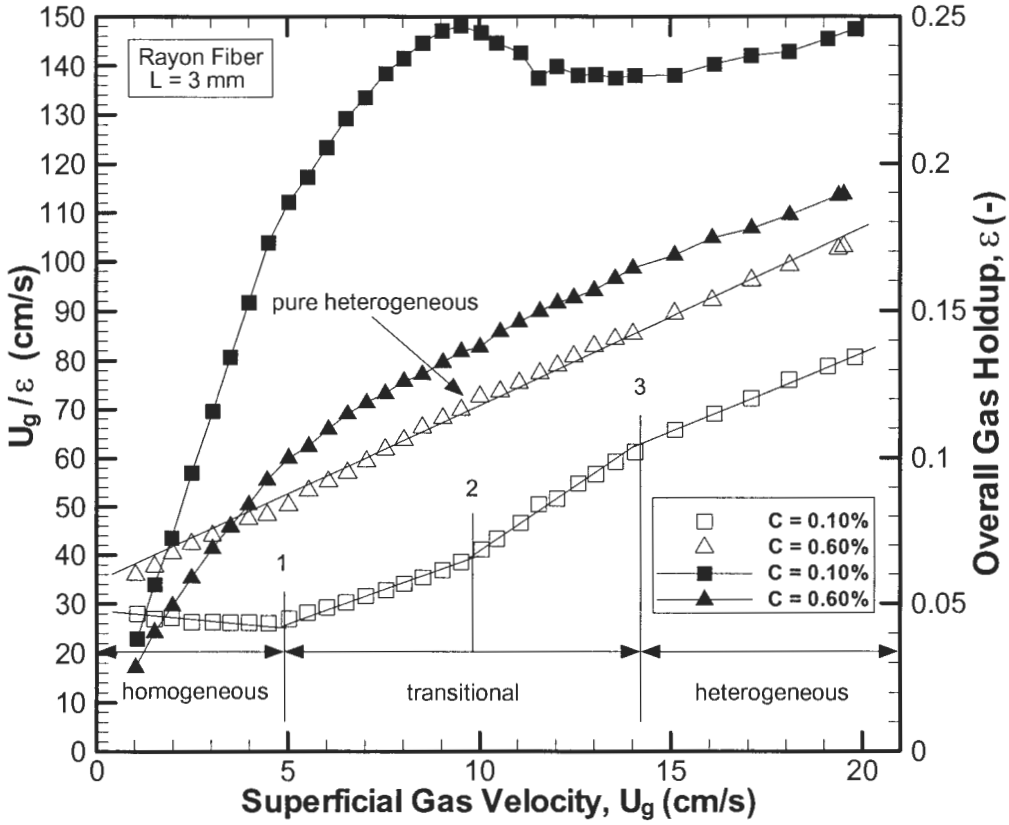

Figure 3.5: Sample drift flux plot for L = 3 mm Rayon fiber.

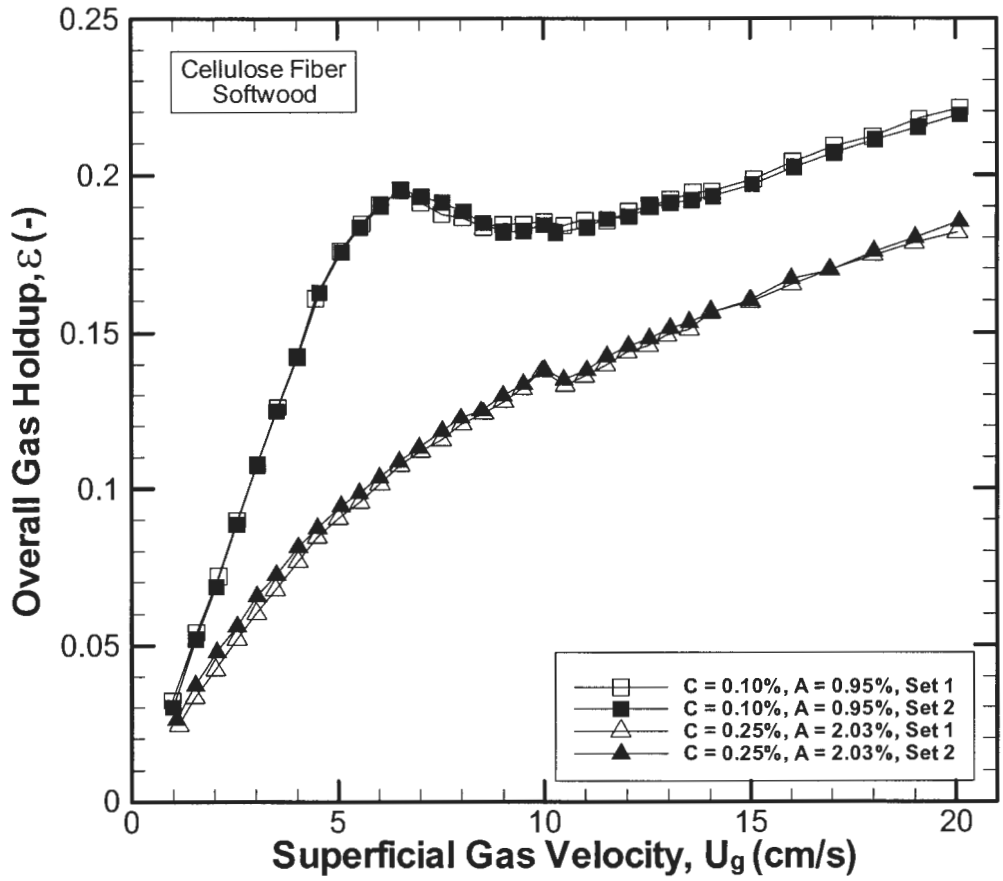

Figure 3.6: Repeatability tests of softwood cellulose fiber.

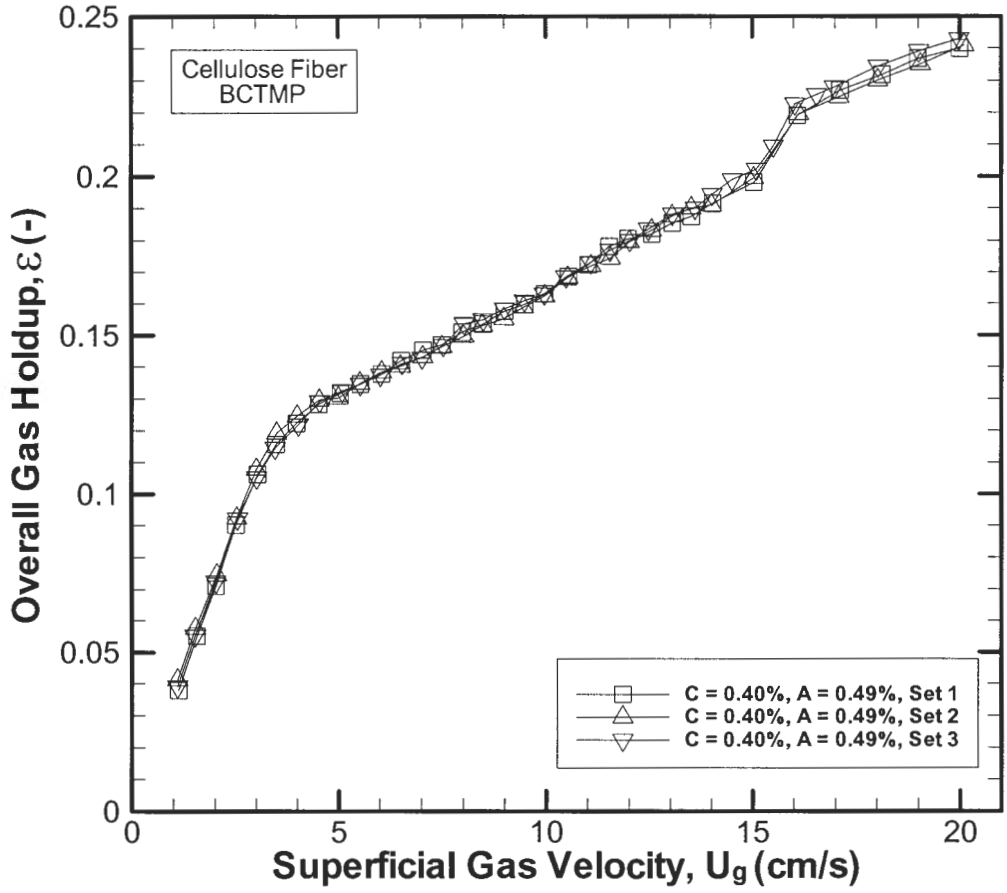

Figure 3.7: Repeatability test example for BCTMP cellulose fiber.

CHAPTER 4: RESULTS

This chapter is divided into three sections. The first section addresses some general experiment observations. The second section discusses overall gas holdup results and data repeatability tests. The third section summarizes local gas holdup results.

4.1 Experimental Observations

This section discusses some general experimental observations that were not discussed in the previous sections.

The main observation is the distribution of the air within the bubble column for an air-water system at low superficial gas velocities, which is shown in Fig. 4.1 for an air-water system at distributing air through the A = 0.95% distributor plate at U_g = 2 cm/s. As a result of the low flow rate, not all the holes in the distributor plate are active at the same time. The flow begins to circulate in a counterclockwise fashion immediately after the air enters the column through the distributor plate, as is evident by the streaklines shown in Fig. 4.2. Thus, the active holes will rotate counterclockwise with the rotation of the flow.

Another observation is the presence of large bubbles near the top of the column in flows at high superficial gas velocity and high fiber mass fraction. Since it is difficult to visually observe large bubbles in a high fiber mass fraction slurry, large bubbles were simulated in an air-water system by turning the air up to a high superficial gas velocity ($U_g \approx 15$ cm/s) for a couple of seconds and then suddenly turning off the air flow rate. The air bubbles were allowed to escape the column and then the air was abruptly turned on to send a surge of air through the column. A vapor layer quickly formed on the bottom of the column and rose. Wall friction caused the shape of the air layer to form a bullet-nose bubble. Many small bubbles were entrained in the wake of the large bubble as it rose up the column. Figure 4.3 shows an example of a large bubble that was produced using this method at a column height

of H $\approx$ 290 cm. Note that the medium above the air bubble in the picture is water. Figure 4.4 shows another large bubble just before it reaches the top of the water. The water height just before the bubble reaches the surface in this picture is approximately 60 cm above the static water height. Figure 4.5 shows the bubble bursting at the air-water interface, which creates large splashes as evident by the water splash shown in the middle of the picture. Figure 4.6 shows an example of the top of a fiber slurry at a high superficial gas velocity and high fiber mass fraction during continuous operation. At times, the splash in the fiber suspension was so violent that a fiber slurry "projectile" was propelled vertically over 1.5 m and escaped the bubble column.

4.2 Overall Gas Holdup Results

This section is divided into four different subsections. The first three sections will cover the effects of superficial gas velocity, fiber mass fraction, and fiber type, respectively, on overall gas holdup for the base case. The base case is all the information gathered for the smallest open area distributor plate (A = 0.49%). The fourth subsection will discuss the effects of distributor open area on the gas holdup and any differences observed from the base case.

4.2.1 Effect of Superficial Gas Velocity

The bubble column hydrodynamics of a low fiber mass fraction slurry (C < 0.60%) is similar to those of an air-water system, as shown in Fig. 4.7. Three different flow regimes are observed as the superficial gas velocity increases over the range of $0 \leq U_g \leq 20$ cm/s. The homogeneous, or bubbly, flow regime is observed at low superficial gas velocities ($U_g \leq$ 5 cm/s) and is characterized by a uniform distribution of similarly sized bubbles that ascend the column with minimal lateral movement. Bubble coalescence typically does not occur

within the homogeneous flow regime and gas holdup increases linearly with respect to superficial gas velocity.

As the superficial gas velocity increases beyond $U_g = 5$ cm/s, the flow begins to enter the transitional flow regime. The onset of the transitional flow regime is characterized by bubble-bubble interaction, the diversion of the bubbles from the nearly vertical motion, and eventual bubble coalescence. Gas holdup no longer increases linearly with superficial gas velocity. The gas holdup versus superficial gas velocity curve within the transitional region will sometimes display a well pronounced local maximum gas holdup value. Figure 4.7 shows the pronounced local maximum gas holdup value within the transitional regime that can be seen for $C \leq 0.25\%$. Figure 4.8 also shows the pronounced local maximum gas holdup value for all fiber types at $C = 0.10\%$. The pronounced local maximum gas holdup value is not observed for all flows that exhibit the homogeneous, transitional, and heterogeneous flow regimes (e.g., $C = 0.40\%$ in Fig. 4.7). The fiber mass fraction at which the maximum value is observed varies among the fiber types and distributor plate open areas. After the local maximum is reached, gas holdup decreases to a local minimum value before it starts to increase again. Su and Heindel (2003) stated that the decrease in gas holdup with increasing superficial gas velocity beyond the local maximum gas holdup is a result of increased bubble coalescence; this causes a bubble size distribution and a wider range of bubble rise velocities. The heterogeneous flow regime begins as the gas holdup curve starts to increase linearly with increasing superficial gas velocity after reaching the local minimum value. The heterogeneous, or churn-turbulent, flow regime is characterized by highly turbulent flow.

When $C \geq 0.60\%$, the flow becomes pure heterogeneous (Ruzicka, 2001b); where heterogeneous flow is observed at all superficial gas velocities. As shown in Fig. 4.8 for $C = 1.00\%$, pure heterogeneous flow is observed for all fiber types. Superficial gas velocity does not have a significant effect on gas holdup in pure heterogeneous flow. Overall gas holdup

increases with increasing superficial gas velocity over the entire range of superficial gas velocities, but the increase is not nearly as dramatic as for flow that demonstrates the three different flow regimes. The specific fiber mass fraction that this flow pattern occurs will be discussed further in the following section.

The Zuber-Findlay drift flux model, as described in Section 3.3.2, is used to identify the superficial gas velocities that define the homogeneous, transitional, and heterogeneous flow regimes. Figure 3.5 shows an example of the drift flux plot for L = 3 mm Rayon fiber at C = 0.10% and C = 0.60%. For flows that demonstrate the three flow regimes, the Zuber-Findlay drift flux plot shows a slope change when the flow transitions from the homogeneous to the transitional regime and from the transitional regime to the heterogeneous flow regime. For flows that demonstrate the local maximum gas holdup, the drift flux plot displays an extra slope change in the transitional flow regime which corresponds to the superficial gas velocity at which the local maximum occurs, as shown in Figure 3.5 for C = 0.10%. The drift flux plot for pure heterogeneous flow displays a constant slope over the entire range of superficial gas velocities, as shown in Fig. 3.5 for C = 0.60%.

4.2.2 Effect of Fiber Mass Fraction

Fiber mass fraction has a significant influence on overall gas holdup as shown in Fig. 4.7 for a hardwood cellulose slurry. Similar results are obtained using other fiber types and distributor open areas as shown in Appendices C – E.

As the fiber mass fraction increases, a decrease in overall gas holdup is observed, which is typical for all fiber types used in this research. Reese et al. (1996) attributed this trend to a larger bubble size which is a result of an increased coalescence rate. The larger bubble size leads to an increase in the bubble rise velocity of the corresponding bubbles. As bubble rise velocity increases, bubble residence time decreases. A range of bubble rise velocities leads to an increase in bubble-bubble interactions, resulting in a further increase in bubble

coalescence. Bubble breakup rate is also reduced with increasing fiber mass fraction due to the suppression of the turbulent intensity (Su and Heindel, 2003). Fibers also tend to retard bubble ascension, which occurs because small bubbles become trapped in the fiber network and need to coalesce to gain the necessary buoyant force to break through the fiber network (Lindsay et al., 1995). The entrapment of small bubbles would actually increase gas holdup, but small bubbles are entrapped for such a small period of time since bubble coalescence and breakup dominate the flow hydrodynamics. Therefore the decrease in gas holdup with increasing fiber mass fraction is a result of increasing bubble coalescence and/or decreasing bubble breakup.

As the fiber mass fraction increases past a certain critical mass fraction, the homogeneous and transitional regimes are no longer observed, and the flow is heterogeneous for all superficial gas velocities. Ruzicka et al. (2001b) classified this typical flow pattern, with the absence of the homogeneous and transitional regimes, as pure heterogeneous flow. The critical mass fraction where pure heterogeneous flow is observed differs among the six fiber types. The flow becomes pure heterogeneous when $C \geq 0.60\%$ for L = 3 and 6 mm Rayon fibers, as well as the hardwood and BCTMP cellulose fibers. Pure heterogeneous flow occurs at $C \geq 0.40\%$ for the softwood cellulose fiber and at $C \geq 0.25\%$ for L = 12 mm Rayon fiber. Figure 4.8 shows the different overall gas holdup versus superficial gas velocity curves for C = 0.10% and 1.00% for all six fiber types.

The influence of fiber mass fraction on gas holdup is less significant at higher mass fractions, as shown in Fig. 4.9. At the highest mass fractions ($C \geq 1.20\%$), the gas holdup decrease is minimal with the increasing mass fraction. This is a result of fiber settling at the column base, thus creating a locally high fiber mass fraction near the bottom of the column. Therefore, the fiber mass fraction throughout the rest of the column may remain relatively similar between the higher fiber mass fractions. It is also noted that the highest overall gas holdup is recorded for an air-water system without any fiber added to the system.

Figure 4.10 shows the comparison of the effect of fiber mass fraction on Rayon fiber for the current study and a similar study conducted by Su and Heindel (2003) in a 15.2 cm ID bubble column with A = 0.57%. The results of these two studies are very similar and show that overall gas holdup decreases with increasing Rayon fiber length. Figure 4.10 also shows that Rayon fiber length has a greater influence on overall gas holdup at lower mass fractions for both studies. Figure 4.11 shows that the rate of gas holdup reduction is similar for $U_g \geq 5$ cm/s and the gas holdup is nearly constant for all mass fractions at $U_g = 1$ cm/s. It can also be noted that gas holdup is more sensitive to increasing fiber mass fraction for $U_g \geq 5$ cm/s at lower fiber mass fractions ($C \leq 0.80\%$).

Fiber mass fraction is observed to have a negligible effect on the superficial gas velocity at which transitional flow is first observed. Transitional flow is first observed at $U_g \approx 5$ cm/s for all Rayon fiber types, hardwood cellulose, and softwood cellulose fiber. Transitional flow for the BCTMP cellulose fiber is first observed at $U_g \approx 4.5$ cm/s. These transitions are determined using the Zuber-Findlay drift flux model as described earlier. This observance is contrary to the results shown by Su and Heindel (2003). They studied three different Rayon fiber lengths in a D = 15.2 cm ID semi-batch bubble column and determined that the superficial gas velocity at which transitional flow was first observed decreased slightly with increasing fiber mass fraction.

Fiber settling and channeling is also observed in the lower region of the column at high fiber mass fractions and low superficial gas velocities for all fiber types. An example of fiber settling and channeling in the lower column regions is shown in Fig. 4.12 for C = 1.80%, L = 6 mm Rayon fiber, and $U_g \approx 2$ cm/s. Typically channeling is observed when the fiber mass fraction is greater than $C \approx 0.80\%$. The amount of settled fiber and the degree of channel formation decreases as the superficial gas velocity increases and disappears once the superficial gas velocity is sufficiently large; this U_g value increases as the fiber mass fraction increases. Channel formation is also a result of fiber settling as the bubbles tend to find a

preferential path of least resistance to rise through the settled fiber. Fiber settling enhances bubble coalescence near the aeration plate as a bubble must gain a sufficient buoyancy force to break through the fiber network. Hence, when channeling is observed, relatively large bubbles exist in the slurry, even at low superficial gas velocities.

4.2.3 Effect of Fiber Type

When the three different flow regimes are observed, the duration of the transitional flow regime and the magnitude of the gas holdup in the heterogeneous flow regime is influence by the fiber type as shown in Fig. 4.8 for A = 0.49%. Appendix F contains similar plots for all distributor open areas. As noted earlier, the transitional flow regime begins at $U_g \approx 5$ cm/s for all fiber types except for BCTMP, which enters the transitional regime at $U_g \approx 4.5$ cm/s. At C = 0.10%, heterogeneous flow begins at $U_g \approx 15$ cm/s for Rayon fiber, $U_g \approx 14$ cm/s for BCTMP cellulose fiber, and $U_g \approx 11$ cm/s for softwood and hardwood cellulose fiber. The superficial gas velocity at which heterogeneous flow begins decreases slightly as the fiber mass fraction increases until the flow becomes pure heterogeneous. Figure 4.8 for C = 1.00% shows that the fiber type influences the magnitude of the overall gas holdup when the flow is pure heterogeneous.

In general, L = 3 mm Rayon fiber has the highest overall gas holdup; with overall gas holdup decreasing within increasing Rayon fiber length for all regimes of three regime flow and pure heterogeneous flow. For heterogeneous and pure heterogeneous flow regimes, BCTMP cellulose has the highest and softwood cellulose has the lowest overall gas holdup for cellulose fibers. Softwood cellulose fiber is expected to be the lowest since it is the longest of the cellulose fibers. BCTMP cellulose may be the highest for these flow conditions due to excessive amounts of foam being generated during operation which will create a higher overall gas holdup. Foam produced by BCTMP cellulose fiber is a result of lignosulfates remaining on the fibers from the fiber bleaching process (Tang and Heindel,

2005). Hardwood and softwood cellulose fibers generate little foam in comparison to BCTMP cellulose. Overall gas holdup for cellulose fibers is similar in the homogeneous regime. Some unexpected trends were observed in the transitional flow regime for cellulose fibers; where hardwood cellulose has the highest and BCTMP cellulose has the lowest overall gas holdup.

4.2.4 Effect of Distributor Open Area

The distributor plate open area has a significant influence on the overall gas holdup. Increasing the open area in an air-water system decreases the overall gas holdup in the transitional and heterogeneous flow regimes, as shown in Figure 4.13. This may be attributed to increased bubble coalescence due to decreased hole spacing with increased open area (Su and Heindel, 2005). Overall gas holdup is similar throughout the entire homogeneous flow regime for A = 0.49% and 0.95%. Gas holdup for A = 2.03% is similar to these plates in the homogeneous regime for $U_g \leq 3$ cm/s, at which the homogeneous regime destabilizes and lower overall gas holdup is observed. Figure 4.14 shows the effect of distributor plate open area on BCTMP cellulose fiber for C = 0.25% and 1.00%. For BCTMP cellulose fiber flows that demonstrate the three different flow regimes ($C \leq 0.40\%$), the effect of distributor plate open area is different for the different flow regimes. Overall gas holdup is highest for A = 0.95% and lowest for A = 2.03% in the homogeneous and transitional flow regime. Increasing open area results in decreasing overall gas holdup in the heterogeneous flow regime. For flows that are pure heterogeneous ($C \geq 0.60\%$), similar overall gas holdup results are observed for A = 0.49% and A = 0.95%, with lower overall gas holdup results for A = 2.03%. Similar trends are observed for hardwood and softwood cellulose, except that overall gas holdup results for pure heterogeneous flow are very similar for all three distributor plates.

Distributor plate effects with L = 3 mm Rayon display similar results to an air-water system for three regime flow ($C \leq 0.40\%$). For pure heterogeneous flow ($C \geq 0.60\%$), highest overall gas holdup results are shown for A = 0.95%, while the lowest overall gas holdup results are shown for A = 0.49%. The results observed for L = 3 mm Rayon are not expected and do not follow the trends of the other fibers. From the cellulose fiber results, increasing the open area results in higher overall gas holdup until the open area becomes too large (hole spacing becomes too small) and the bubbles interact with each other immediately after entering the column through the distributor plate (Su and Heindel, 2005).

Appendix G shows the effect of fiber mass fraction on the overall gas holdup for the range of superficial gas velocities for each distributor plate open area. From these graphs, it is determined that fiber mass fraction effect on overall gas holdup does not depend on distributor plate open area, except at low fiber mass fractions. For the base case, overall gas holdup is the highest for the air-water set without any fiber. But for the larger two plates, overall gas holdup for the air-water system is not the highest gas holdup. For A = 0.95%, overall gas holdup for C = 0.05% was higher than that of an air-water system for $U_g \geq 10$ cm/s. For A = 2.03%, overall gas holdup for $C \leq 0.25\%$ was higher than that of an air-water system for $U_g \geq 5$ cm/s. Further exploration is necessary to understand the causes of this phenomenon.

The local maximum gas holdup value within the transitional flow regime was observed in air-water flow and low fiber mass fractions for the smallest distributor plate open area (A = 0.49%). The larger plates (A = 0.95% and 2.03%) displayed three regime flow, but the local maximum gas holdup value was not observed. Gas holdup increases with increasing fiber mass fraction through the entire range of superficial gas velocities, although the influence of superficial gas velocity became less as the flow entered the transitional and heterogeneous regimes.

The critical fiber mass fraction at which the flow becomes pure heterogeneous is the same for each distributor plate open area, therefore distributor plate open area does not effect the value of the critical fiber mass fraction for which pure heterogeneous flow is observed. The distributor plate open area also does not affect the superficial gas velocity at which the transitional flow regime begins for each fiber type.

4.3 Local Gas Holdup Results

This section is divided into five subsections. The first subsection will discuss the definition of local gas holdup, the method for calculating local gas holdup, and the general local gas holdup trend. The remaining subsections will discuss the effects of superficial gas velocity, fiber mass fraction, fiber type, and distributor open area on local gas holdup, respectively. Once again, the effects of superficial gas velocity, fiber mass fraction, and fiber type will be discussed for the base case (A = 0.49%) and the effects of distributor plate open area subsection will discuss the deviations from the base case.

4.3.1 Definition and General Trends

Local gas holdup discussed in this thesis is merely local in comparison to the overall gas holdup. Local gas holdup is not a true local value, but is an average over a small axial distance. Local gas holdup is calculated over a smaller height difference instead of the difference between the top and bottom pressure transducers used to calculate overall gas holdup.

The local gas holdup in this study corresponding to the location of pressure transducer i is defined as the average of the gas holdup obtained using pressure transducers i and i + 1 and that of pressure transducers i – 1 and i. The local gas holdup is calculated using this method to dampen the axial fluctuations in gas holdup resulting from small changes in the pressure

difference. Therefore, local gas holdup values are determined at axial locations every 30.5 cm over the range $45 \leq H \leq 290$ cm, where H is the height from the column bottom.

The local gas holdup trends observed in this study were not expected. Therefore, four pressure transducers were switched around and all pressure transducers were recalibrated to be sure that the trends observed were an actual representation of the flow patterns within the column. Similar trends were observed before and after pressure transducer relocation and recalibration. Hence, the trends observed are an actual representation of the flow patterns within the bubble column.

The main observation of the local gas holdup is that it tends to have similar local maximum values at two different locations within the column. The first is located approximately 130 – 160 cm and the second is located approximately 260 – 290 cm from the bottom of the column. The axial gas holdup trends and location of the local maximum gas holdup values observed depend on fiber type, superficial gas velocity, and fiber mass fraction.

The observance of the local maximum gas holdup values at different axial locations suggests the existence of recirculation cells within the bubble column. Millies and Mewes (1995a, b) identified recirculation cells within GL bubble column flow to be on the order of one column diameter in size. Grevskott et al. (1996) observed two recirculation cells within two air-water-glass bead systems, with the bottom cell being on the order of one column diameter and the upper cell extending to the top of 0.14 m and 0.26 m diameter bubble columns with static heights of approximately 7 and 5 column diameters, respectively. These researchers also stated that the gas holdup was maximized in the center of the recirculation cell. Visual observation of the bubble column in the current study showed that the local gas holdup maximum actually occurred between two adjacent recirculation cells. The flow was observed to be downward along the column wall for the entire column height; therefore the slurry flow must be upward in the column center. The flow was also observed to be more

horizontal around the regions of the column corresponding to the locations of the local gas holdup maxima. The horizontal flow swirled about a fixed axial location such that it had an angular variation. Figure 4.15 is a schematic representation of the flow observation for a single instant in time at the location of one of the local maximum values. The horizontal flow follows the solid arrows at one instant in time and the dashed arrows are followed at another instant. Thus the flow rotates in a circular fashion at this particular axial location. The swirling movement likely retains small bubbles as it swirls, thus leading to the higher gas holdup in this region.

4.3.2 Effect of Superficial Gas Velocity

The recirculation cells are not present at low superficial gas velocities for flows in which the homogeneous, transitional, and heterogeneous flow regimes are all observed. The homogeneous flow regime is observed at low superficial gas velocities. Therefore, the bubbles are uniformly dispersed and rise nearly vertically, no back mixing occurs, and thus recirculation cells are suppressed. Local gas holdup tends to increase slightly with increasing height in the bubble column in the homogeneous regime. When the flow enters the transitional regime, the recirculation cells are more pronounced. As the superficial gas velocity increases in the transitional regime, the recirculation cells become stronger. The recirculation cells are well developed in the heterogeneous and pure heterogeneous flow regimes.

Figures 4.16 and 4.17 show the effects of superficial gas velocity on local gas holdup for L = 3 mm Rayon fiber at C = 0.10% and C = 1.00%, respectively. The local gas holdup maxima for flows that demonstrate the three different flow regimes become more pronounced with the onset of the transitional flow regime. The local gas holdup maxima are not well pronounced within the homogeneous regime since the bubbles are uniformly distributed, rise nearly vertical, and no back mixing occurs. As the superficial gas velocity

increases into the transitional flow regime at $U_g \approx 5$ cm/s, the locations of the local gas holdup maxima become evident at $H \approx 130$ cm and 260 cm in Fig. 4.16. Therefore, the size of the recirculation cell in Fig. 4.16 is $H_c \approx 130$ cm, or approximately four column diameters. Superficial gas velocity does not have any influence on the local gas holdup curve for flows that are pure heterogeneous, as shown in Fig. 4.17. The local gas holdup maxima are clearly identifiable and occur at the same locations for all superficial gas velocities. The local gas holdup maxima occur at $H \approx 160$ cm and 290 cm for the pure heterogeneous flow in Fig. 4.17, which corresponds to a recirculation cell size of $H_c \approx 130$ cm.

4.3.3 Effect of Fiber Mass Fraction

As shown in Fig. 4.18, the fiber mass fraction has a negligible effect on the local gas holdup trend, except at the critical fiber mass fraction when the flow becomes pure heterogeneous. The critical fiber mass fraction for each fiber type was described in Section 4.2.2. The locations of the local gas holdup maxima increase 30.5 cm, or one pressure transducer difference, when the flow becomes pure heterogeneous. Before and after this critical fiber mass fraction the fiber mass fraction has a negligible effect on the local gas holdup trend. The decrease in local gas holdup, at fixed axial locations, with increasing fiber mass fraction is analogous to the decrease in overall gas holdup with increasing fiber mass fraction. This decrease is due to an increased rate of bubble coalescence as fiber mass fraction increases.

4.3.4 Effect of Fiber Type

The influence of fiber type on the local gas holdup variation is found in Fig. 4.19. Small changes in the location of the local gas holdup maxima are observed. The location of the lower local maximum is consistent among fiber types, but the location of the upper local maximum is higher for Rayon fibers than cellulose fibers. This implies that the size of the

recirculation cells is slightly larger for Rayon fiber slurries. The differing upper local gas holdup maximum for Rayon and cellulose fiber may be due to the difference in length and fiber characteristics in this study. The Rayon fiber in this study is longer than the cellulose fiber, which may enhance the fiber dampening effect and thus create a longer recirculation cell. The different characteristics of the fibers may also have an effect on the size of the recirculation cells; such as the ability of the cellulose fiber to swell and form flocs.

4.3.5 Effect of Distributor Plate Open Area

Appendices H and I show the effect of superficial gas velocity on local gas holdup for L = 3 mm Rayon fiber at C = 0.10% and 1.00%, respectively. The same trends that are described in Section 4.3.2 are observed for all distributor plate open areas.

Appendix J shows the effect of fiber mass fraction on local gas holdup for BCTMP cellulose at all distributor plate open areas. From the figures in Appendix J it can be seen that the influence of the fiber mass fraction on local gas holdup does not depend on the distributor plate open area.

The trend that the size of the recirculation cells for Rayon fiber slurries is slightly larger than cellulose fiber slurries is consistent for all distributor plate open areas, as shown by Appendix K. Therefore, the effect of fiber type is consistent for all distributor plate open areas.

The locations of the local gas holdup maxima are increased by one column diameter between the A = 0.49% and A = 2.03% plates, as shown in Appendix K. The location of the lower local maximum was H $\approx$ 130 cm for A = 0.49%, where as H $\approx$ 160 cm for A = 2.03%. The location of the upper local maximum for cellulose fiber increase from H $\approx$ 230 cm to 260 cm between the smallest and largest open area plates. The upper local maximum increased from H $\approx$ 260 cm to 290 cm for the Rayon fiber. The sizes of the recirculation cells remain the same for all the distributor plates. The size of the recirculation cell for

Rayon fiber is $H_c \approx 130$ cm, or four column diameters, and the size for cellulose fibers is $H_c \approx 100$ cm, or three column diameters. This phenomenon can be attributed to increased bubble coalescence and higher bubble rise velocities due to the increased open area (Su and Heindel, 2005).

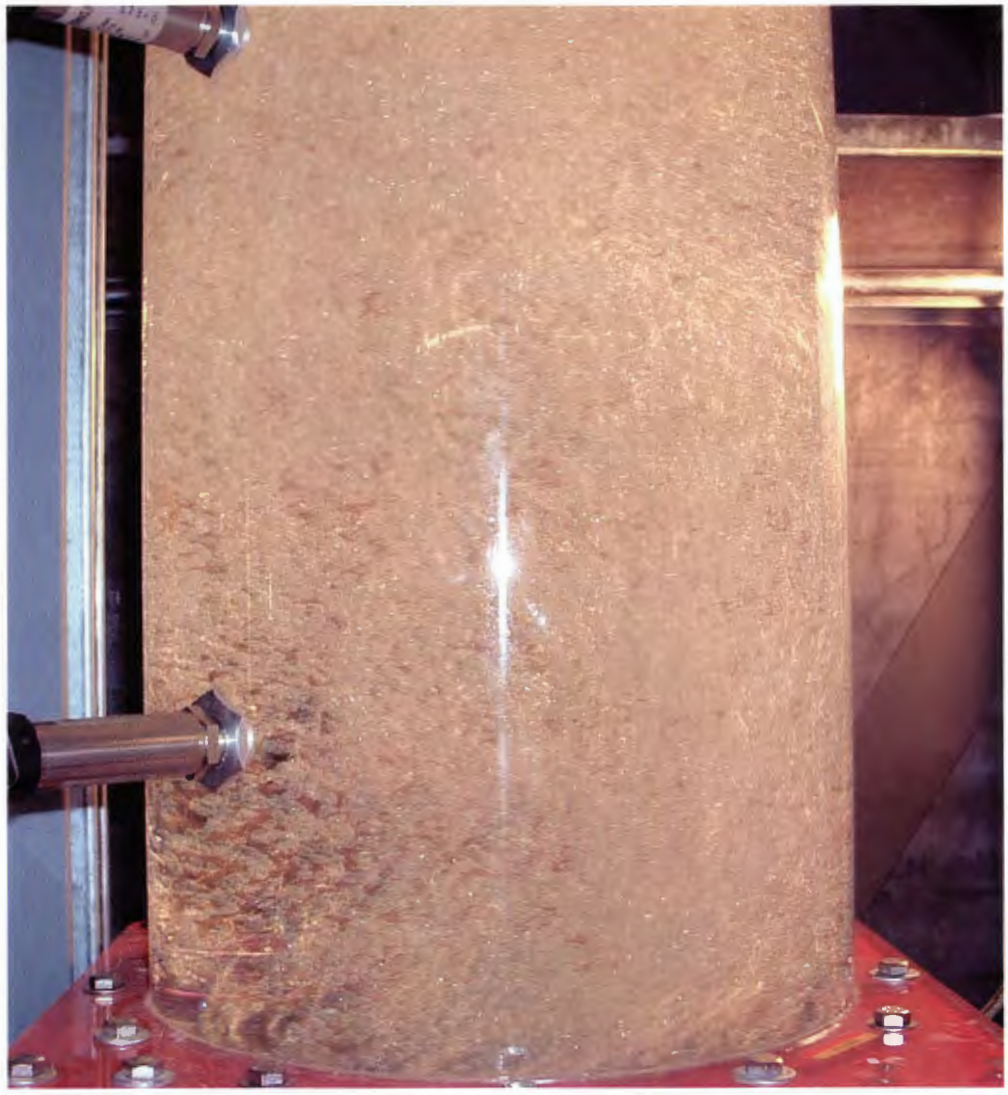

Figure 4.1: Air entering column through the A = 0.95% distributor plate at U_g = 2 cm/s in an air-water system.

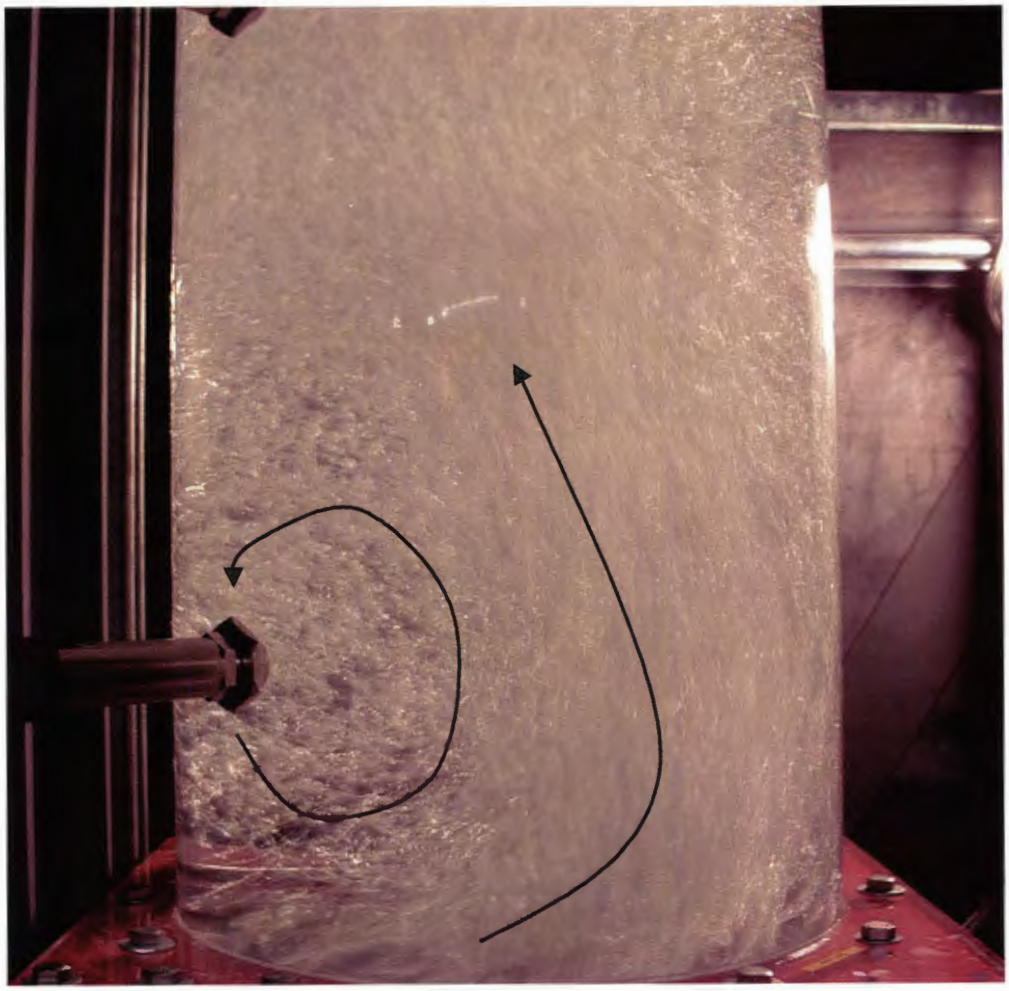

Figure 4.2: Air entering column through the A = 0.95% distributor plate at U_g = 2 cm/s in an air-water system without camera flash to show streaklines.

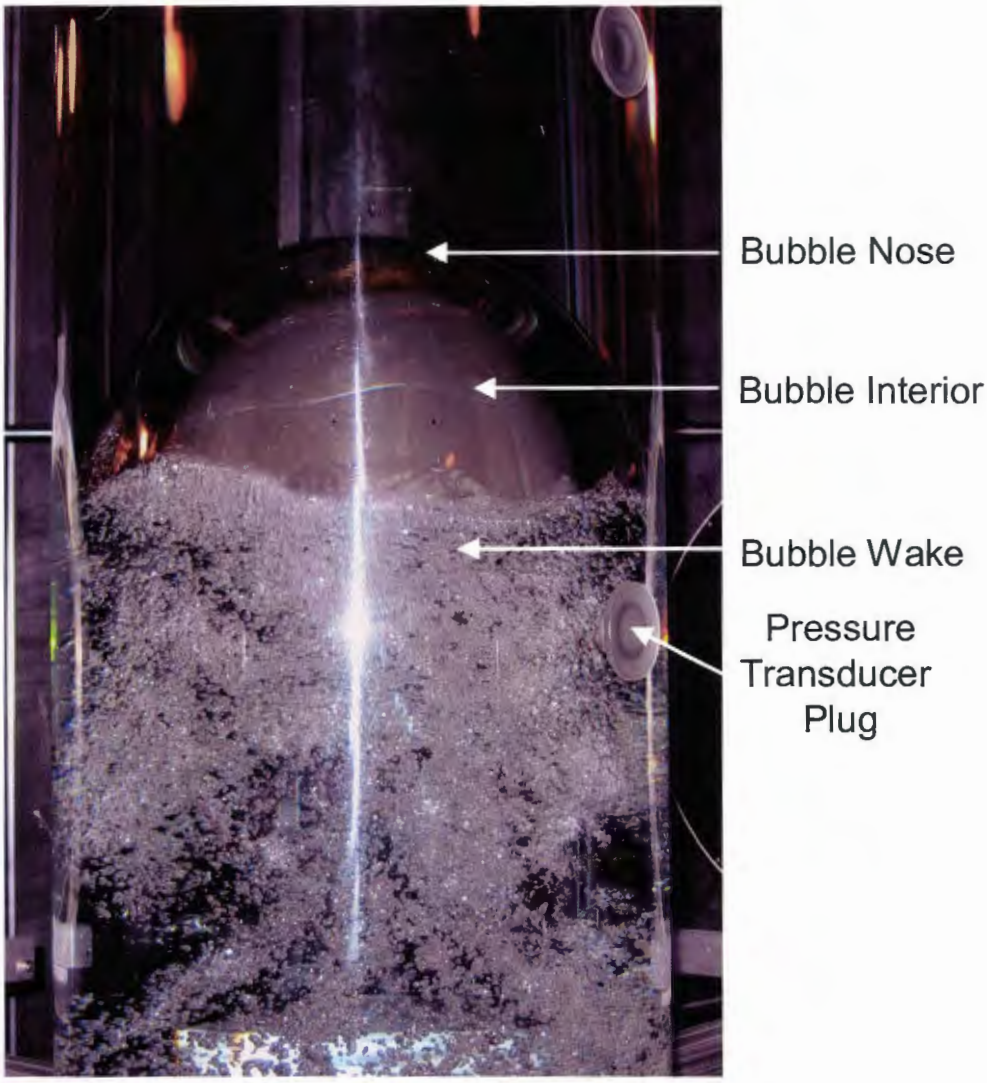

Figure 4.3: Simulated large bubble through an air-water system.

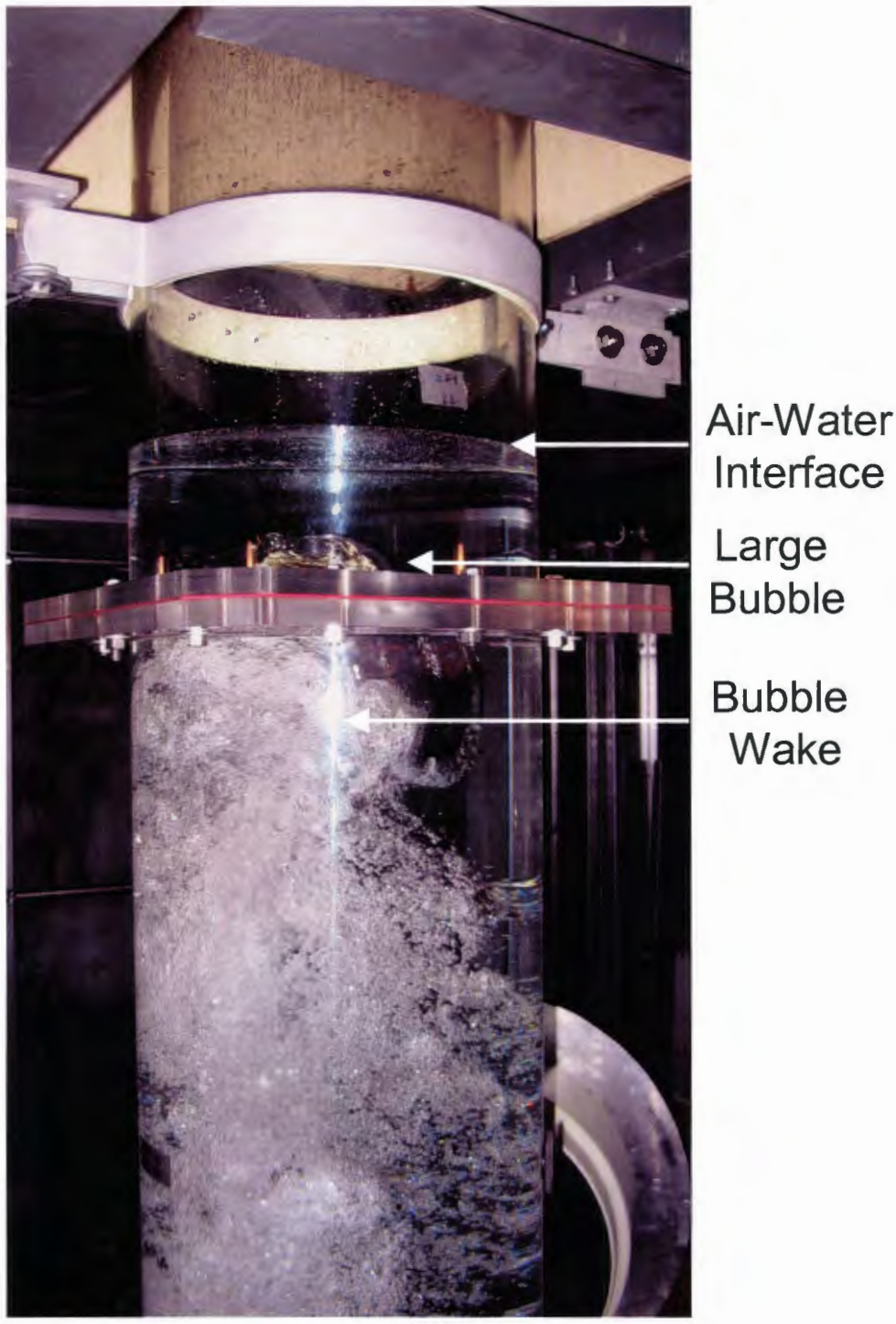

Figure 4.4: Picture of an air bubble just before it reaches the top of the water in the column.

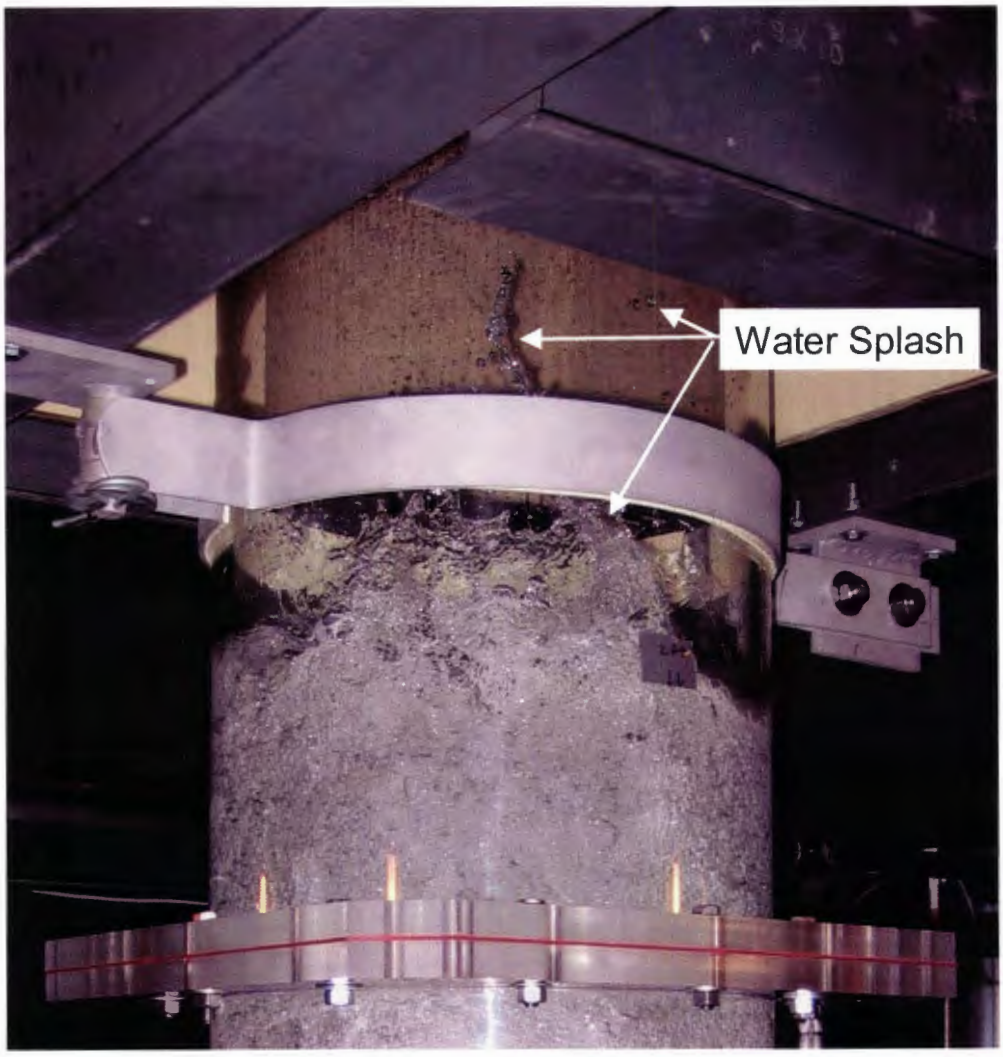

Figure 4.5: Picture of an air-bubble bursting at the top of the water in the bubble column.

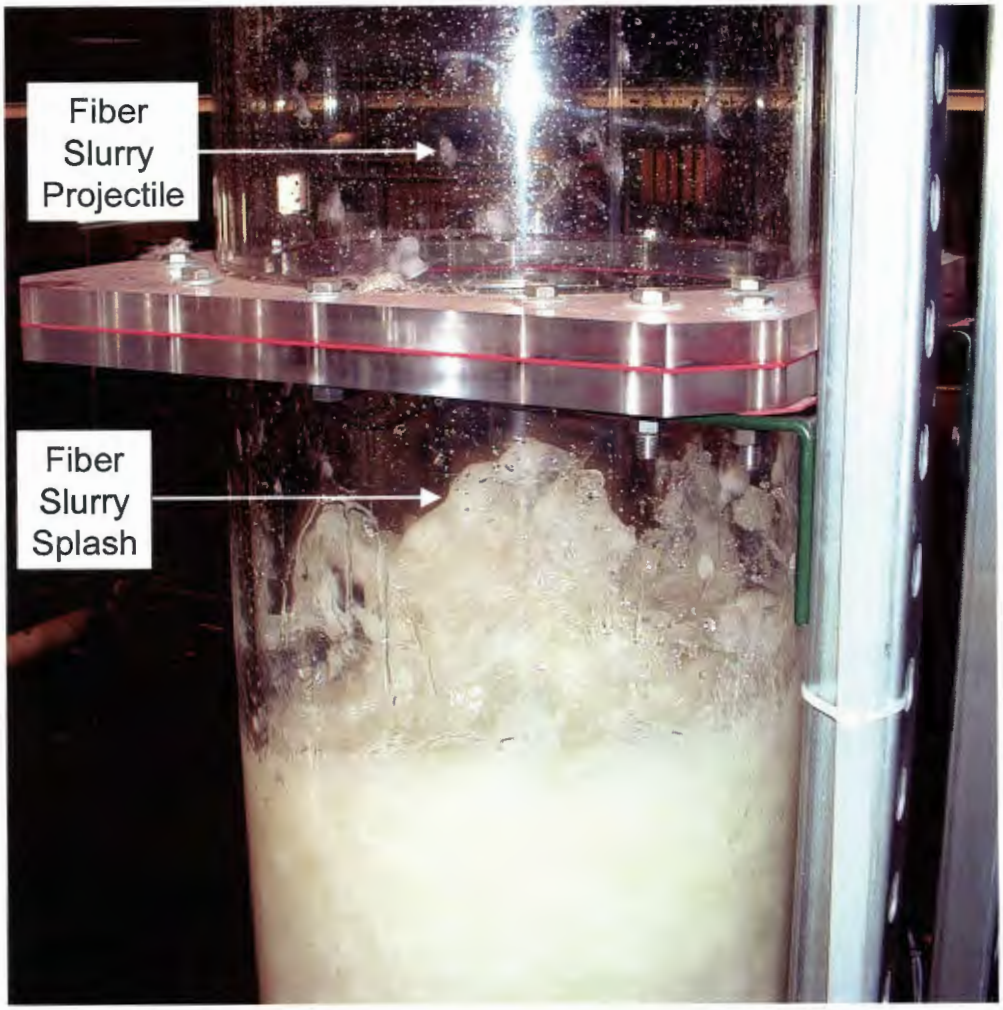

Figure 4.6: Picture of the top of a C = 1.80%, L = 6 mm Rayon fiber slurry operating at U_g ≈7 cm/s.

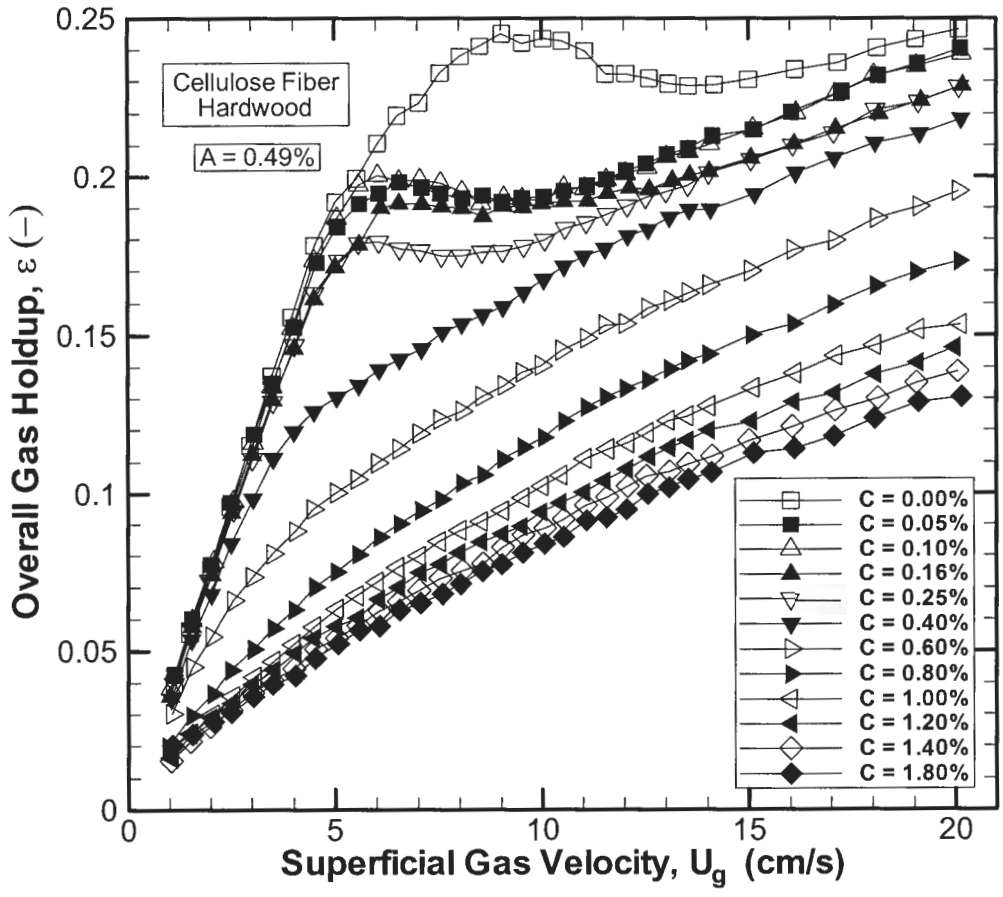

Figure 4.7: Effect of fiber mass fraction and superficial gas velocity on overall gas holdup for hardwood cellulose fiber at A = 0.49%.

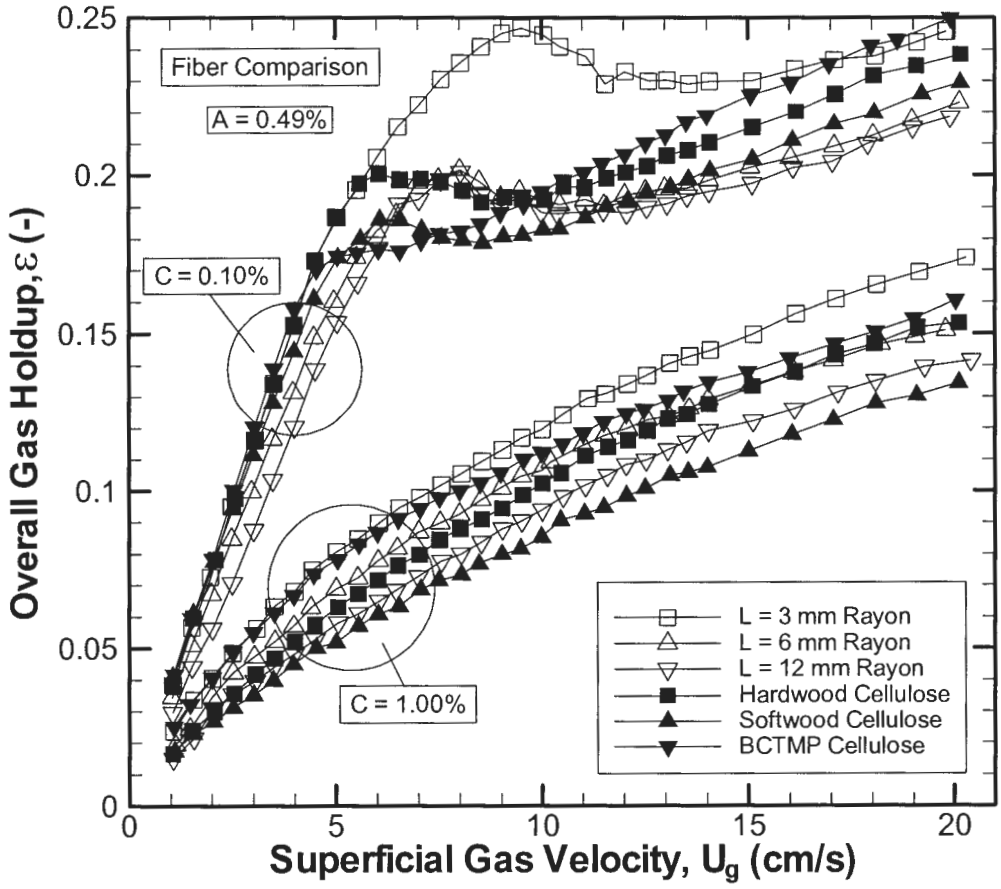

Figure 4.8: Effect of fiber type on overall gas holdup at C = 0.10% and C = 1.00% for A = 0.49%.

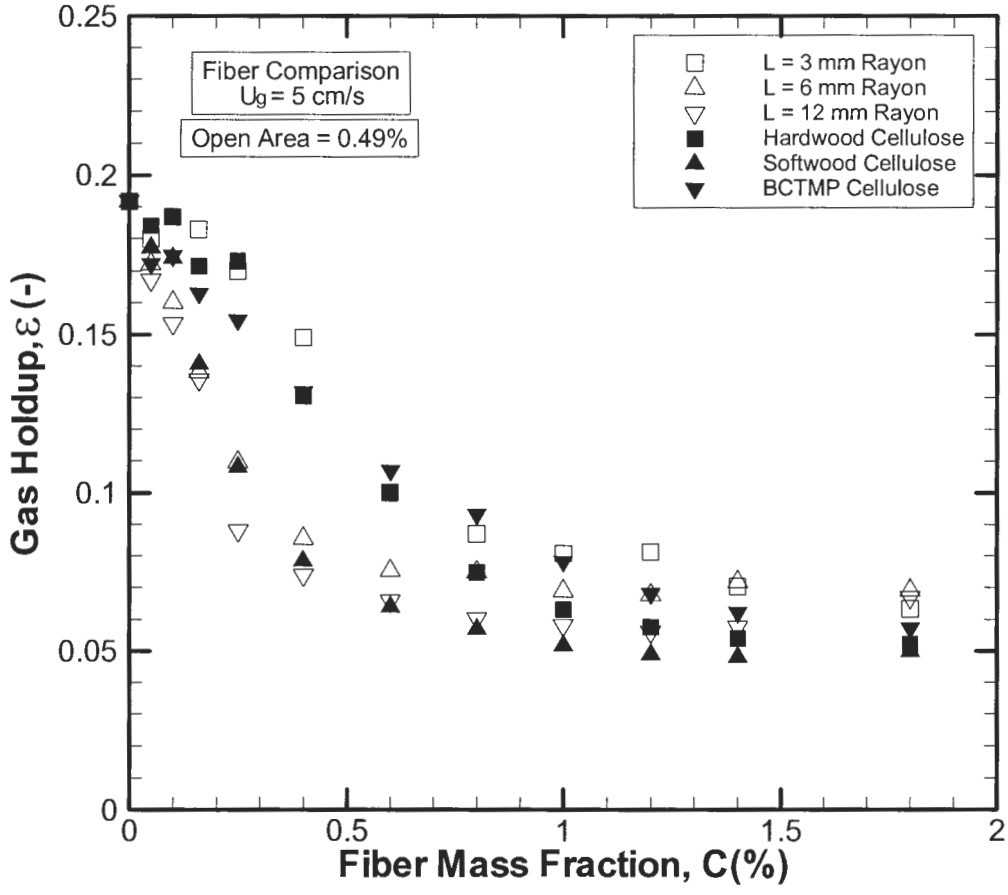

Figure 4.9: Gas holdup as a function of fiber mass fraction for all fiber types studied for A = 0.49% at U_g = 5 cm/s.

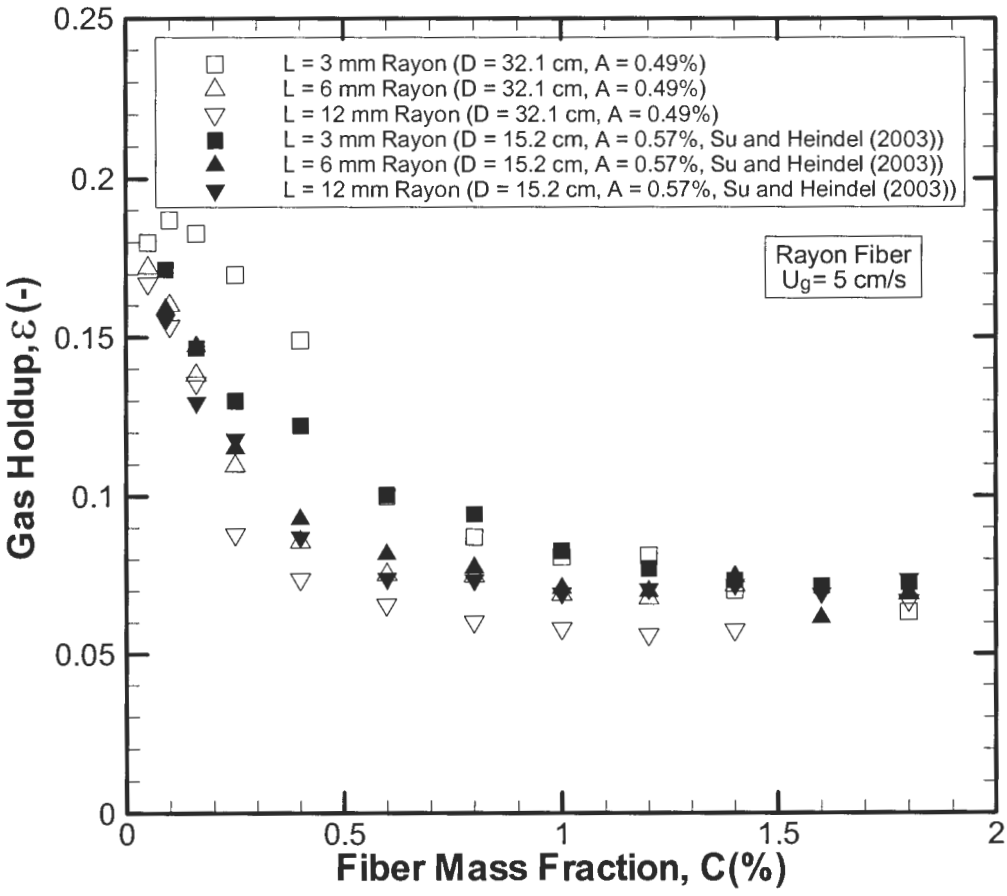

Figure 4.10: Comparison of the effect of fiber mass fraction on overall gas holdup for Rayon fiber to Su and Heindel (2003).

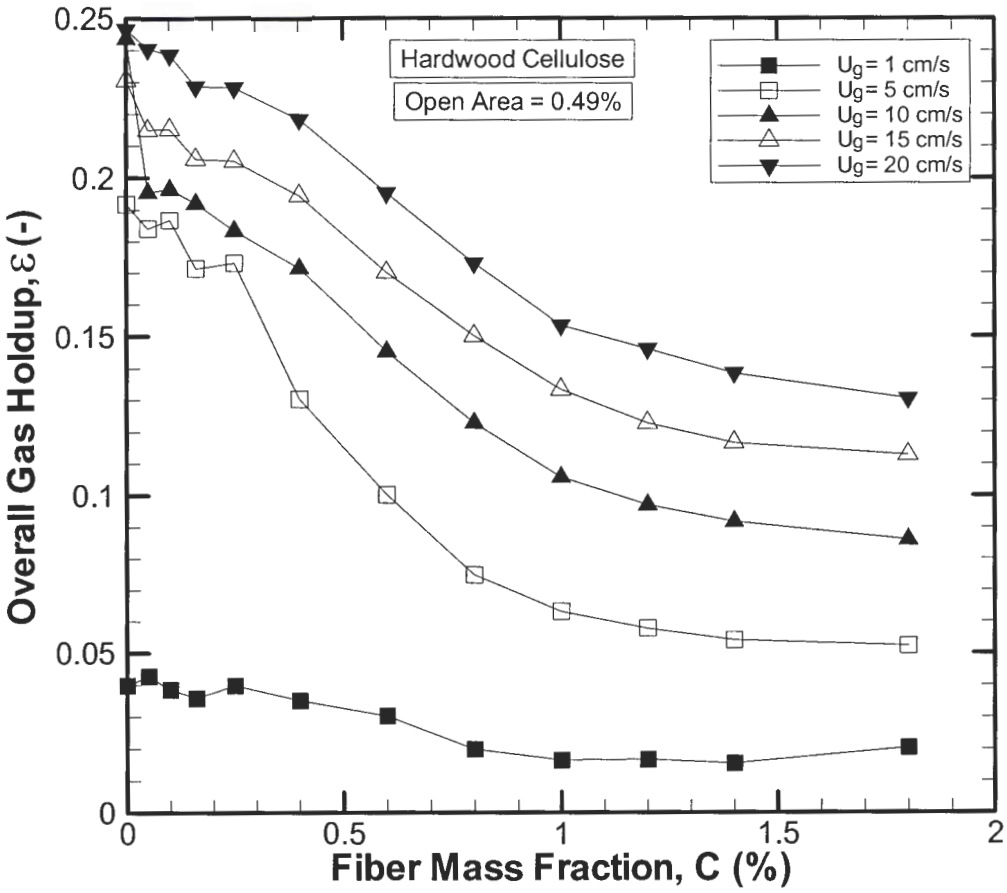

Figure 4.11: Gas holdup as a function of fiber mass fraction for hardwood cellulose for various superficial gas velocities at A = 0.49%.

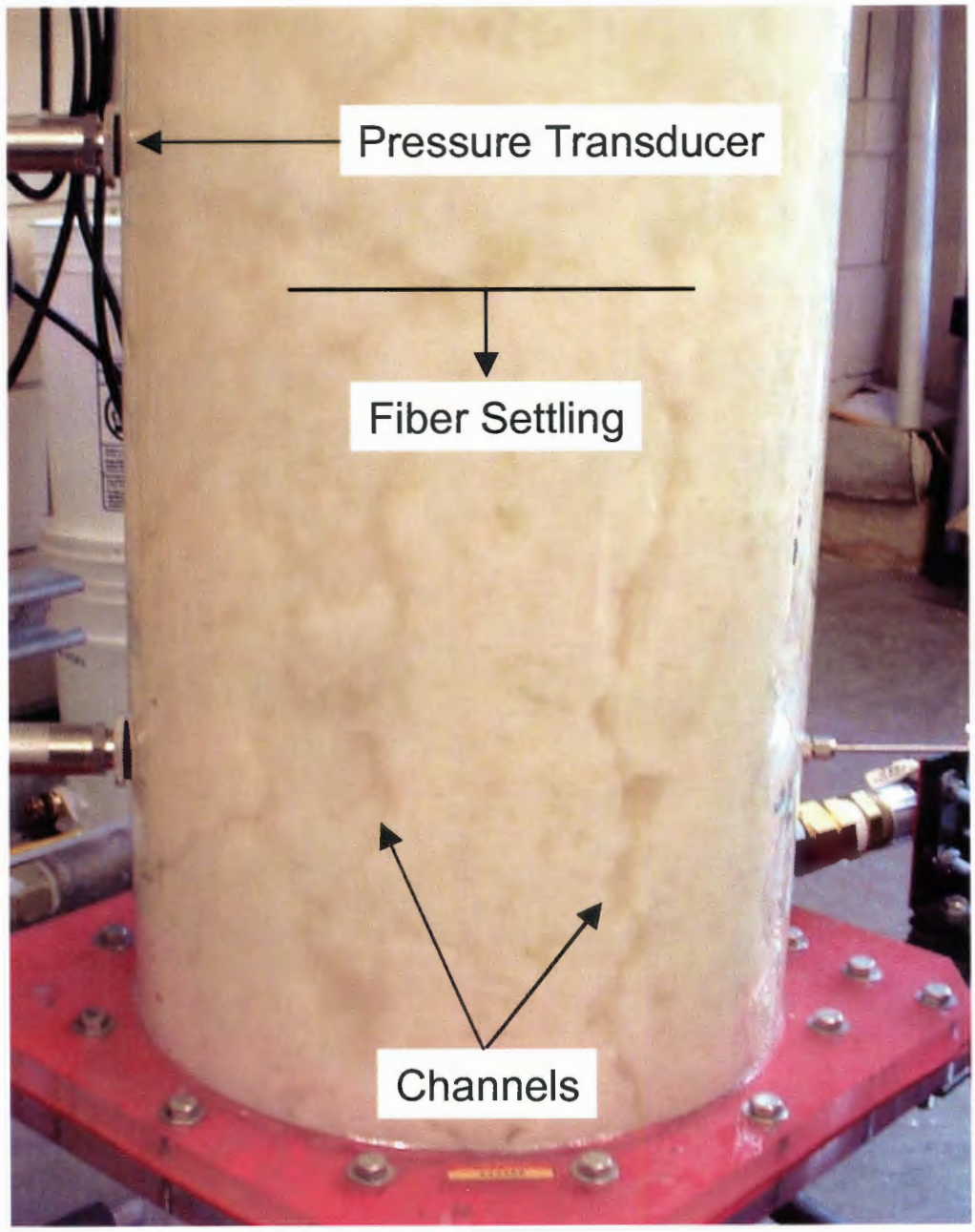

Figure 4.12: Fiber settling and channeling in a C = 1.80%, L = 6 mm Rayon fiber slurry operating at $U_g \approx 2$ cm/s.

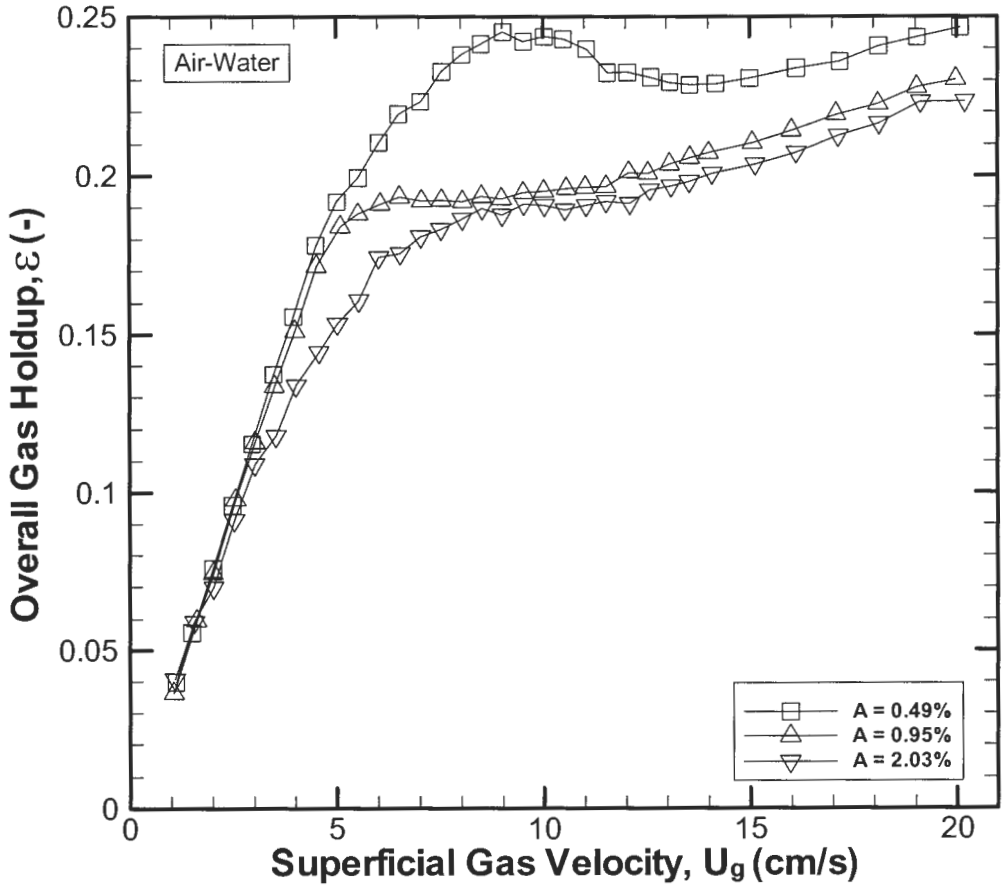

Figure 4.13: Effect of distributor plate open area on overall gas holdup for an air-water system.

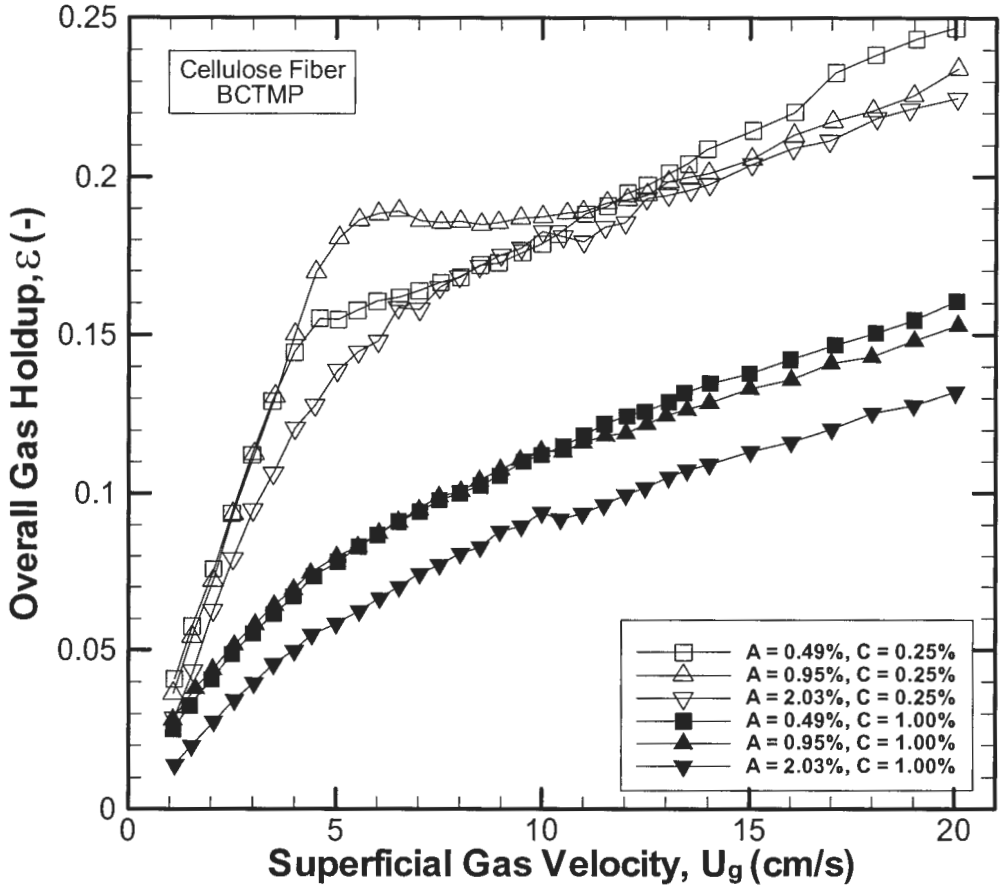

Figure 4.14: Effects of distributor plate open area on overall gas holdup for C = 0.25% and C = 1.00% BCTMP cellulose fiber.

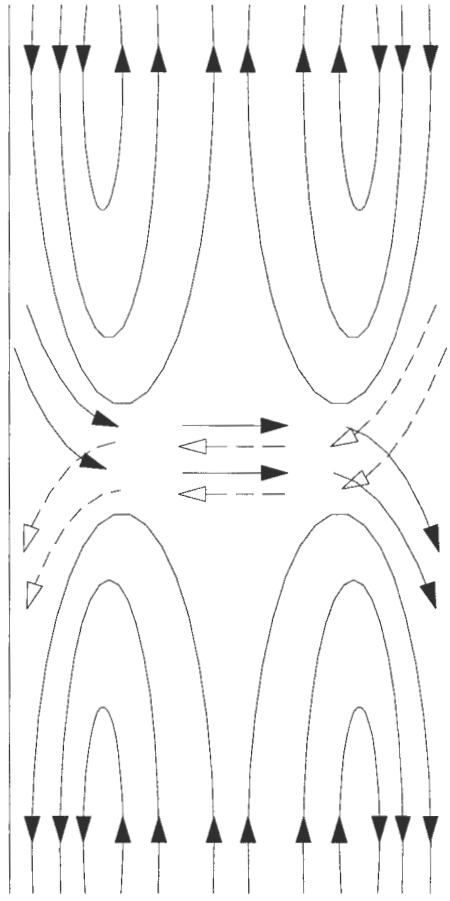

Figure 4.15: Schematic representation of column recirculation. At one instant in time the horizontal flow follows the solid arrows. At another instant, the dashed arrows are followed. Hence the horizontal flow rotates in a circular fashion at this axial location.

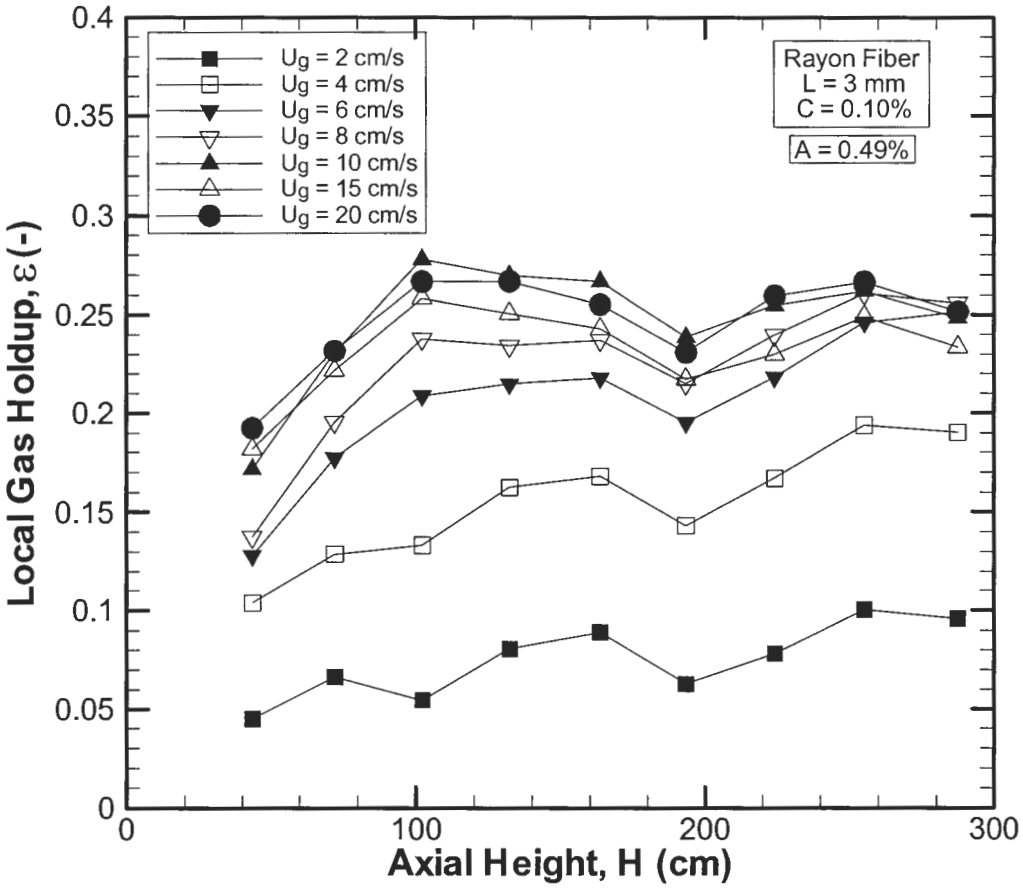

Figure 4.16: Effect of superficial gas velocity on L = 3 mm Rayon fiber for C = 0.10% and A = 0.49%.

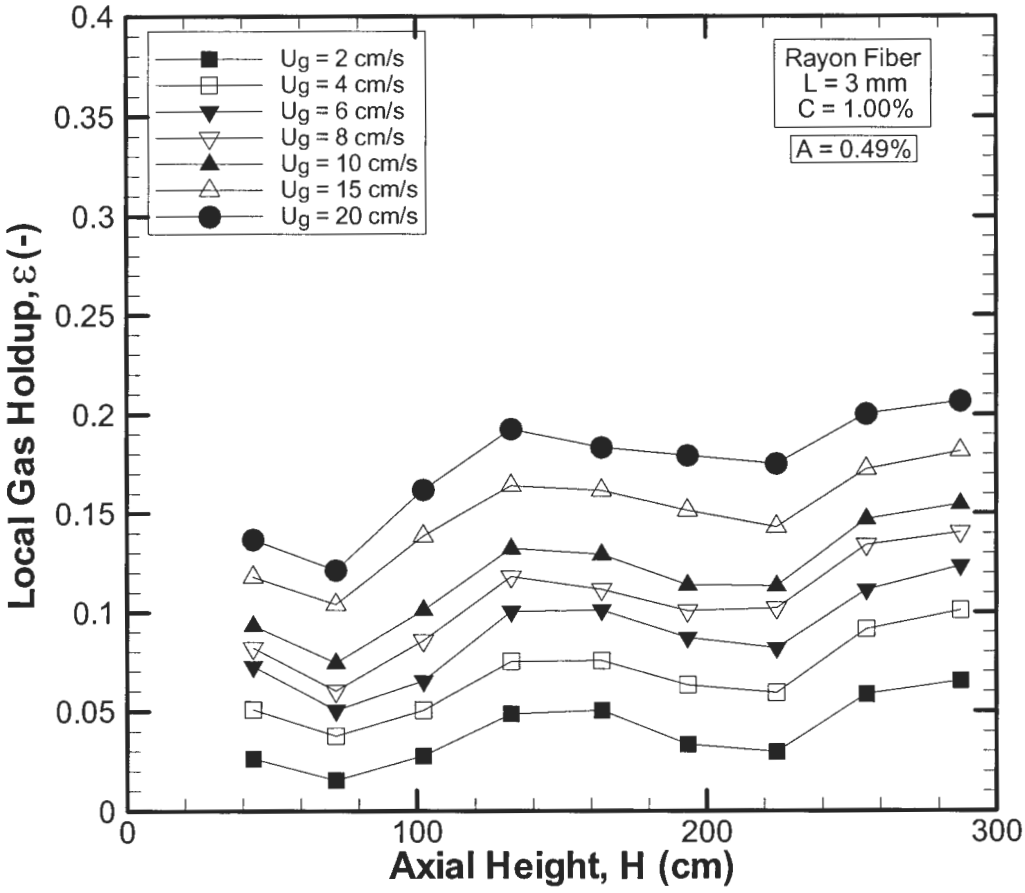

Figure 4.17: Effect of superficial gas velocity on local gas holdup for L = 3 mm Rayon fiber at C = 1.00% and A = 0.49%.

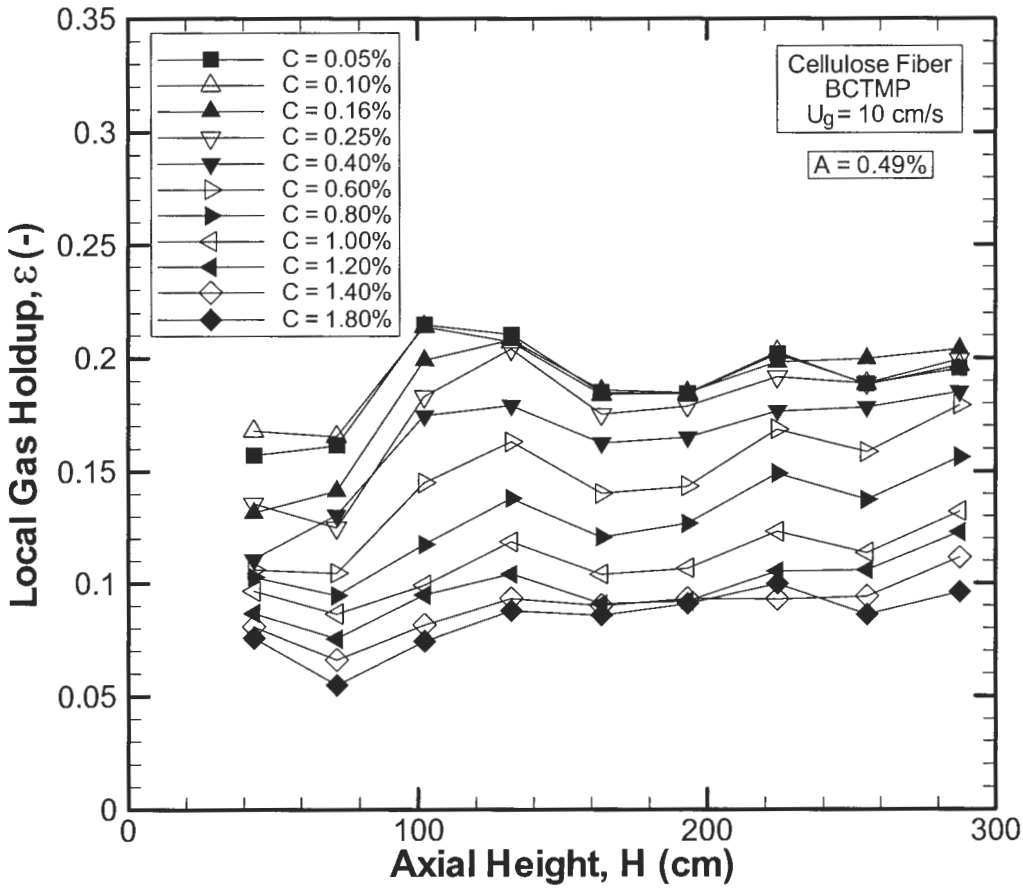

Figure 4.18: Effect of fiber mass fraction on local gas holdup for BCTMP cellulose fiber at U_g = 10 cm/s and A = 0.49%.

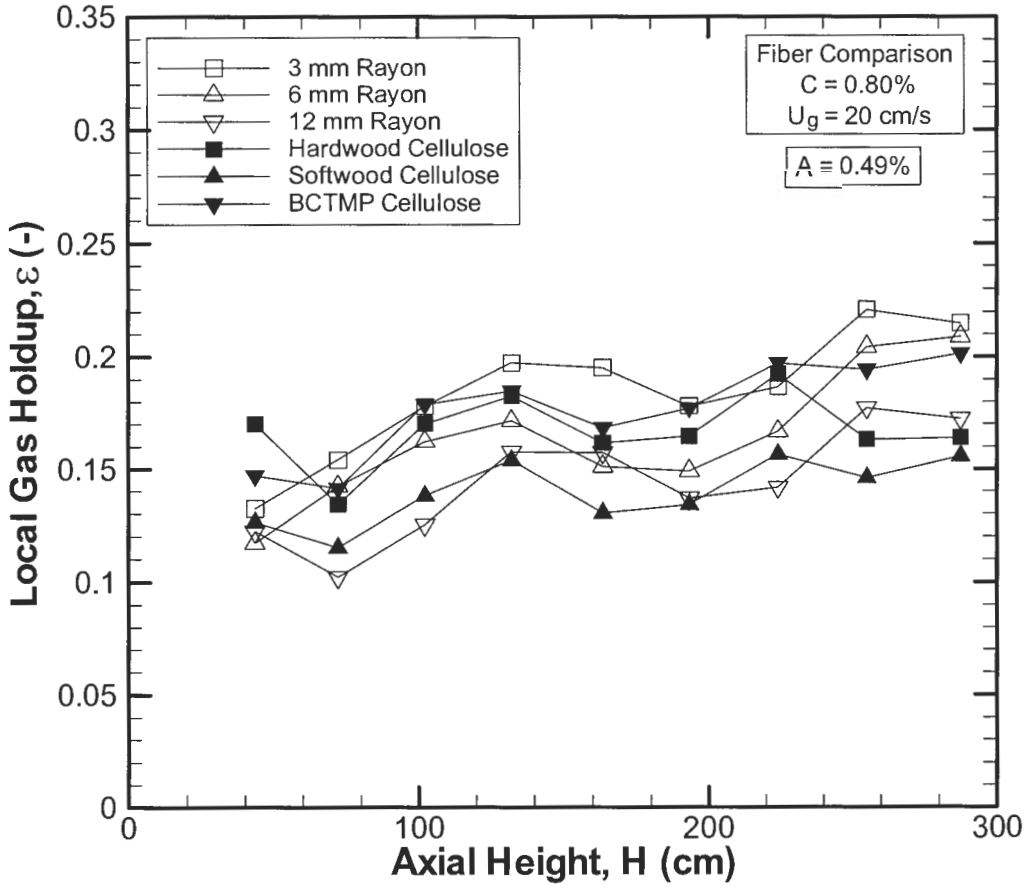

Figure 4.19: Effect of fiber type on local gas holdup for C = 0.80%, U_g = 20 cm/s, and A = 0.49%.

CHAPTER 5: CONCLUSIONS

5.1 Conclusions

The effects of fiber mass fraction, superficial gas velocity, fiber type, and distributor open area on overall and local gas holdup in a semi-batch 32 cm ID bubble column were researched. The effects of these four factors are summarized below:

- Fiber mass fraction had the most significant influence on overall and local gas holdup. An increase in the fiber mass fraction decreased the overall and local gas holdup. The influence of fiber mass fraction became less as the fiber mass fraction increased; this was very apparent when the flow became pure heterogeneous. For high fiber mass fractions ($C \geq 1.20\%$), the fiber mass fraction had a minimal effect on gas holdup. Fiber mass fraction did not influence the superficial gas velocity at which transitional flow began for flows that demonstrated the homogeneous, transitional, and heterogeneous flow regimes. There was a critical mass fraction for each fiber type at which the flow became pure heterogeneous for all superficial gas velocities. The local gas holdup maxima location increased by one column diameter when the flow changed to pure heterogeneous.
- Superficial gas velocity also had a significant influence on overall and local gas holdup. Increasing the superficial gas velocity for fiber mass fractions less than the critical mass fraction resulted in the flow changing from homogeneous to transitional to heterogeneous flow. The transitional regime began at $U_g \approx 5$ cm/s for all fiber types, but the superficial gas velocity range over which transitional flow was observed depended on fiber type. The superficial gas velocity at which heterogeneous flow began decreased slightly as the fiber mass fraction increased until the flow became pure heterogeneous. An increase in superficial gas velocity resulted in increased gas holdup for pure heterogeneous flow.

- Fiber type influenced the superficial gas velocity range over which transitional flow regime was observed, as well as the location of the upper local gas holdup maximum and the size of the recirculation cell. The range of superficial gas velocities that encompassed the transitional flow regime was smaller for cellulose fiber than Rayon fiber. The location of the upper local gas holdup maximum was higher for Rayon fiber than for cellulose fiber. Therefore, the recirculation cell size was larger in Rayon fiber slurries than cellulose fiber slurries.
- The distributor plate open area had some interesting influences on overall gas holdup. Increased open area resulted in higher gas holdup until the open area became too large (hole spacing became too small) and the bubbles interacted with each other immediately upon entering the column through the distributor plate. This caused a decrease in the overall gas holdup. The locations of the local gas holdup maxima increased by one column diameter between the smallest and largest open area plates.

5.2 Recommendations

The results obtained from this study should be compared to results obtained using similar semi-batch bubble columns in this laboratory. These columns have inner diameters of D = 10.2 cm and D = 15.2 cm. Therefore, the effect of column diameter on gas holdup can be determined.

Interesting local gas holdup trends have been observed in the 32.1 cm bubble column in this research. Since little research has been completed on bubble columns of this size, the results obtained should be validated by using another method. Hubers (2005) completed some initial studies on this 32.1 cm bubble column by using X-ray computed tomography. His research should be expanded to cover similar operating conditions used in this current study to completely verify the results using a noninvasive method.

Different liquids could also be used within the column for the liquid phase. Highly viscous liquids such as Tellus oil, paraffin oil, and glucose solutions have been used by other researchers (Urseanu et al., 2003; Krishna et al., 2000). The bubble column could also be operated as a GLS system by using various sizes of glass beads as the solid phase. The column could also be placed within a pressurized vessel to record gas holdup information while operating the bubble column at an elevated pressure. Urseama et al. (2003) stated that substantially higher overall gas holdup can be observed at increased operating pressures.

BIBLIOGRAPHY

Becker, S.; De Bie, H.; Sweeney, J. Dynamic Flow Behaviour in Bubble Columns. *Chemical Engineering Science*. **1999**, 54, 4929-4935.

Bennett, M.A.; West, R.M.; Luke, S.P.; Jia, X.; Williams, R.A. Measurement and Analysis of Flows in a Gas-Liquid Column Reactor. *Chemical Engineering Science*. **1999**, 54, 5003-5012.

Bennington, C.P.J.; Kerekes, R.J.; Grace, J.R. Mixing in Pulp Bleaching. *Journal of Pulp and Paper Science*. **1989**, 15(3), 186-195.

Buwa, V.V.; Ranade, V.V. Characterization of Dynamics of Gas-Liquid Flows in Rectangular Bubble Columns. *AIChE Journal*. **2004**, 50(10), 2394-2407.

Chen, R.C.; Reese, J.; Fan, L.-S. Flow Structure in a Three-Dimensional Bubble Column and Three-Phase Fluidized Bed. *AIChE Journal*. **1994**, 40(7), 1093-1104.

Dudukovic, M.P.; Larachi, F.; Mills, P.L. Multiphase Reactors – Revisited. *Chemical Engineering Science*. **1999**, 54, 1975-1995.

Gandhi, B.; Prakash, A.; Bergougnou, M.A. Hydrodynamic Behavior of Slurry Bubble Column at High Solids Concentrations. *Powder Technology*. **1999**, 103, 80-94.

Grevskott, S.; Sannaes, B.H.; Dudukovic, M.P.; Hjarbo, K.W.; Svendsen, H.F. Liquid Circulation, Bubble Size Distributions, and Solids Movement in Two- and Three-Phase Bubble Columns. *Chemical Engineering Science*. **1996**, 51(10), 1703-1713.

Heindel, T.J. A Review of Gas Flows in Fiber Suspensions. *Tappi Spring Technical Conference and Exhibit*. **2003**, 119-135.

Heindel, T.J. Gas Flow Regime Changes in a Bubble Column Filled with a Fiber Suspension. *Canadian Journal of Chemical Engineering*. **2000**, 78, 1017-1022.

Hol, P.D.; Heindel, T.J. Local Gas Holdup Variation in a Fiber Slurry. *Industrial and Engineering Chemistry Research*. **2005**, In Review.

Hubers, J.L. An X-ray Visualization Facility for Large-Scale Multiphase Flows. M.S. Thesis. **2005**. Iowa State University. Ames, Iowa.

Janse, P.; Gomez, C.O.; Finch, J.A. Effect of Pulp Fibers on Gas Holdup in a Flotation Column. *Canadian Journal of Chemical Engineering*. **1999**, 77, 22-25.

Jianping, W.; Shonglin, X. Local Hydrodynamics in a Gas-Liquid-Solid Three-Phase Bubble Column Reactor. *Chemical Engineering Journal*. **1998**, 70, 81-84.

Krishna, R.; Ellenberger, J.; Hennephof, D.E. Analogous Description of the Hydrodynamics of Gas-Solid Fluidized Beds and Bubble Columns. *Chemical Engineering Journal*. **1993**, 53, 89-101.

Krishna, R.; Urseanu, M.I.; de Swart, J.; Ellenberger, J. Gas Holdup in Bubble Columns: Operation with Concentrated Slurries Versus High Viscosity Liquid. *Canadian Journal of Chemical Engineering*. **2000**, 78(3), 442-448.

Lain, S.; Broder, D.; Sommerfeld, M. Experimental and Numerical Studies of the Hydrodynamics in a Bubble Column. *Chemical Engineering Science*. **1999**, 54, 4913-4920.

Lefebvre, S.; Guy, C. Characterization of Bubble Column Hydrodynamics with Local Measurements. *Chemical Engineering Science*. **1999**, 54, 4895-4902.

Lehr, F.; Millies, M.; Mewes, D. Bubble-Size Distributions and Flow Fields in Bubble Columns. *AIChE Journal*. **2002**, 48(11), 2426-2443.

Li, H.; Prakash, A. Heat Transfer and Hydrodynamics in a Three-Phase Slurry Bubble Column. *Industrial and Engineering Chemistry Research*. **1997**, 36, 4688-4694.

Lindsay, J.D.; Ghiaasiaan, S.M.; Abdel-Khalik, S.I. Macroscopic Flow Structures in a Bubbling Paper Pulp-Water Slurry. *Industrial and Engineering Chemistry Research*. **1995**, 34, 3342-3354.

Lubbert, A.; Paaschen, T.; Lapin, A. Fluid Dynamics in Bubble Column Bioreactors: Experiments and Numerical Simulations. *Biotechnology and Bioengineering*. **1996**, 52, 248-258.

Millies, M.; Mewes, D. Back-Mixing of the Continuous Phase in Bubble Columns. *Chemical Engineering Science*. **1995a**, 50(13), 2107-2115.

Millies, M.; Mewes, D. Calculation of Circulating Flows in Bubble Columns. *Chemical Engineering Science*. **1995b**, 50(13), 2093-2106.

Moustiri, S.; Hebrard, G.; Thakre, S.S.; Roustan, M. A Unified Correlation for Predicting Liquid Axial Dispersion Coefficient in Bubble Columns. *Chemical Engineering Science*. **2001**, 56, 1041-1047.

Olmos, E.; Gentric, C.; Poncin, S.; Midoux, N. Description of Flow Regime Transitions in Bubble Columns via Laser Doppler Anemometry Signals Processing. *Chemical Engineering Science*. **2003**, 58, 1731-1742.

Pelton, R.; Piette, R. Air Bubble Holdup in Quiescent Wood Pulp Suspensions. *Canadian Journal of Chemical Engineering*. **1992**, 70, 660-663.

Reese, J.; Jiang, P.; Fan, L.-S. Bubble Characteristics in Three-Phase Systems Used for Pulp and Paper Processing. *Chemical Engineering Science*. **1996**, 51, 2501-2510.

Reese, J.; Silva, E.M.; Yang, S.-T.; Fan, L.-S. Industrial Applications of Three-Phase Fluidization Systems. *Fluidization, Solids Handling, and Processing – Industrial Applications*, W.-C. Yang, Ed. Westwood, NJ, Noyes Publications. **1999**, 582-682.

Ruzicka, M.C.; Zahradnik, J.; Drahos, J.; Thomas, N.H. Effect of Bubble Column Dimensions on Flow Regime Transition. *Chemical Engineering Science*. **2001a**, 56, 4609-4626.

Ruzicka, M.C.; Zahradnik, J.; Drahos, J.; Thomas, N.H. Homogeneous-Heterogeneous Regime Transition in Bubble Columns. *Chemical Engineering Science*. **2001b**, 56, 4609-4626.

Sarrafi, A.; Jamialahmadi, M.; Muller-Steinhagen, H.; Smith, J.M. Gas Holdup in Homogeneous and Heterogeneous Gas-Liquid Bubble Column Reactors. *Canadian Journal of Chemical Engineering*. **1999**, 77, 11-21.

Schulz, T.H.; Heindel, T.J. A Study of Gas Holdup in a Cocurrent Air/Water/Fiber System. *TAPPI Journal*. **2000**, 83(6), 58.

Schweitzer, J.-M.; Bayle, J.; Gauthier, T. Local Gas Hold-Up Measurements in Fluidized Bed and Slurry Bubble Column. *Chemical Engineering Science*. **2001**, 56, 1103-1110.

Seifert, P. Recent Innovations in Paper Recycling. *Tappi Journal*. **1994**, 77(2), 149-152.

Shah, Y.T.; Kelkar, B.G.; Godbole, S.P.; Deckwer, W.-D. Design Parameters Estimations for Bubble Column Reactors. *AIChE Journal*. **1982**, 28(3), 353-379.

Su, X.; Heindel, T.J. Effect of Perforated Plate Open Area on Gas Holdup in Rayon Fiber Suspensions. *Journal of Fluids Engineering*. **2005**, Accepted for Publication.

Su, X.; Heindel, T.J. Gas Holdup Behavior in Nylon Fiber Suspensions. *Industrial and Engineering Chemistry Research*. **2004**, 43, 2256-2263.

Su, X.; Heindel, T.J. Gas Holdup in a Fiber Suspension. *Canadian Journal of Chemical Engineering*. **2003**, 81, 412-418.

Sundaresan, S. Modeling the Hydrodynamics of Multiphase Flow Reactors: Current Status and Challenges. *AIChE Journal*. **2000**, 46(6), 1102-1105.

Tang, C.; Heindel, T.J. Effect of Fiber Type on Gas Holdup in a Cocurrent Air-Water-Fiber Bubble Column. *Chemical Engineering Journal*. **2005**, In Review.

Tsuchiya, K; Nakanishi, O. Gas Holdup Behavior in a Tall Bubble Column with Perforated Plate Distributors. *Chemical Engineering Science*. **1992**, 47, 3347-3354.

Urseanu, M.I.; Guit, R.P.M.; Stankiewicz, A.; van Kranenburg, G.; Lommen, J.H.G.M. Influence of Operating Pressure on the Gas Holdup in Bubble Columns for High Viscous Media. *Chemical Engineering Science*. **2003**, 58, 697-704.

Walmsley, M.R.W. Air Bubble Motion in Wood Pulp Fiber Suspension. *Appita Proceedings*. **1992**, 509-515.

Walter, J.F.; Blanch, H.W. Liquid Circulation Patterns and Their Effect on Gas Holdup and Axial Mixing in Bubble Columns. *Chemical Engineering Communications*. **1983**, 19, 243-262.

Warsito; Ohkawa, M.; Maezawa, A.; Uchida, S. Flow Structure and Phase Distributions in a Slurry Bubble Column. *Chemical Engineering Science*. **1997**, 53, 3941-3947.

Went, J.; Jamailahmadi, M.; Muller-Steinhagen, H. Effect of Wood Pulp Fiber Concentration on Gas Hold-up in Bubble Columns. *Chemie-Ingenieur-Technik*. **1993**, 65(3), 306-308.

Xie, T.; Ghiaasiaan, S.M.; Karrila, S.; McDonough, T. Flow Regimes and Gas Holdup in Paper Pulp-Water-Gas Three-Phase Slurry Flow. *Chemical Engineering Science*. **2003**, 58, 1417-1430.

Zahradnik, J.; Fialova, M. The Effect of Bubbling Regime on Gas and Liquid Phase Mixing in Bubble Column Reactors. *Chemical Engineering Science*. **1996**, 51(10), 2491-2500.

Zahradnik, J.; Fialova, M.; Ruzicka, M.; Drahos, J.; Kastanek, F.; Thomas, D.H. Duality of the Gas-Liquid Flow Regimes in Bubble Column Reactors. *Chemical Engineering Science*. **1997**, 52, 3811-3826.

Zuber, N.; Findlay, J.A. Average Volumetric Concentration in Two-Phase Flow Systems. *ASME Journal of Heat Transfer*. **1965**, 87, 453-468.

Appendix A: Fiber Mass Fraction Equation Derivation

The following appendix shows the derivation of the fiber mass fraction equation that is used to find the appropriate dry fiber mass used in this study. The dry fiber mass is determined by the volume of liquid and fiber in the column such that

$$V_c = V_l + V_f \tag{A.1}$$

where the column volume (V_c), liquid volume (V_l), and fiber volume (V_f) are given by

$$V_c = \frac{\pi}{4} D^2 H \tag{A.2}$$

$$V_l = \frac{m_l}{\rho_l} \tag{A.3}$$

$$V_f = \frac{m_f}{\rho_f} \tag{A.4}$$

where D is the column diameter and H is the initial unaerated slurry height in the column, which is ten column diameters (10D). Substituting Equations (A.2) – (A.4) into Equation (A.1) and rearranging yields

$$V_c \rho_f = m_f + m_l \frac{\rho_f}{\rho_l} \tag{A.5}$$

The fiber mass fraction, C, is given by the ratio of the dry fiber mass to the total mass of the liquid and fiber such that

$$C = \frac{m_f}{m_l + m_f} \tag{A.6}$$

Rearranging Equation (A.6), the mass of the liquid can be written in terms of the fiber mass fraction and the dry fiber mass such that

$$m_l = \frac{1-C}{C} m_f \tag{A.7}$$

Substituting Equations (A.7) into (A.5) yields

$$V_c \rho_f = m_f \left[1 + \left(\frac{1-C}{C} \right) \frac{\rho_f}{\rho_l} \right] \tag{A.8}$$

Rearranging and solving for the dry fiber mass results in the final equation

$$m_f = \frac{V_c \rho_l \rho_f C}{\rho_f + C(\rho_l - \rho_f)} \tag{A.9}$$

Appendix B: Gas Holdup Equation Derivation

This appendix contains the derivation of the gas holdup equation used to determine overall and local gas holdup in this study. The equation is based on the hydrostatic pressure difference between the pressure transducers being evaluated. For a gas-liquid-fiber system in which the liquid flow rate is assumed to be small, the static pressure difference is given by

$$\Delta P = \rho_{eff} g \Delta h \tag{B.1}$$

where the effective density, ρ_{eff}, is given by

$$\rho_{eff} = \rho_g \varepsilon_g + \rho_l \varepsilon_l + \rho_f \varepsilon_f \tag{B.2}$$

The respective volumetric phase holdups, ϵ_i, and densities, ρ_i, are from the gas, liquid, and fiber phases. The distance between the pressure transducer readings is denoted by Δh. The volumetric phase holdups must also satisfy

$$\varepsilon_g + \varepsilon_l + \varepsilon_f = 1 \tag{B.3}$$

The liquid and fiber volumetric phase holdups can be written by using the respective liquid, Φ_l, and fiber, Φ_f, volume fractions within a liquid-fiber slurry such that

$$\varepsilon_l = \Phi_l(\varepsilon_l + \varepsilon_f) = \Phi_l(1 - \varepsilon_g) \tag{B.4}$$

$$\varepsilon_f = \Phi_f(\varepsilon_l + \varepsilon_f) = \Phi_f(1 - \varepsilon_g) \tag{B.5}$$

Since the density of the gas phase is much less than the densities of the liquid and fiber phases, the density of the gas phase gas be neglected. Along with this assumption, and combining Equations (B.2), (B.4), and (B.5) into Equation (B.1) yields

$$\Delta P = \left[\rho_l \Phi_l (1 - \varepsilon_g) + \rho_f \Phi_f (1 - \varepsilon_g)\right] g \Delta h \tag{B.6}$$

Simplifying and rearranging the above equation yields the final gas holdup equation that is used for the analysis in this study

$$\varepsilon = \varepsilon_g = 1 - \frac{\Delta P}{\left[\rho_l + \Phi_f (\rho_f - \rho_l)\right] g \Delta h} \tag{B.7}$$

Appendix C: Overall Gas Holdup for All Fibers at A = 0.49%

The information presented in this appendix displays the overall gas holdup as a function of superficial gas velocity for all fiber types and lengths that were studied for the distributor open area of A = 0.49%.

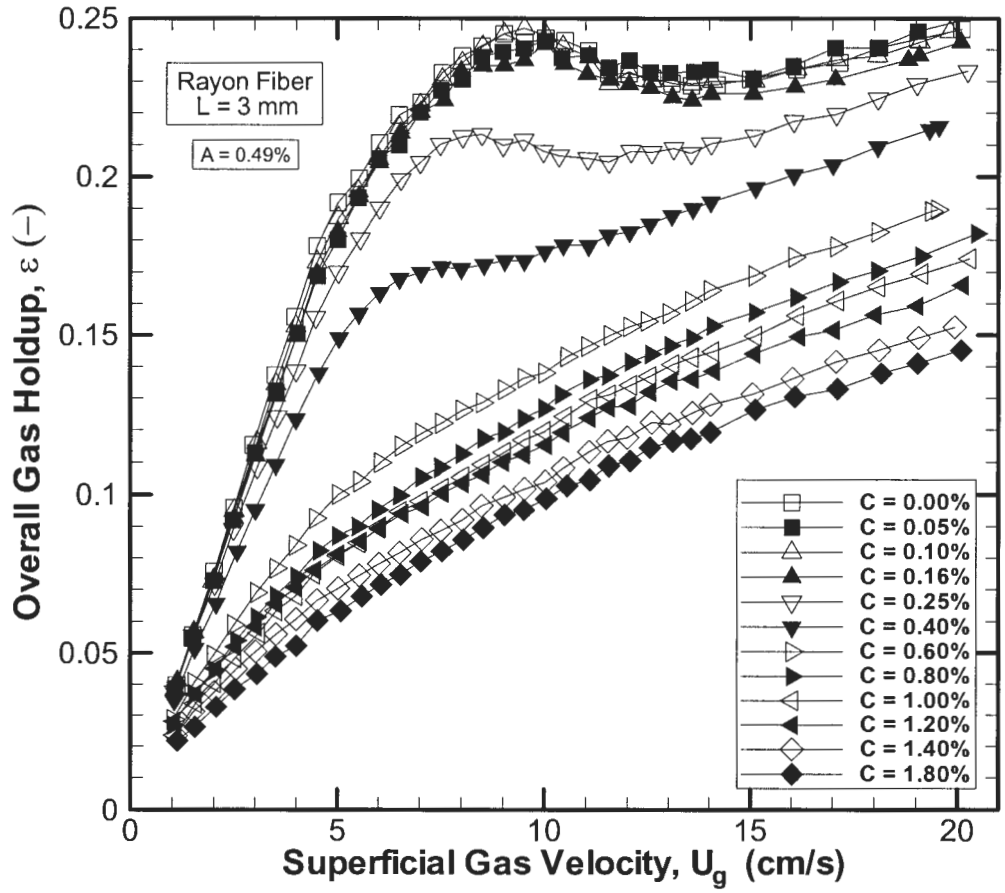

Figure C.1: Overall gas holdup versus superficial gas velocity for all fiber mass fractions for L = 3 mm Rayon fiber with A = 0.49%.

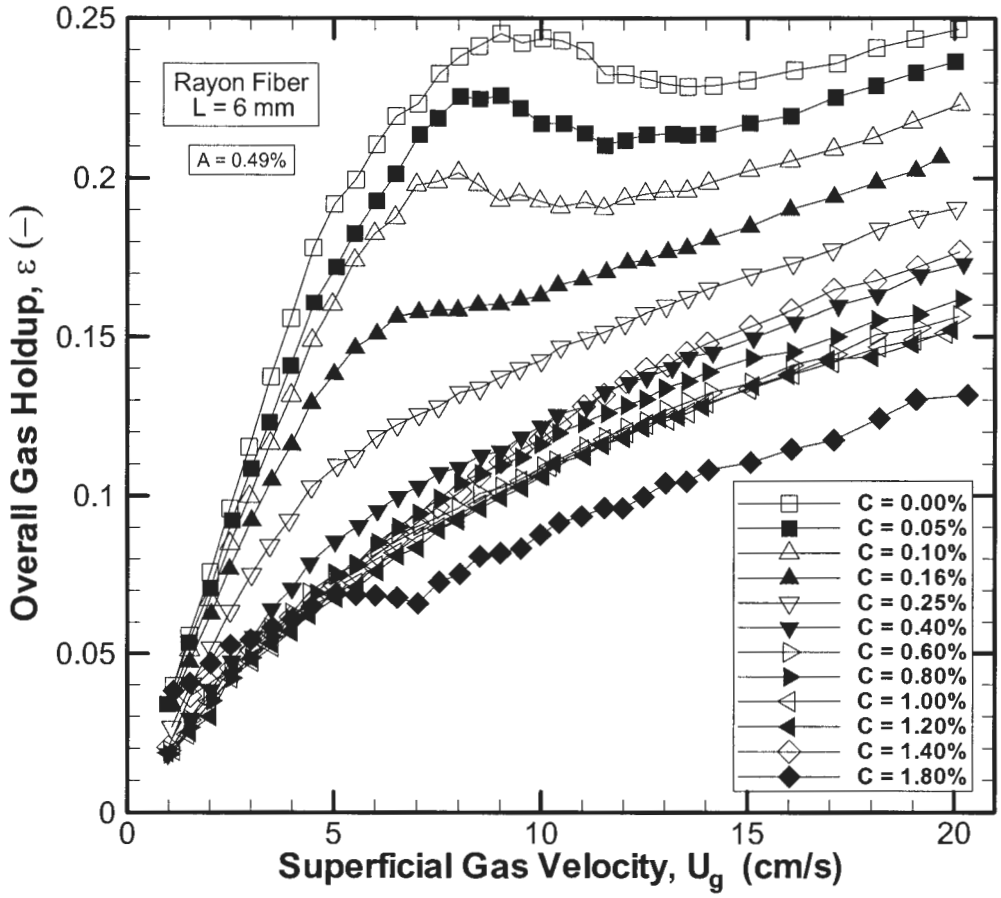

Figure C.2: Overall gas holdup versus superficial gas velocity for all fiber mass fractions for L = 6 mm Rayon fiber with A = 0.49%.

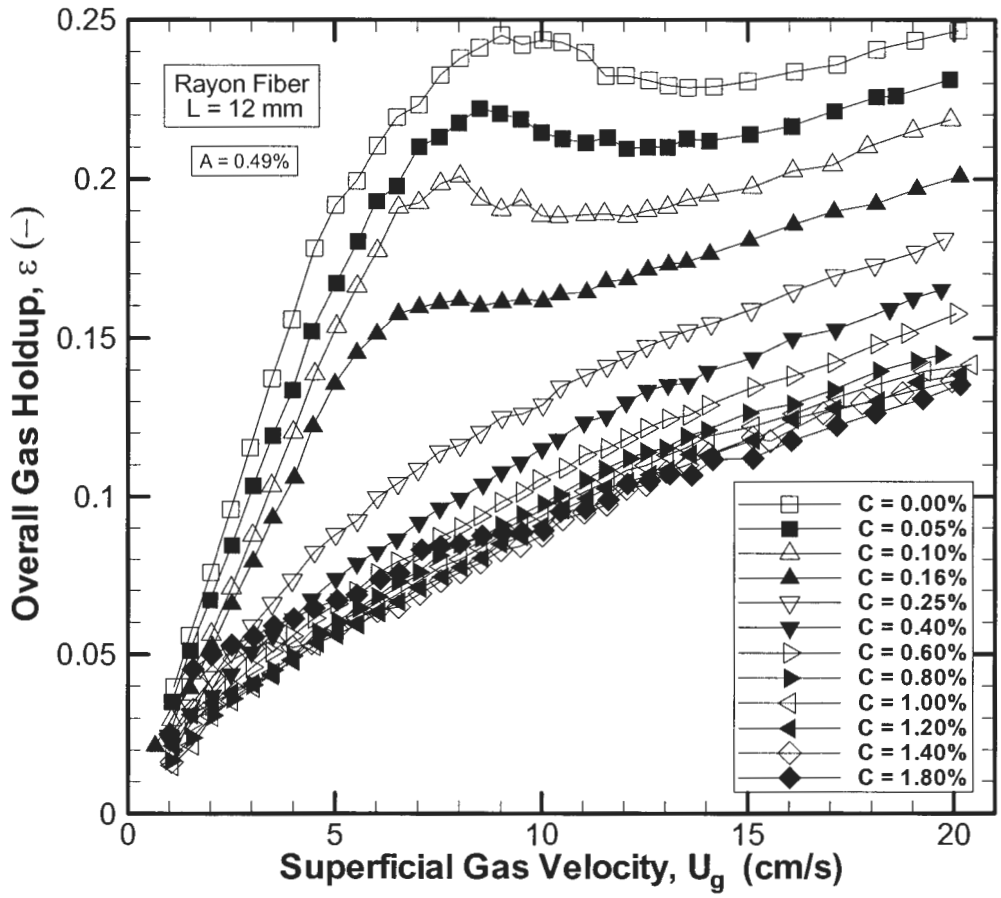

Figure C.3: Overall gas holdup versus superficial gas velocity for all fiber mass fractions for L = 12 mm Rayon fiber with A = 0.49%.

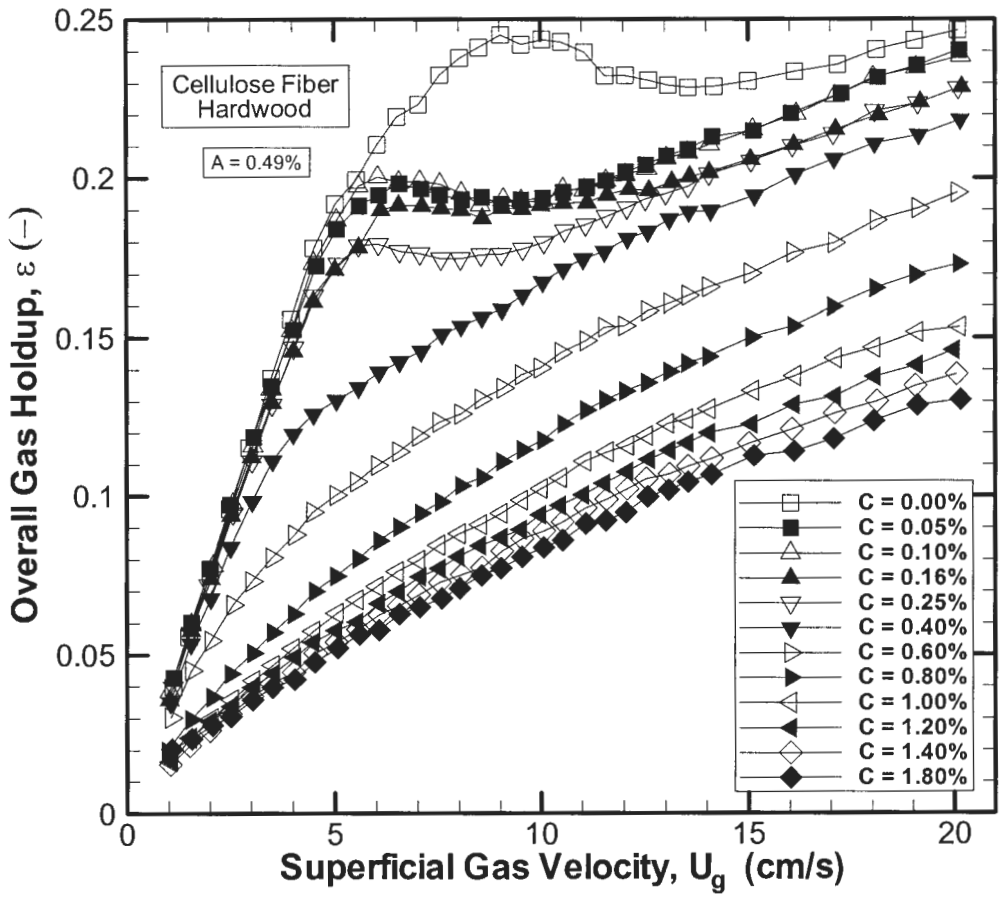

Figure C.4: Overall gas holdup versus superficial gas velocity for all fiber mass fractions for hardwood cellulose fiber with A = 0.49%.

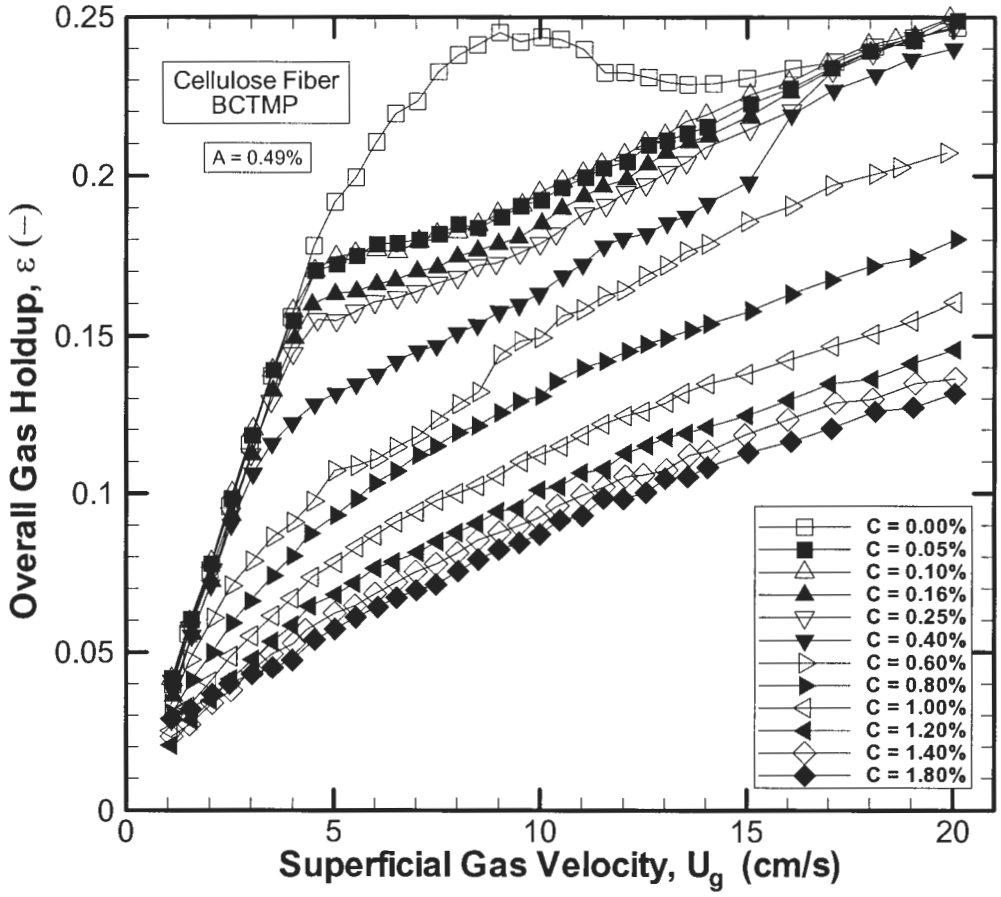

Figure C.5: Overall gas holdup versus superficial gas velocity for all fiber mass fractions for BCTMP cellulose fiber with A = 0.49%.

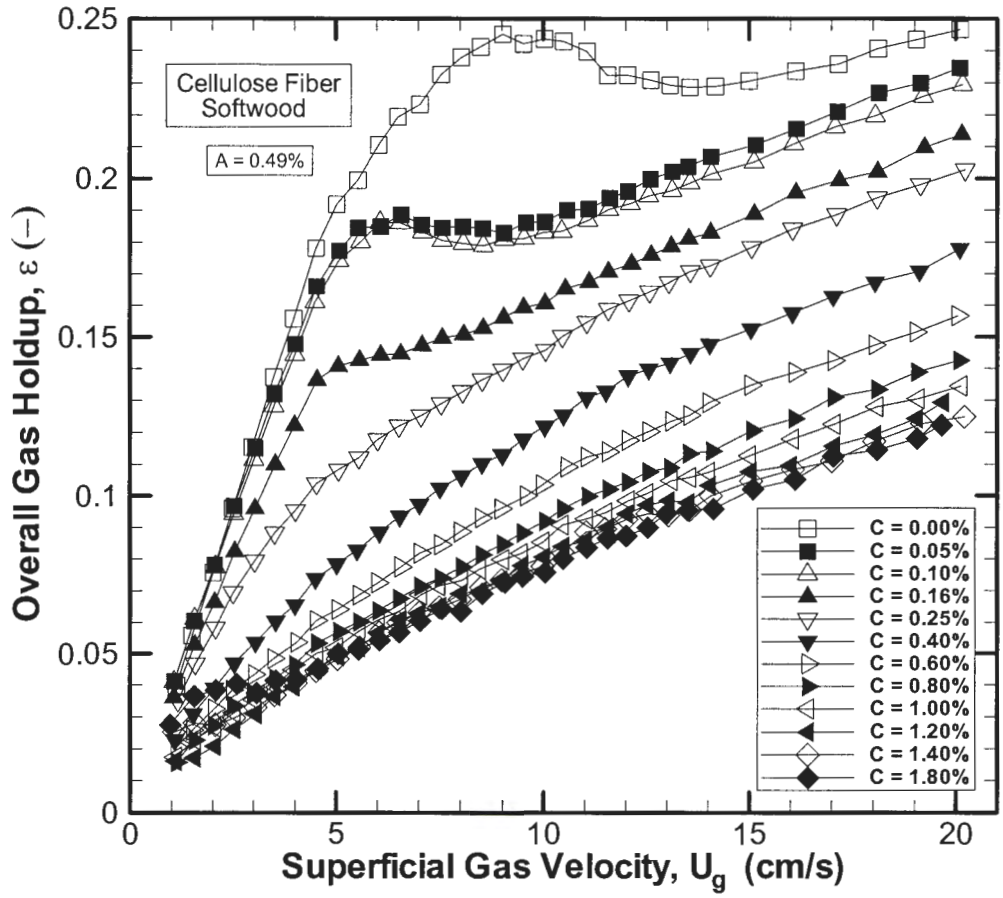

Figure C.6: Overall gas holdup versus superficial gas velocity for all fiber mass fractions for softwood cellulose fiber with A = 0.49%.

Appendix D: Overall Gas Holdup for All Fibers at A = 0.95%

The information presented in this appendix displays the overall gas holdup as a function of superficial gas velocity for all fiber types and lengths that were studied for the distributor open area of A = 0.95%.

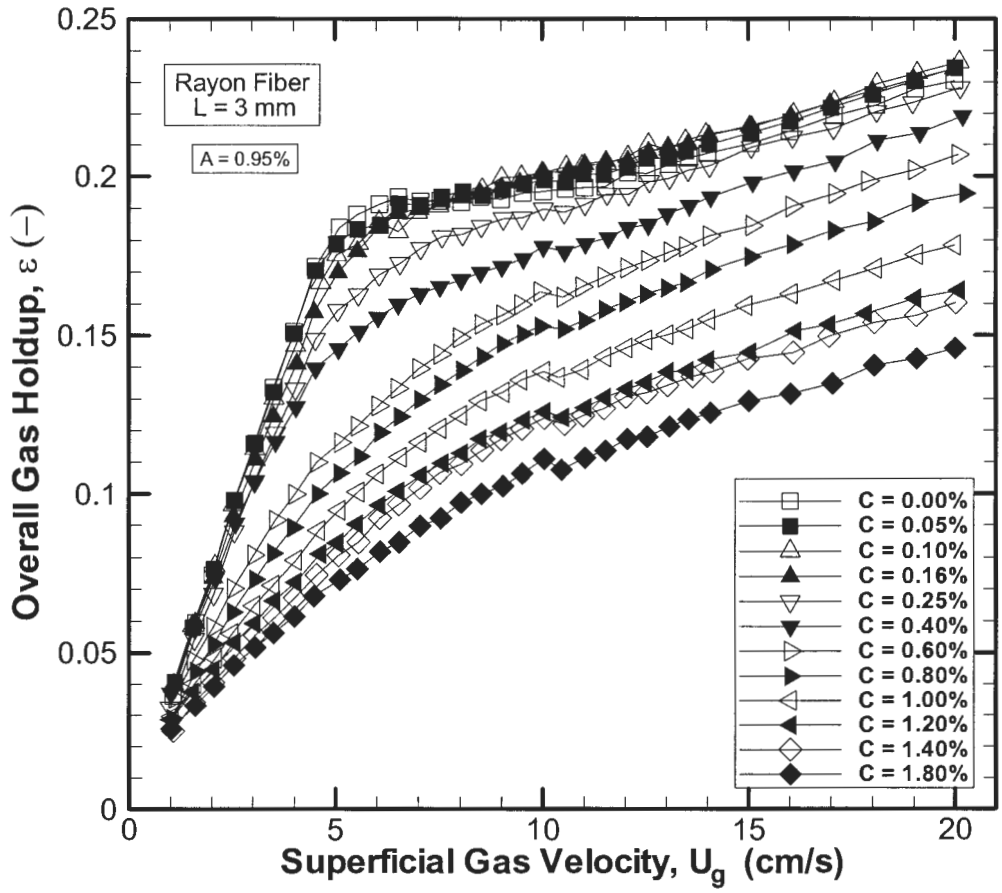

Figure D.1: Overall gas holdup versus superficial gas velocity for all fiber mass fractions for L = 3 mm Rayon fiber with A = 0.95%.

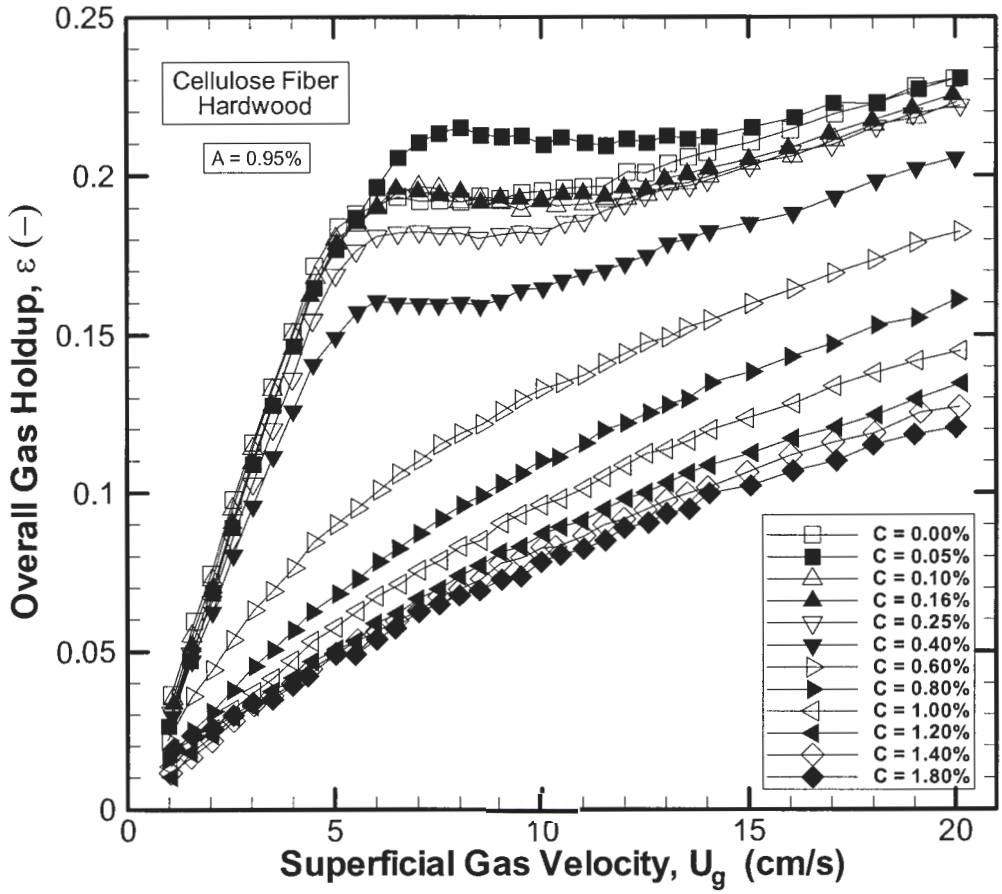

Figure D.2: Overall gas holdup versus superficial gas velocity for all fiber mass fractions for hardwood cellulose fiber with A = 0.95%.

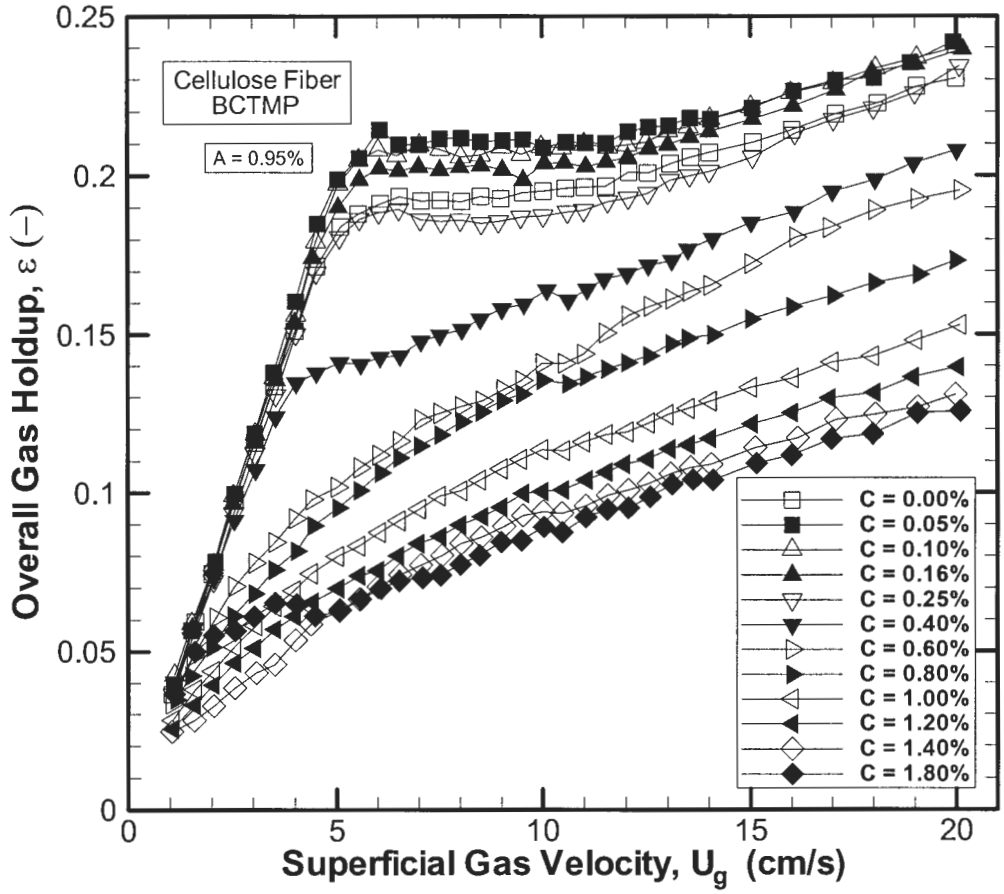

Figure D.3: Overall gas holdup versus superficial gas velocity for all fiber mass fractions for BCTMP cellulose fiber with A = 0.95%.

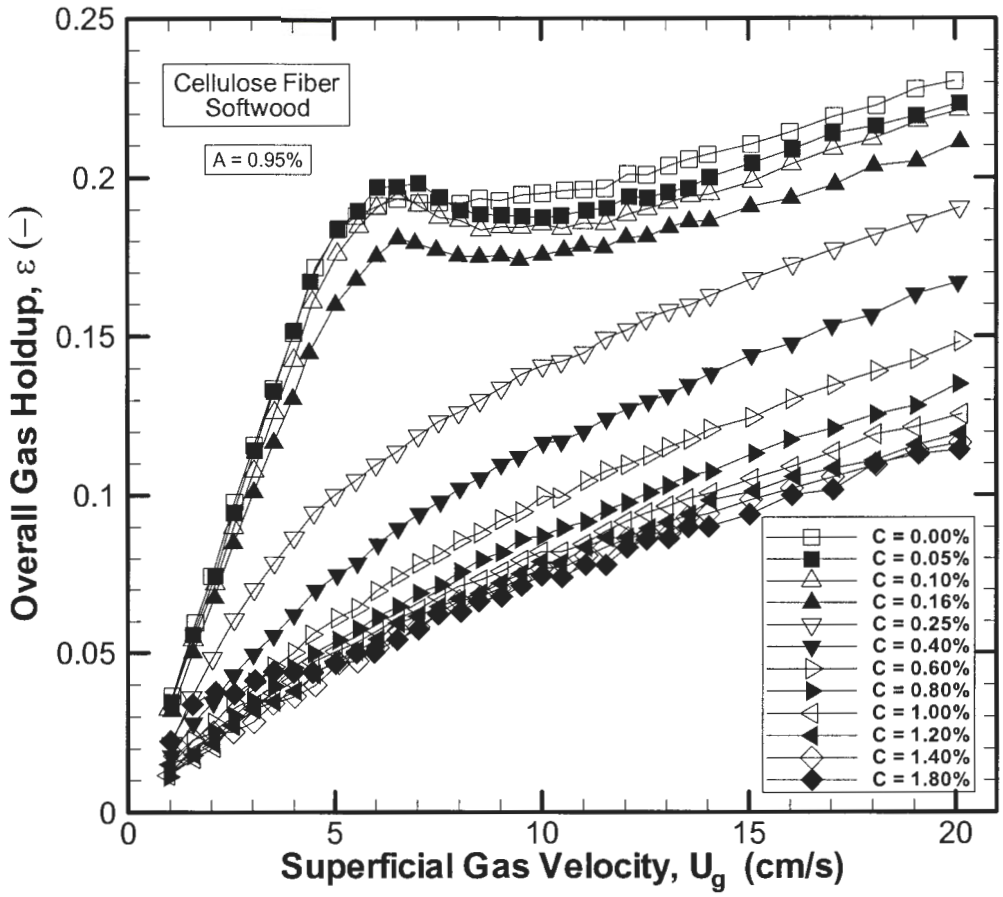

Figure D.4: Overall gas holdup versus superficial gas velocity for all fiber mass fractions for softwood cellulose fiber with A = 0.95%.

Appendix E: Overall Gas Holdup for All Fibers at A = 2.03 %

The information presented in this appendix displays the overall gas holdup as a function of superficial gas velocity for all fiber types and lengths that were studied for the distributor open area of A = 2.03%.

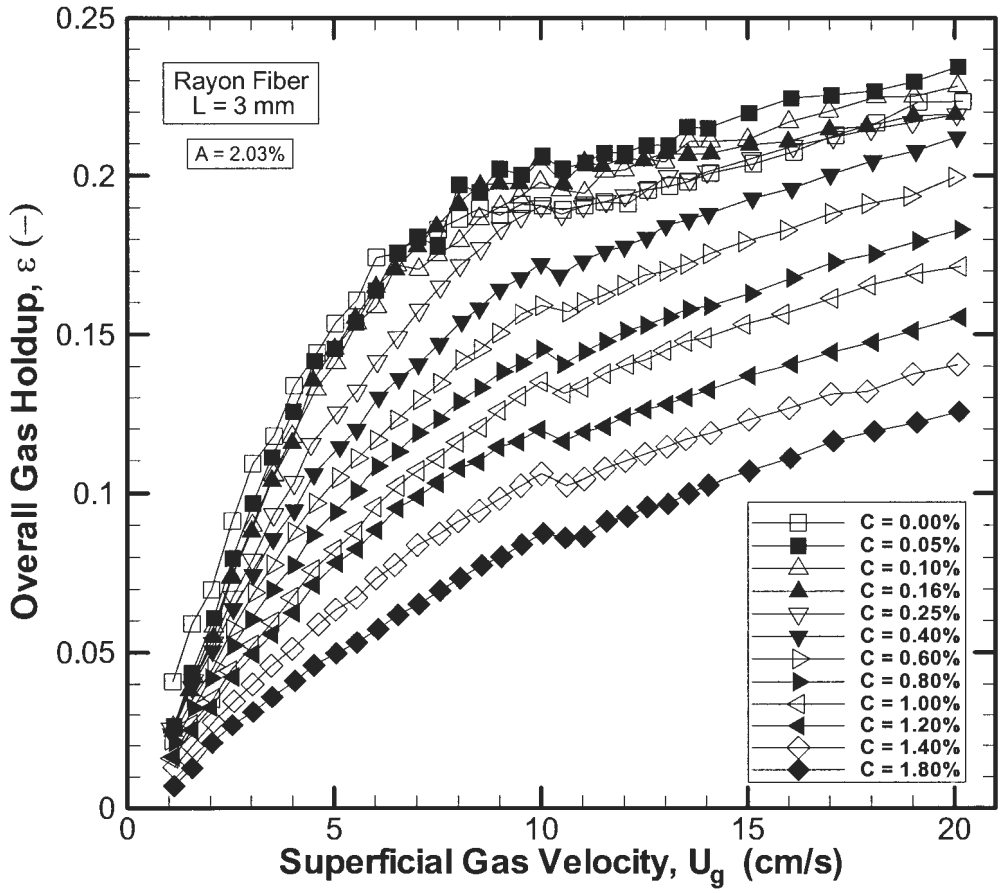

Figure E.1: Overall gas holdup versus superficial gas velocity for all fiber mass fractions for L = 3 mm Rayon fiber with A = 2.03%.

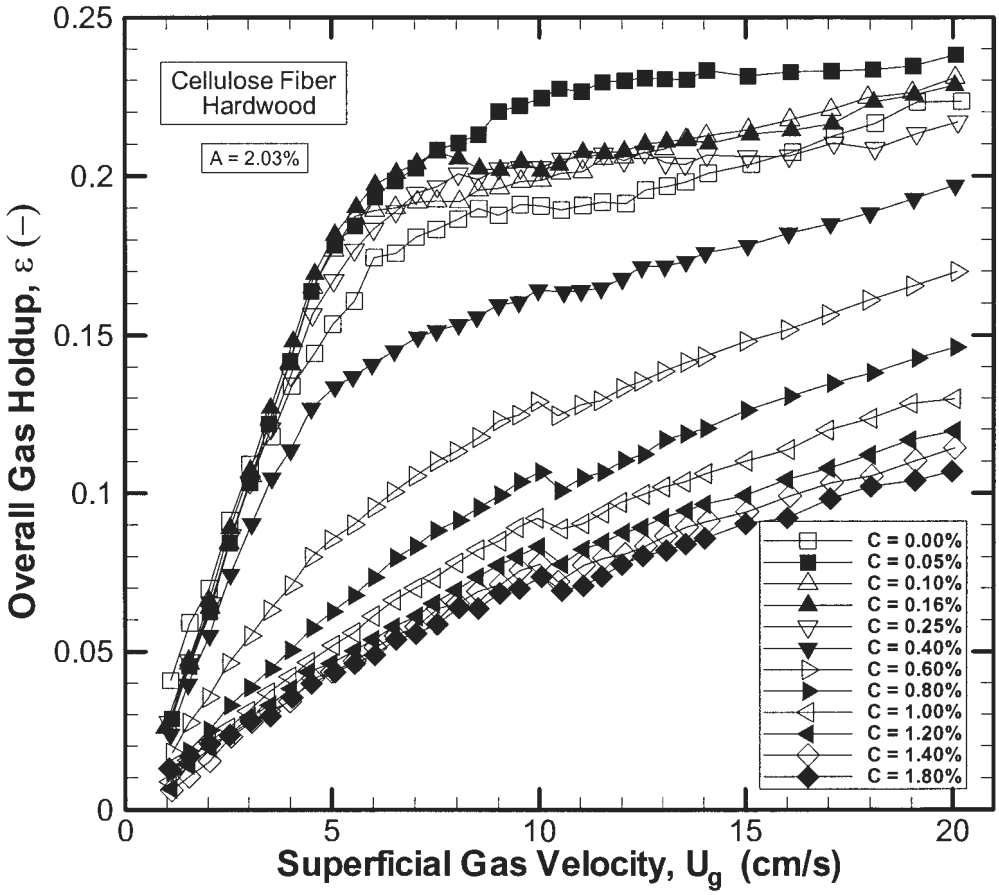

Figure E.2: Overall gas holdup versus superficial gas velocity for all fiber mass fractions for hardwood cellulose fiber with A = 2.03%.

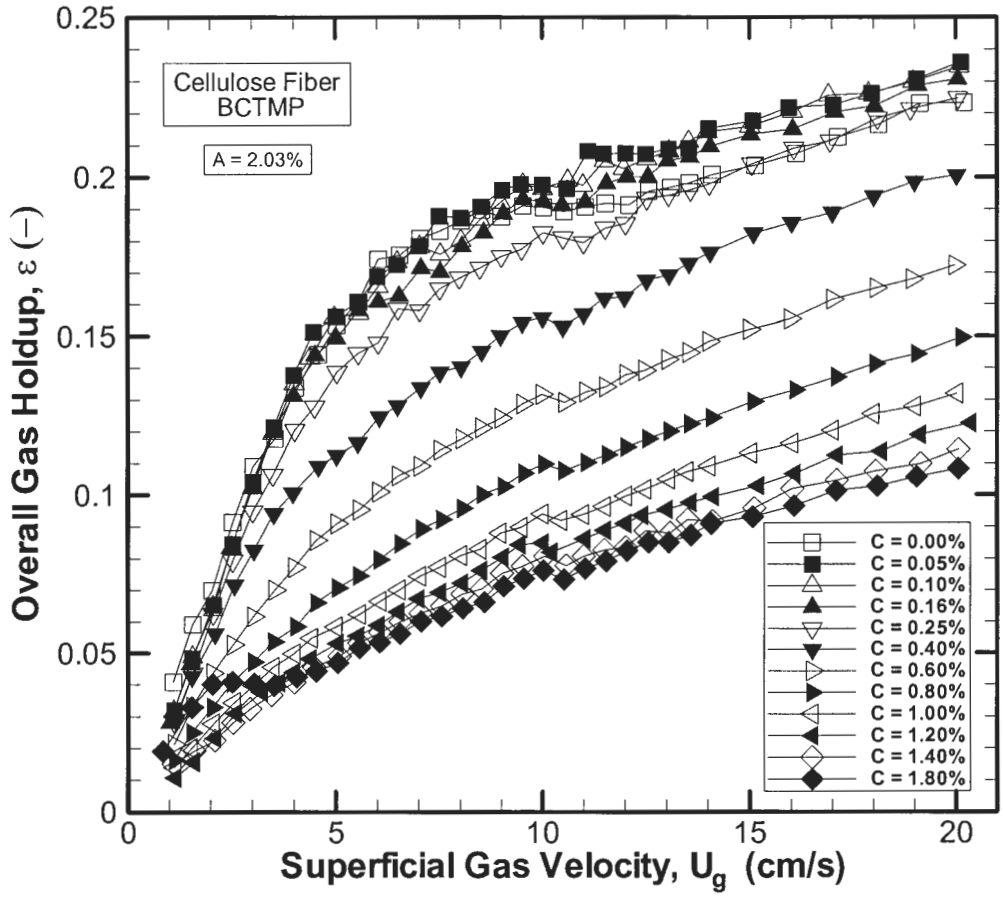

Figure E.3: Overall gas holdup versus superficial gas velocity for all fiber mass fractions for BCTMP cellulose fiber with A = 2.03%.

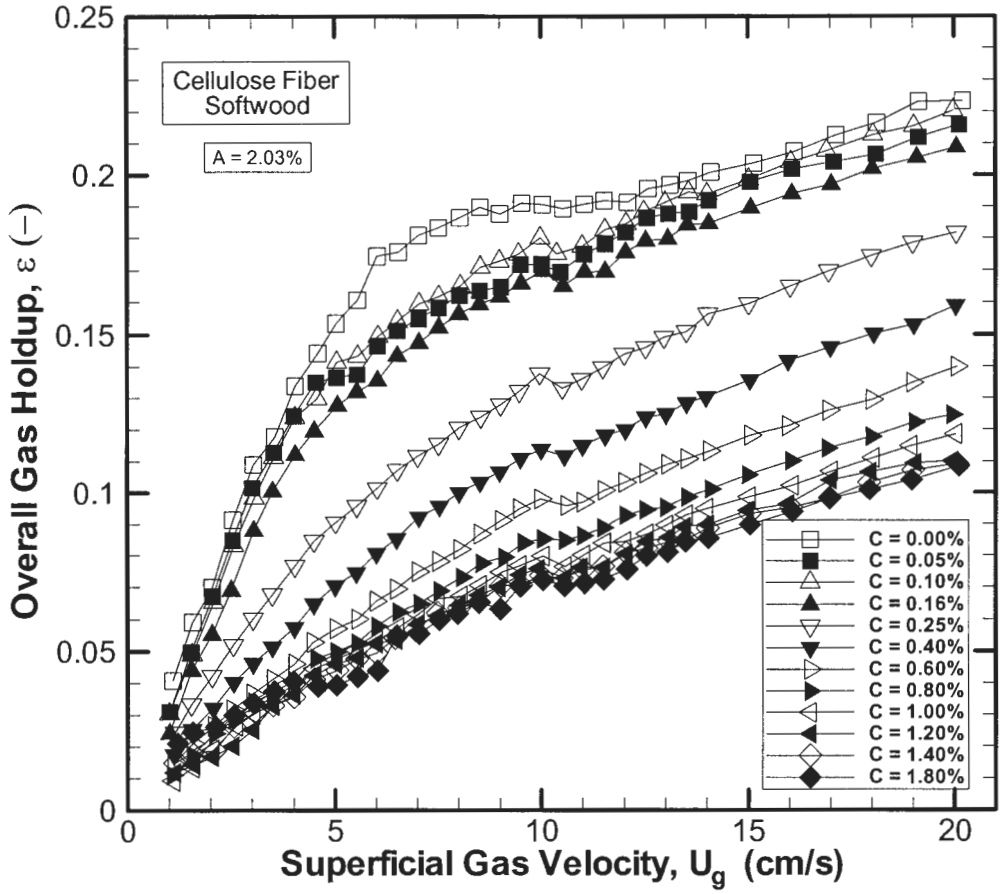

Figure E.4: Overall gas holdup versus superficial gas velocity for all fiber mass fractions for softwood cellulose fiber with A = 2.03%.

Appendix F: Overall Gas Holdup for all fiber types at C = 0.10% and C = 1.00%

The information presented in this appendix displays the overall gas holdup as a function of superficial gas velocity for all fiber types at C = 0.10% and C = 1.00%. Information is provided for all three distributor plate open areas.

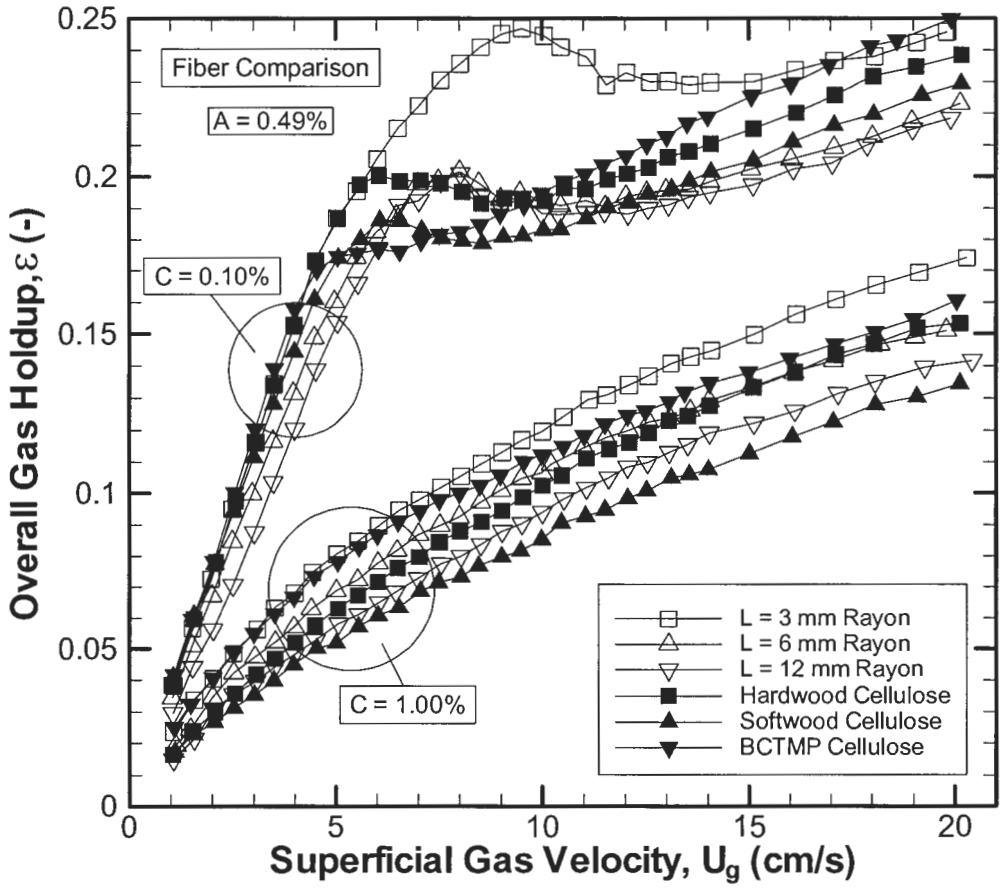

Figure F.1: Overall gas holdup versus superficial gas velocity showing the effect of fiber type at C = 0.10% and C = 1.00% for A = 0.49%.

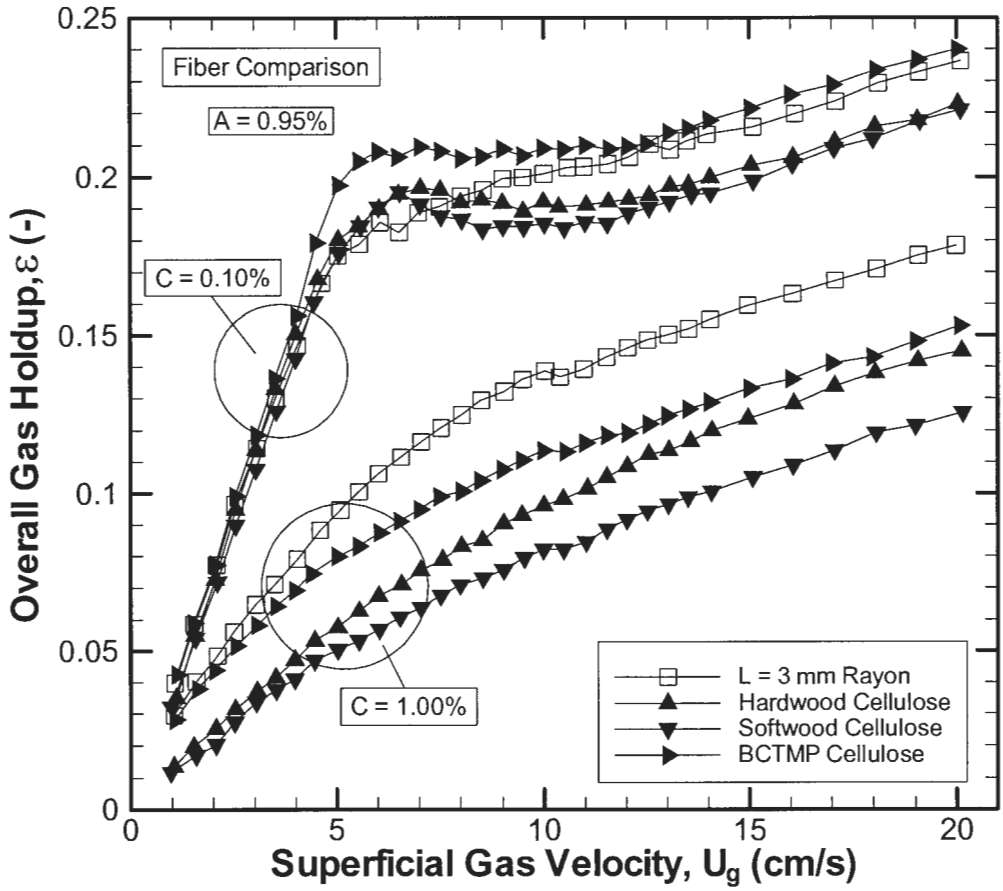

Figure F.2: Overall gas holdup versus superficial gas velocity showing the effect of fiber type at C = 0.10% and C = 1.00% for A = 0.95%.

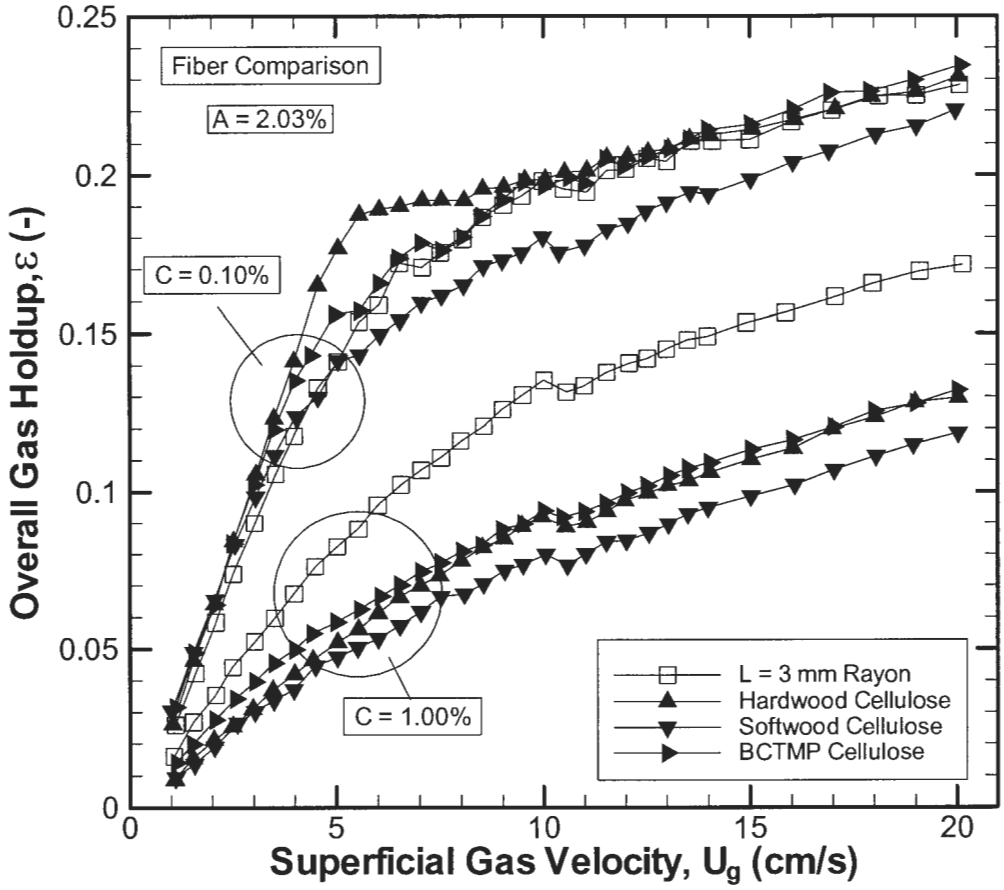

Figure F.3: Overall gas holdup versus superficial gas velocity showing the effect of fiber type at C = 0.10% and C = 1.00% for A = 2.03%.

Appendix G: Effect of Fiber Mass Fraction on Overall Gas Holdup

This appendix shows the effects of hardwood fiber mass fraction on overall gas holdup for the range of superficial gas velocities for the three different distributor plate open areas.

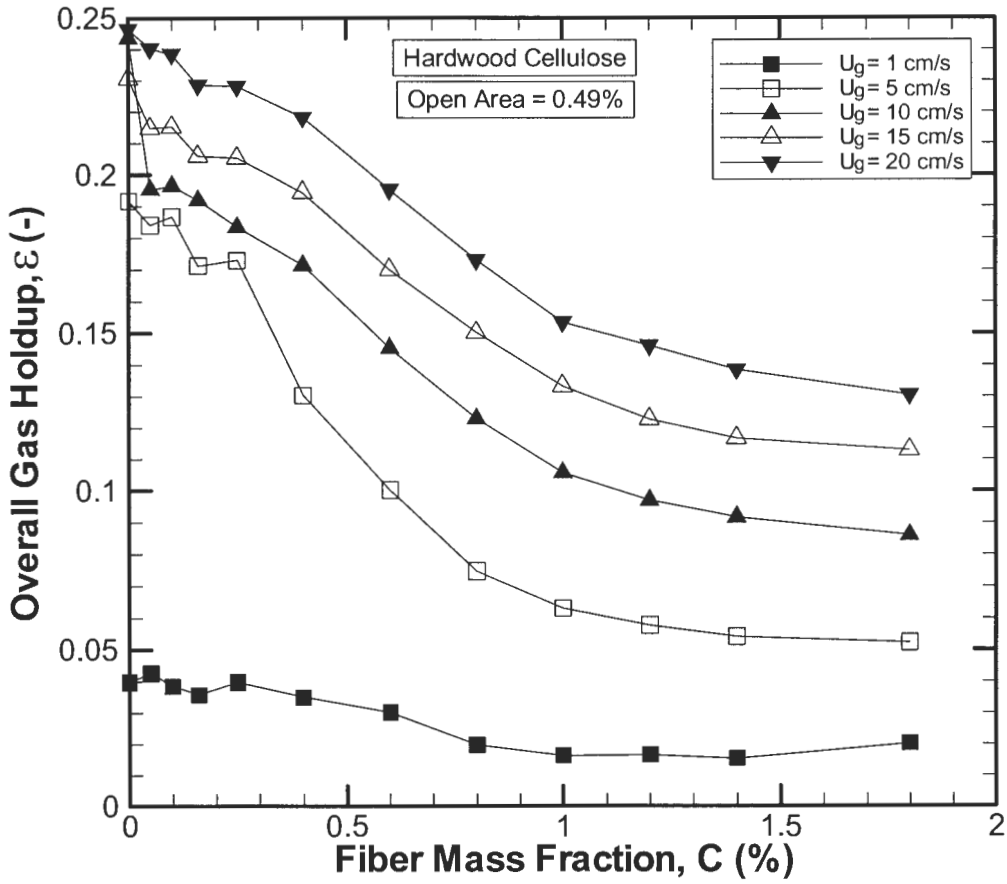

Figure G.1: Gas holdup as a function of fiber mass fraction for hardwood cellulose for various superficial gas velocities at A = 0.49%.

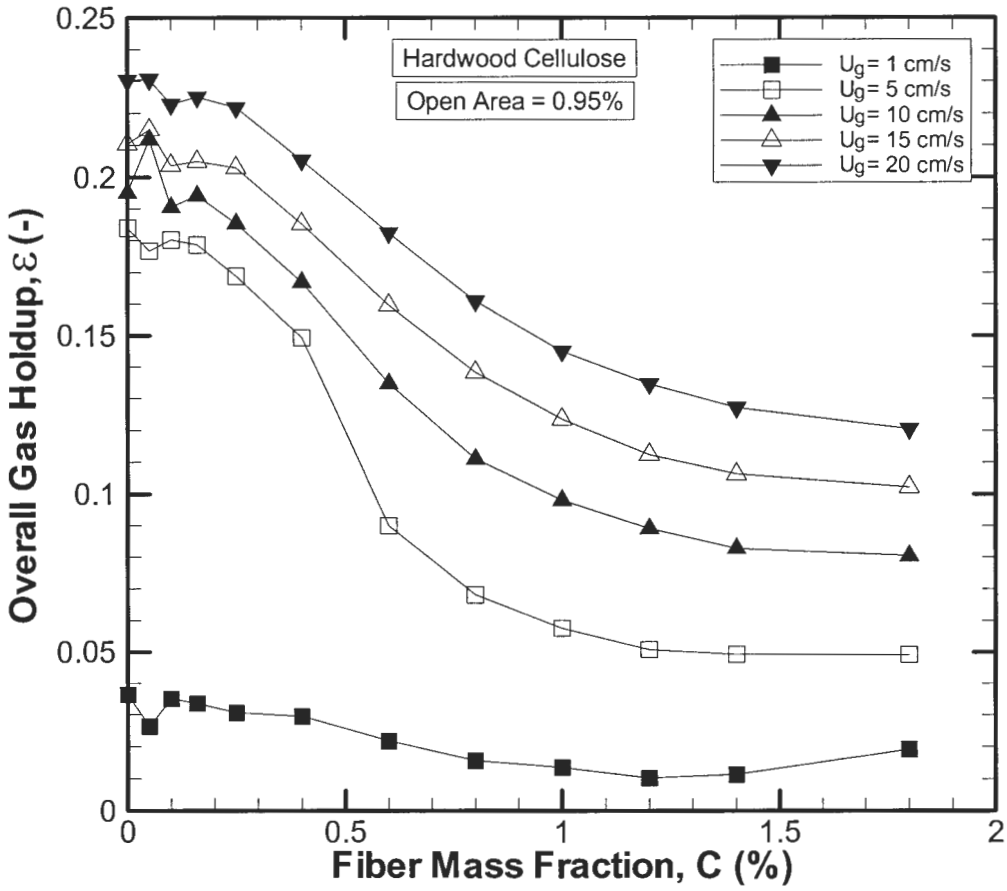

Figure G.2: Gas holdup as a function of fiber mass fraction for hardwood cellulose for various superficial gas velocities at A = 0.95%.

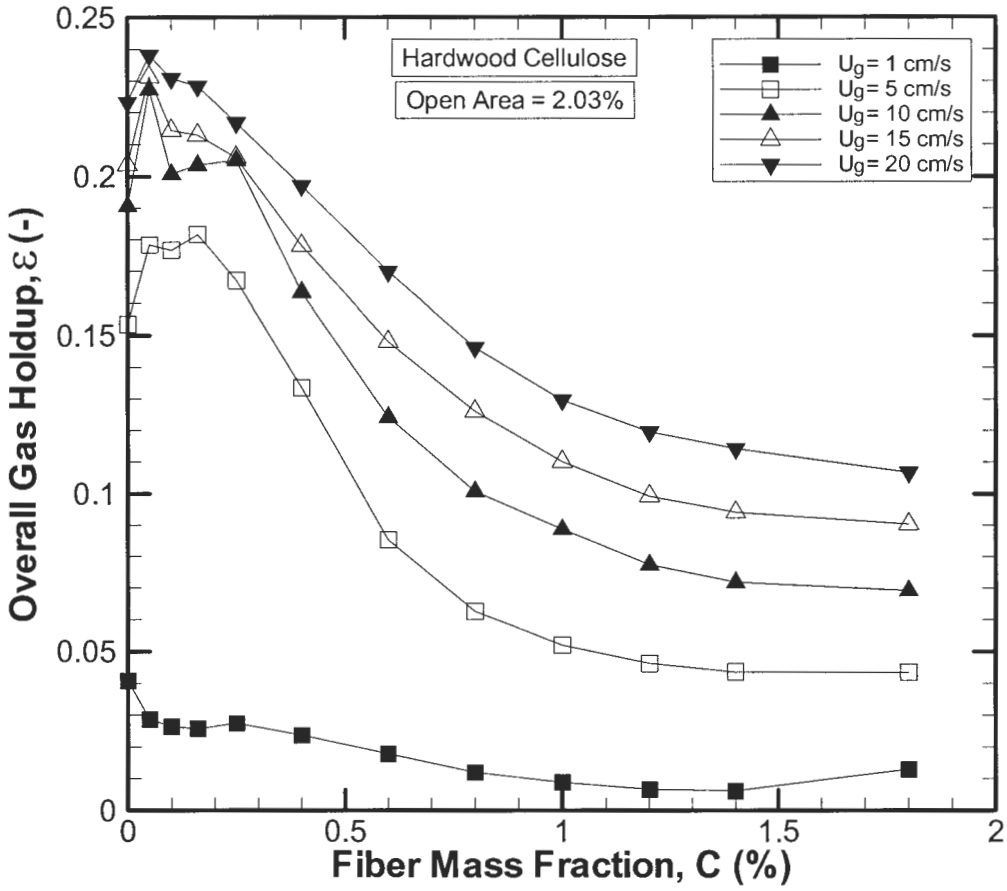

Figure G.3: Gas holdup as a function of fiber mass fraction for hardwood cellulose for various superficial gas velocities at A = 2.03%.

Appendix H: Effect of Superficial Gas Velocity on Local Gas Holdup for L = 3 mm Rayon Fiber at C = 0.10%

This appendix displays the effect of superficial gas velocity on L = 3 mm Rayon fiber at C = 0.10% for distributor plate open areas.

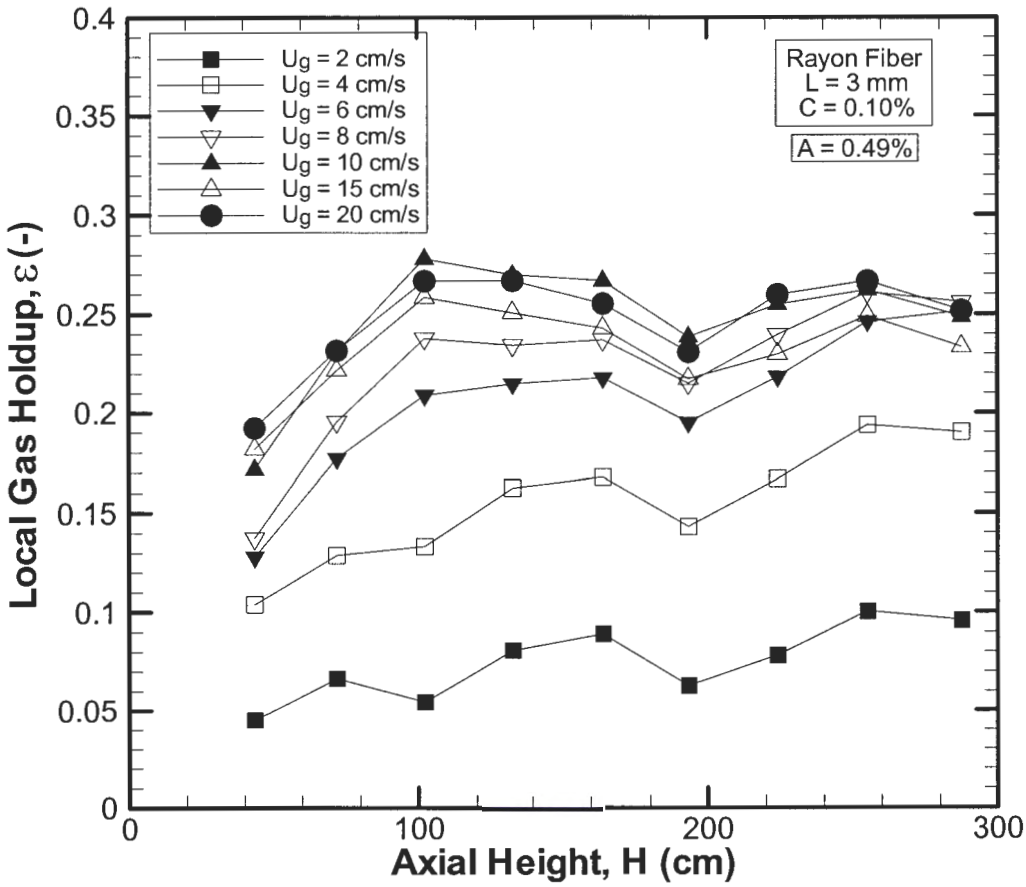

Figure H.1: Effect of superficial gas velocity on L = 3 mm Rayon fiber for C = 0.10% and A = 0.49%.

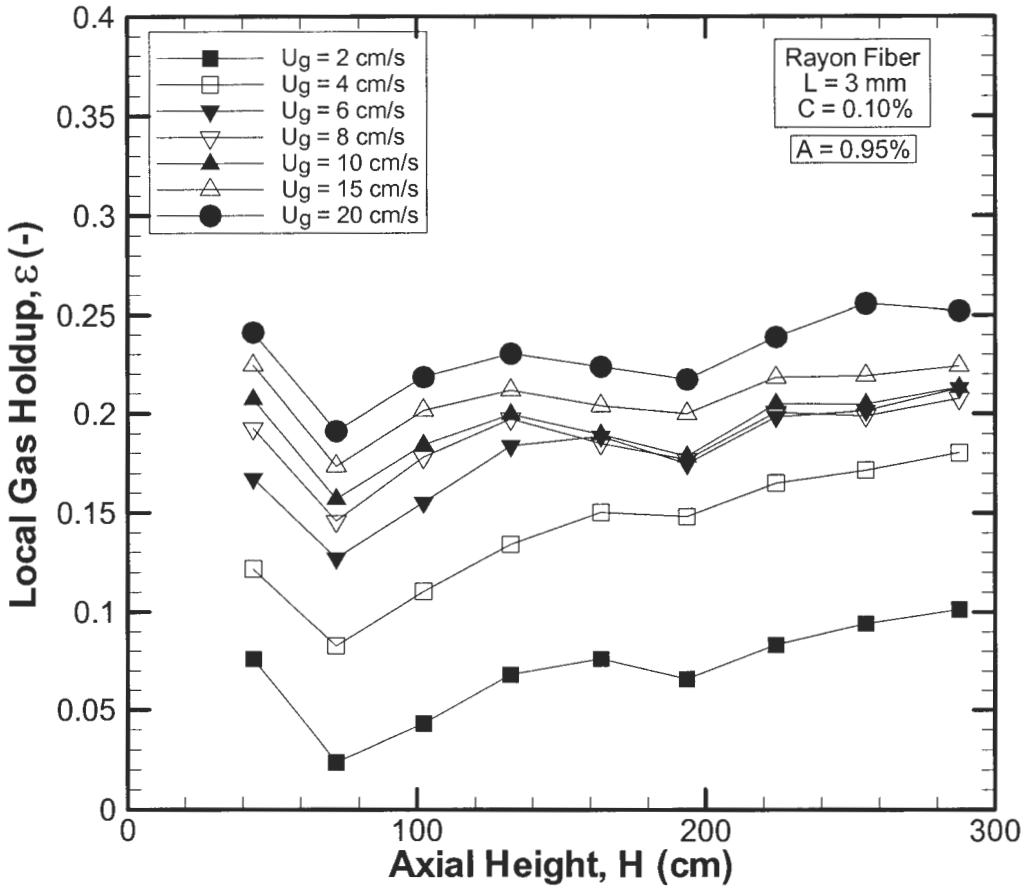

Figure H.2: Effect of superficial gas velocity on L = 3 mm Rayon fiber for C = 0.10% and A = 0.95%.

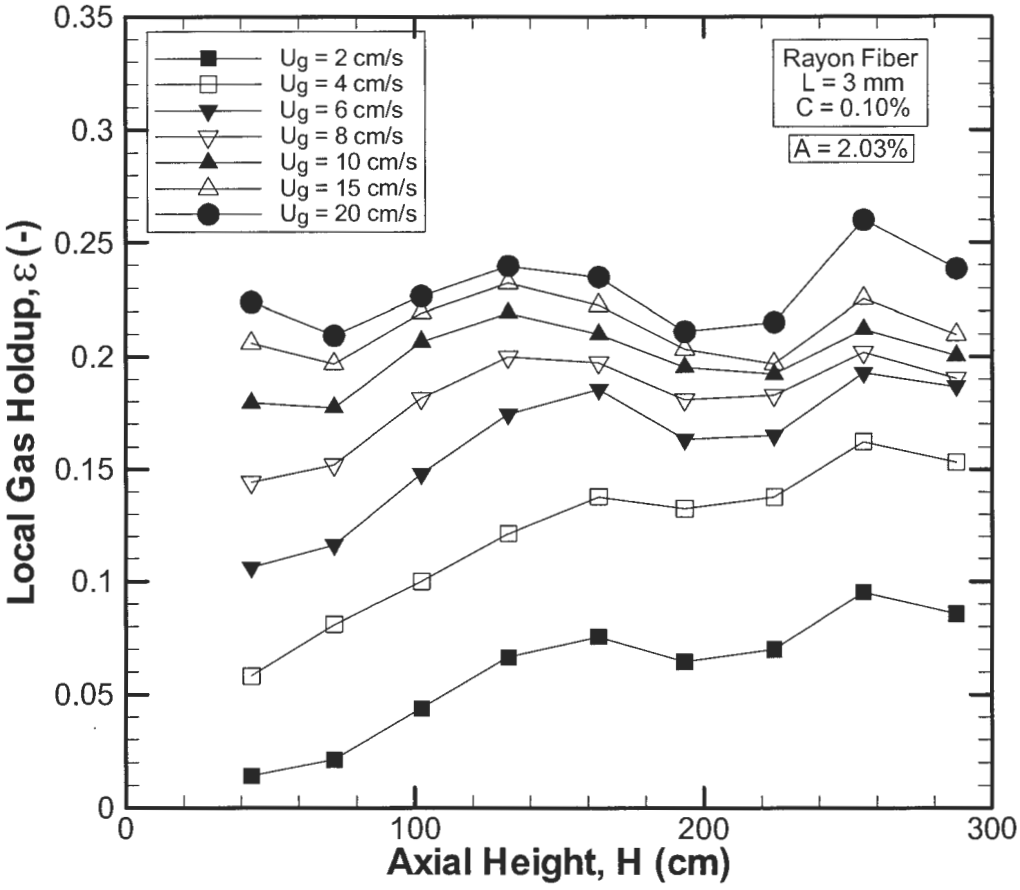

Figure H.3: Effect of superficial gas velocity on L = 3 mm Rayon fiber for C = 0.10% and A = 2.03%.

Appendix I: Effect of Superficial Gas Velocity on Local Gas Holdup for L = 3 mm Rayon fiber at C = 1.00%

This appendix displays the effect of superficial gas velocity on L = 3 mm Rayon fiber at C = 1.00% for all distributor plate open areas.

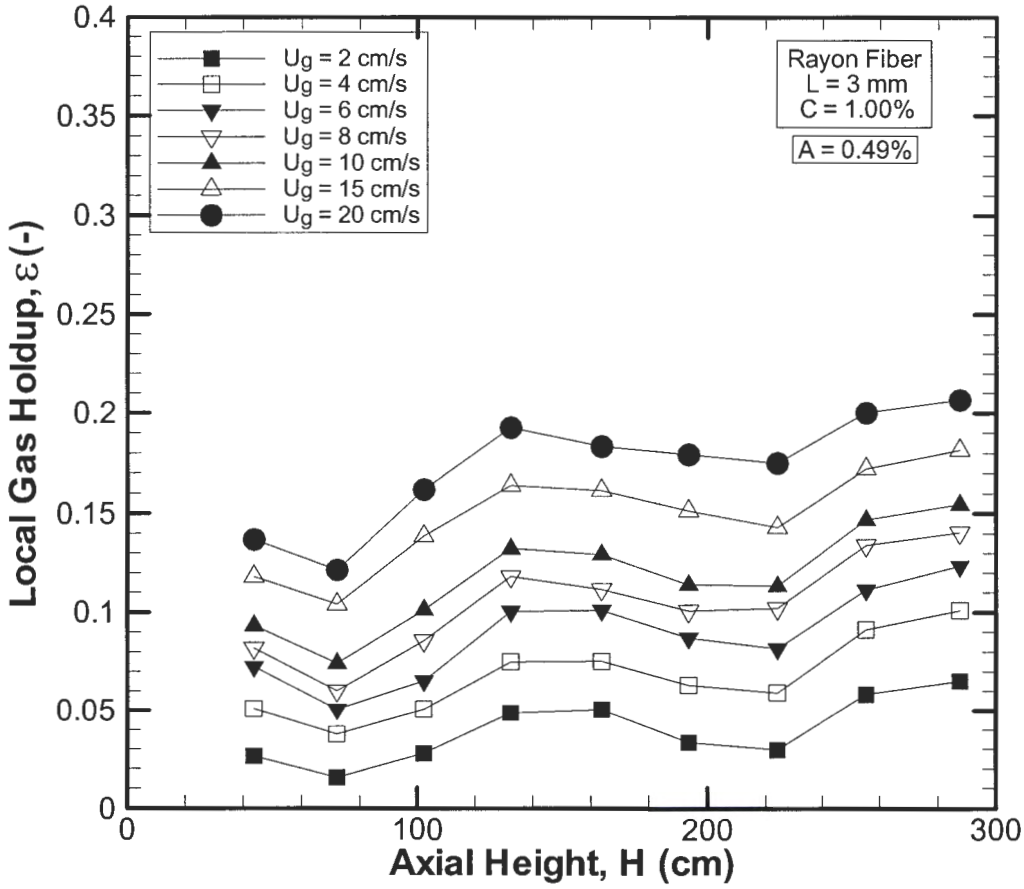

Figure I.1: Effect of superficial gas velocity on local gas holdup for L = 3 mm Rayon fiber at C = 1.00% and A = 0.49%.

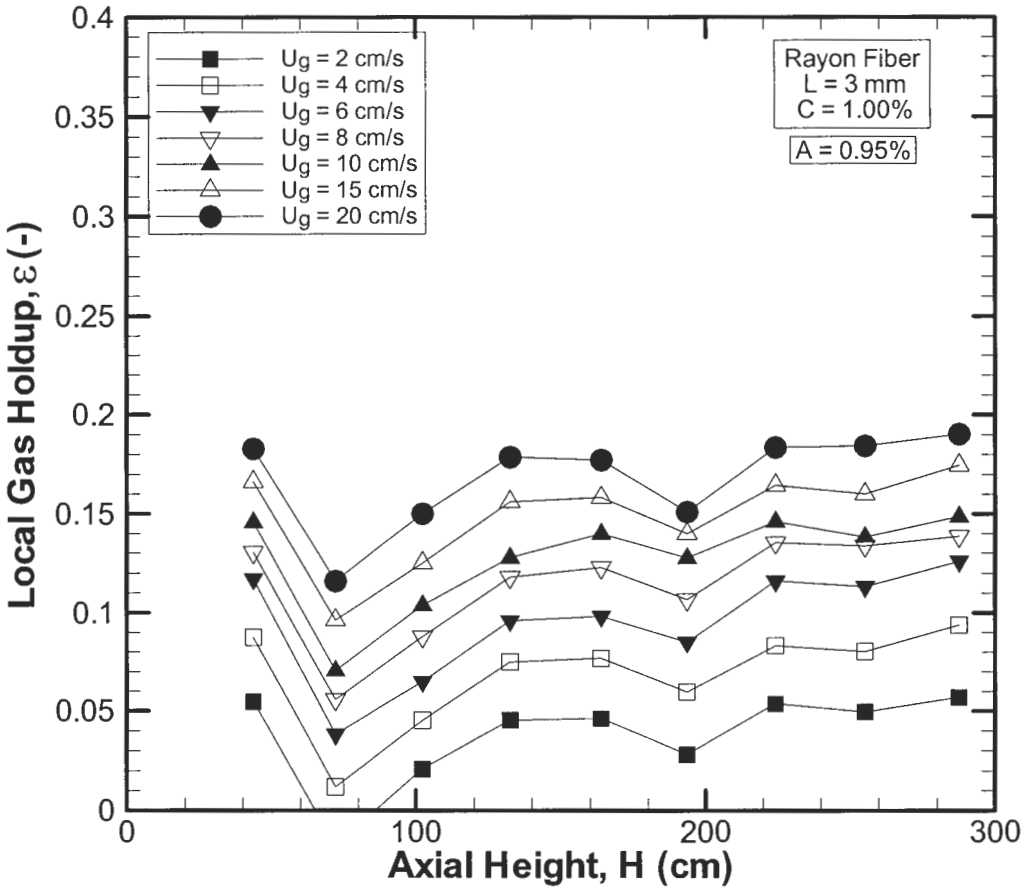

Figure I.2: Effect of superficial gas velocity on local gas holdup for L = 3 mm Rayon fiber at C = 1.00% and A = 0.95%.

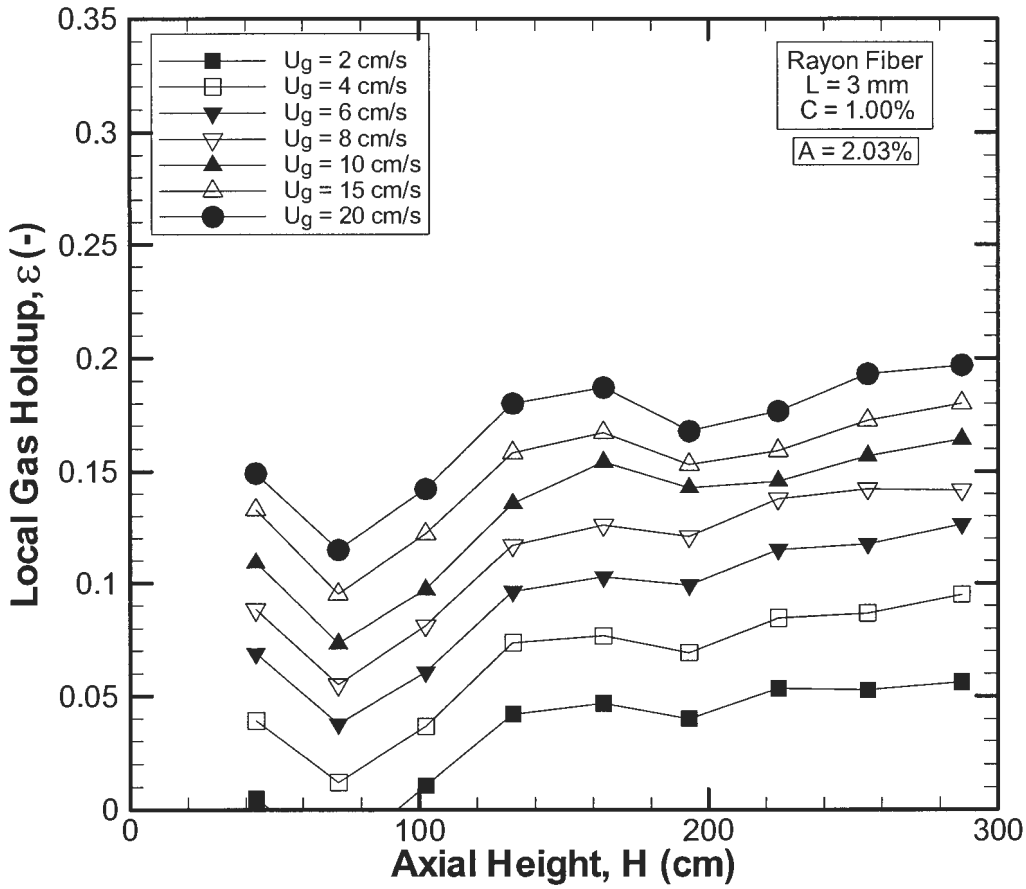

Figure I.3: Effect of superficial gas velocity on local gas holdup for L = 3 mm Rayon fiber at C = 1.00% and A = 2.03%.

Appendix J: Effect of Fiber Mass Fraction on Local Gas Holdup for BCTMP Cellulose Fiber

This appendix displays local gas holdup for BCTMP cellulose at all fiber mass fractions and U_g = 10 cm/s. Results are shown for all three distributor plate open areas.

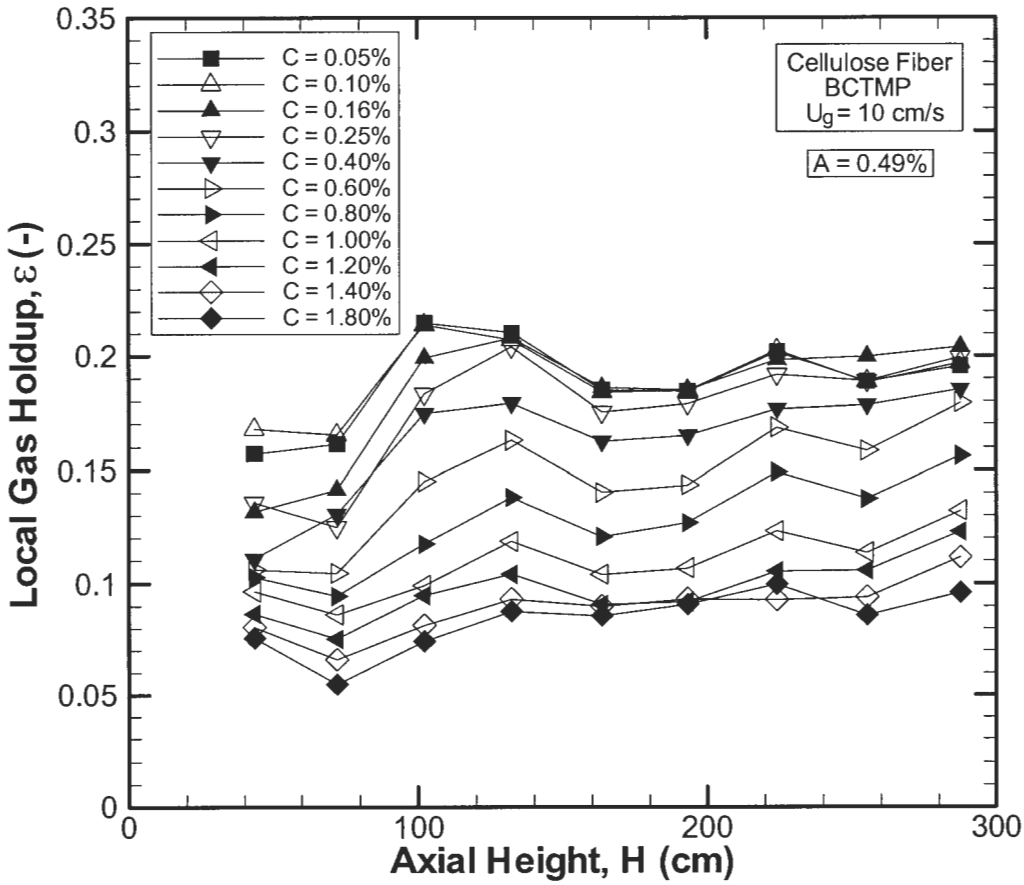

Figure J.1: Effect of fiber mass fraction on local gas holdup for BCTMP cellulose fiber at U_g = 10 cm/s and A = 0.49%.

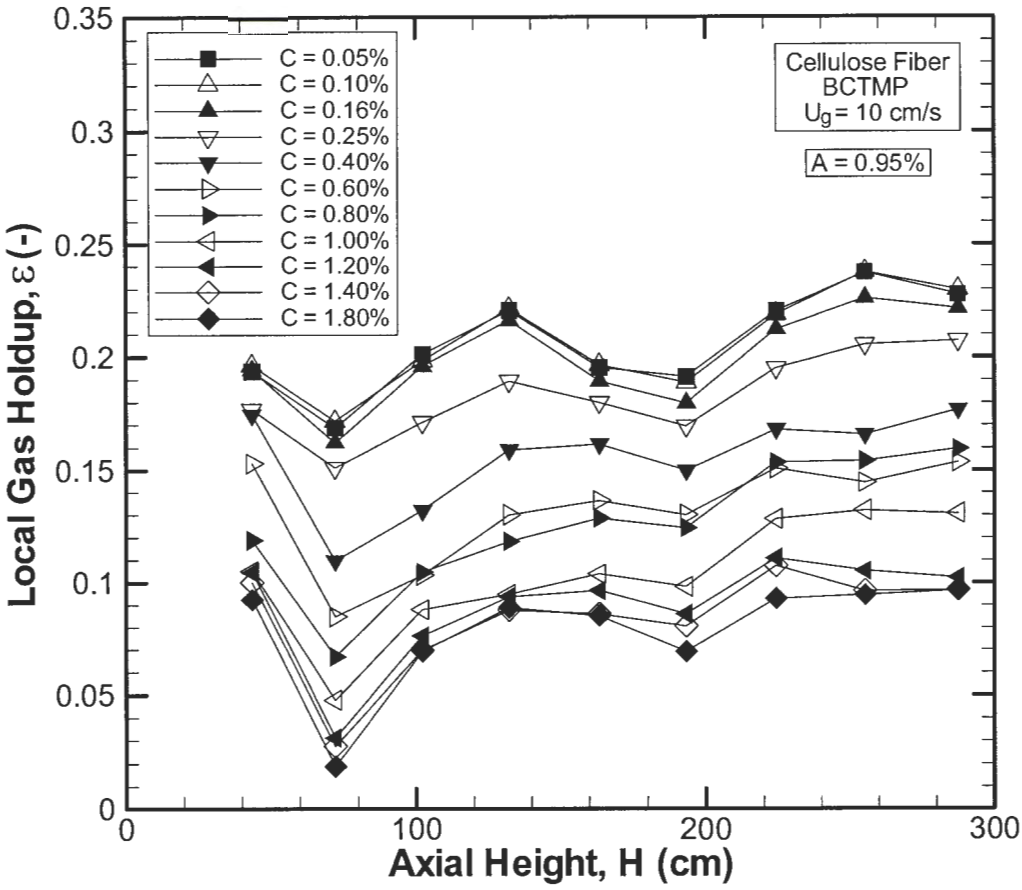

Figure J.2: Effect of fiber mass fraction on local gas holdup for BCTMP cellulose fiber at U_g = 10 cm/s and A = 0.95%.

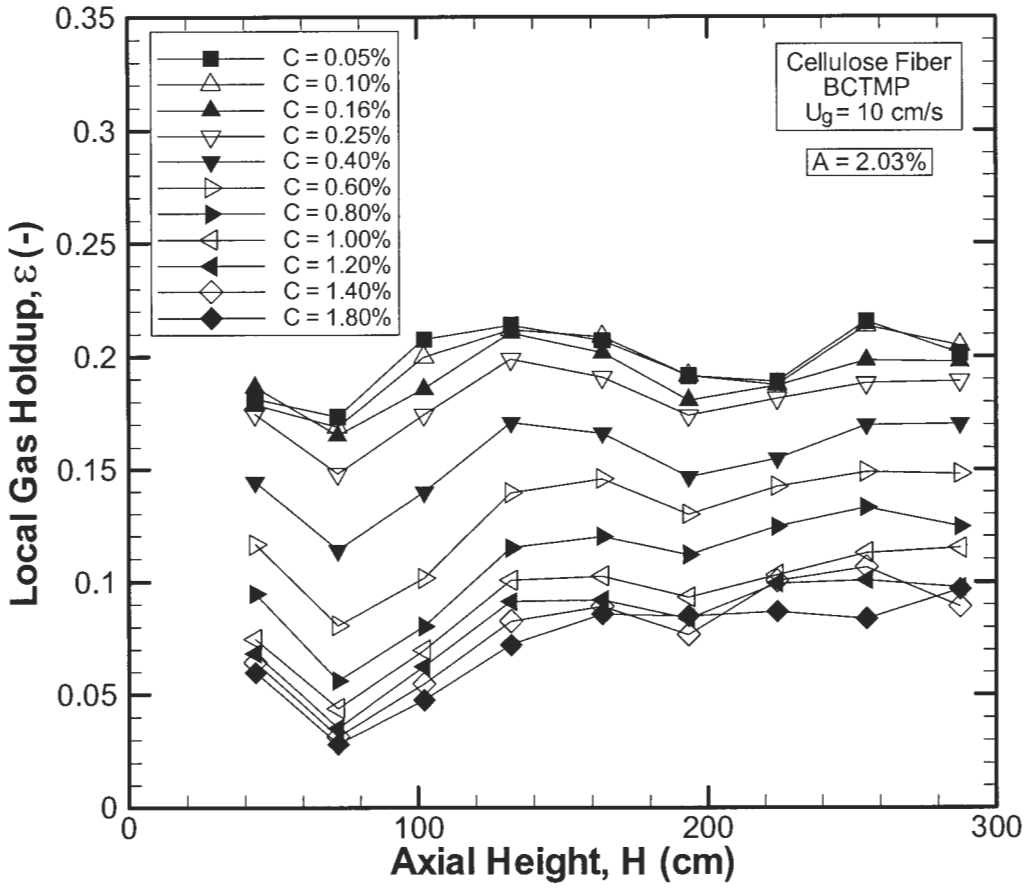

Figure J.3: Effect of fiber mass fraction on local gas holdup for BCTMP cellulose fiber at U_g = 10 cm/s and A = 2.03%.

Appendix K: Effect of Fiber Type on Local Gas Holdup

This appendix displays the effect of fiber type on local gas holdup for all fiber types at C = 0.80% and U_g = 20 cm/s for all distributor plate open areas.

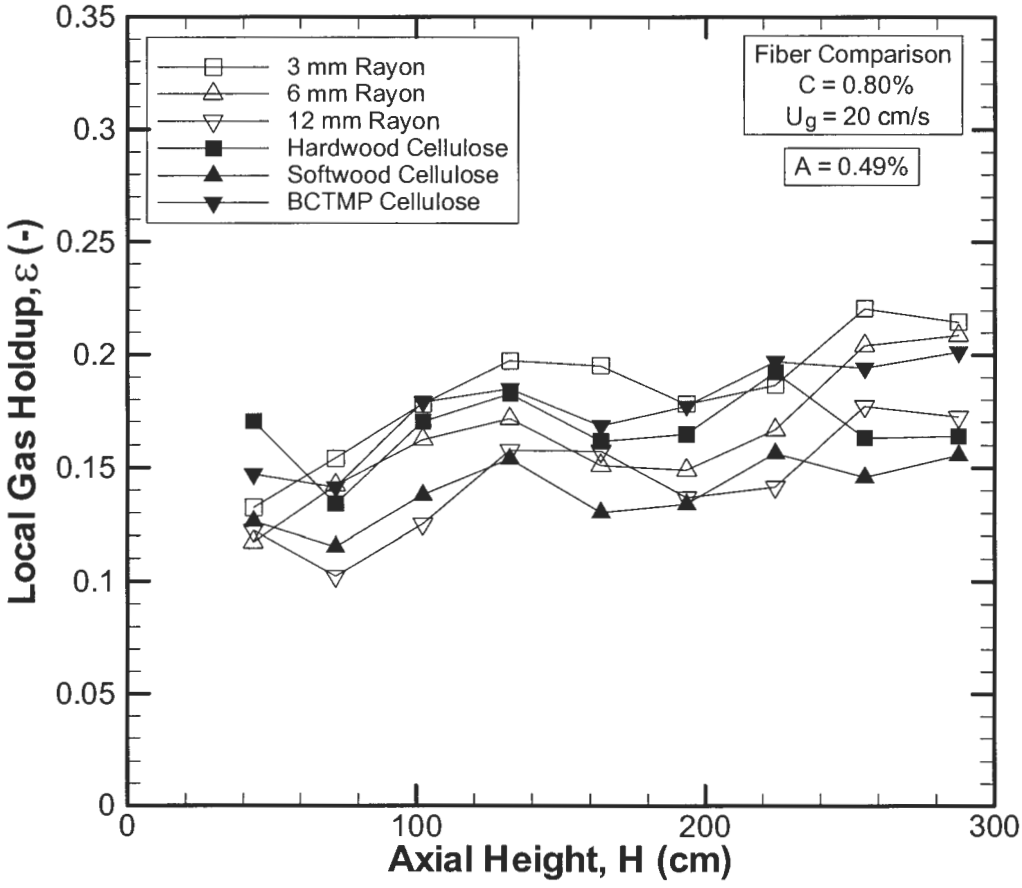

Figure K.1: Effect of fiber type on local gas holdup for C = 0.80%, U_g = 20 cm/s, and A = 0.49%.

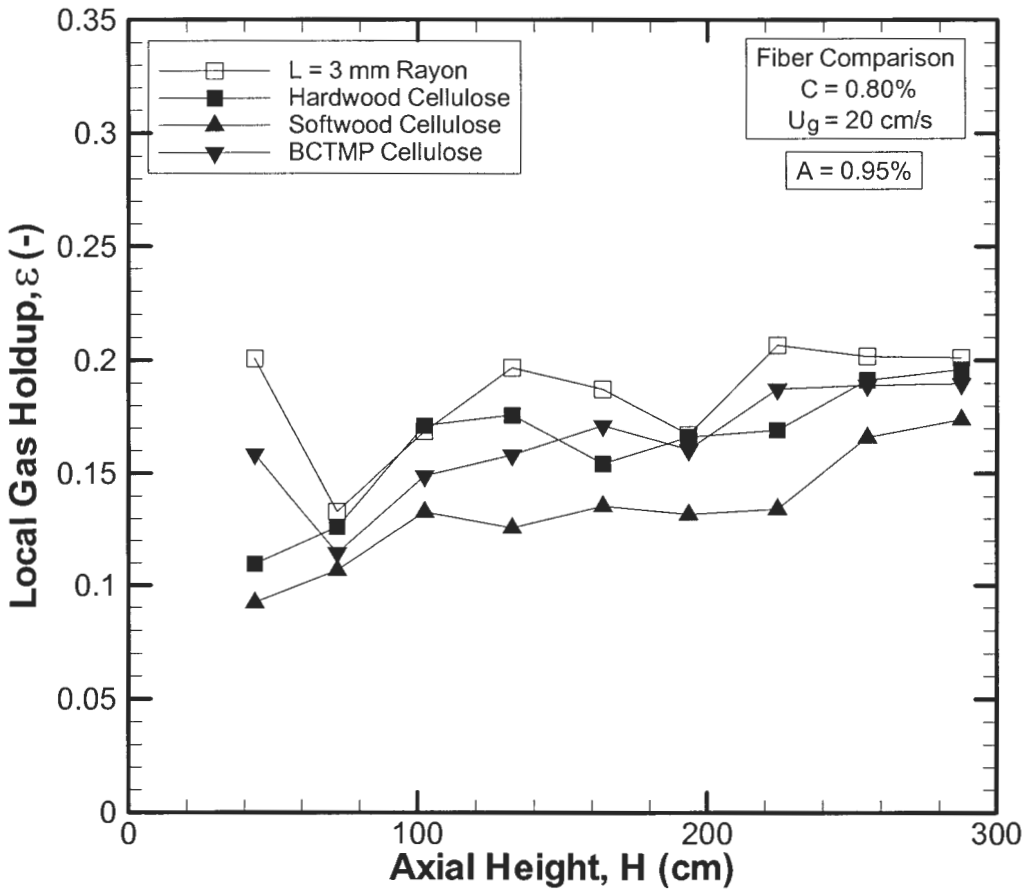

Figure K.2: Effect of fiber type on local gas holdup for C = 0.80%, U_g = 20 cm/s, and A = 0.95%.

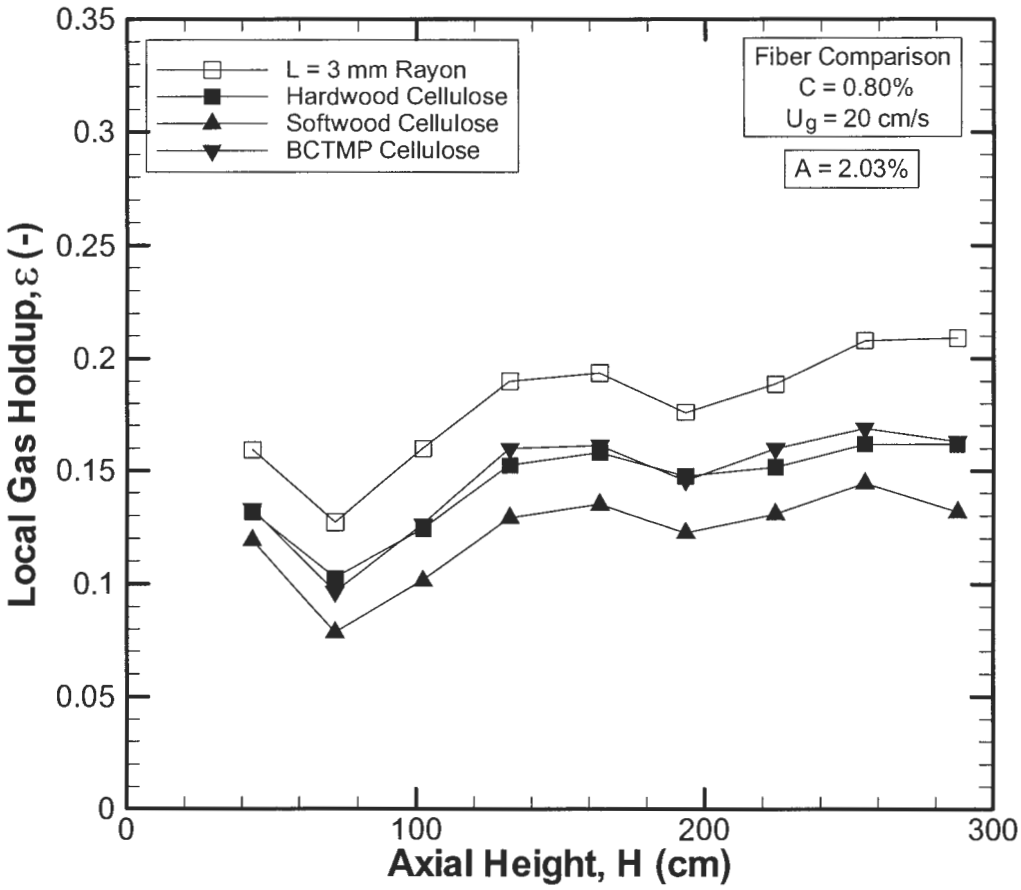

Figure K.3: Effect of fiber type on local gas holdup for C = 0.80%, U_g = 20 cm/s, and A = 2.03%.

Appendix L: Unexpected Result

The major unexpected result was the various trends observed while taking multiple data sets of the same fiber mass fraction to test data repeatability. An example is shown in Fig. L.1 for air-water data sets at A = 0.95%. Eight different data sets were taken, with many different overall gas holdup trends being observed. Different trends were observed for air-water flows for all three distributor plate open areas, as well as for some low fiber mass fraction data sets ($C \leq 0.16\%$). For higher fiber mass fraction sets ($C \geq 0.25\%$), the data sets were almost always repeatable due to the fibers suppressing turbulence.

Random fiber mass fraction data sets were repeated for each fiber type and distributor plate to test the repeatability of the data. If the repeated data set did not match the original data set, the set was repeated at least once more to determine which data set was the actual curve that could be repeated. The "correct" data set for that particular fiber mass fraction and distributor plate open area was chosen based on the repeatability of the data and how it compared to the surrounding fiber mass fraction sets.

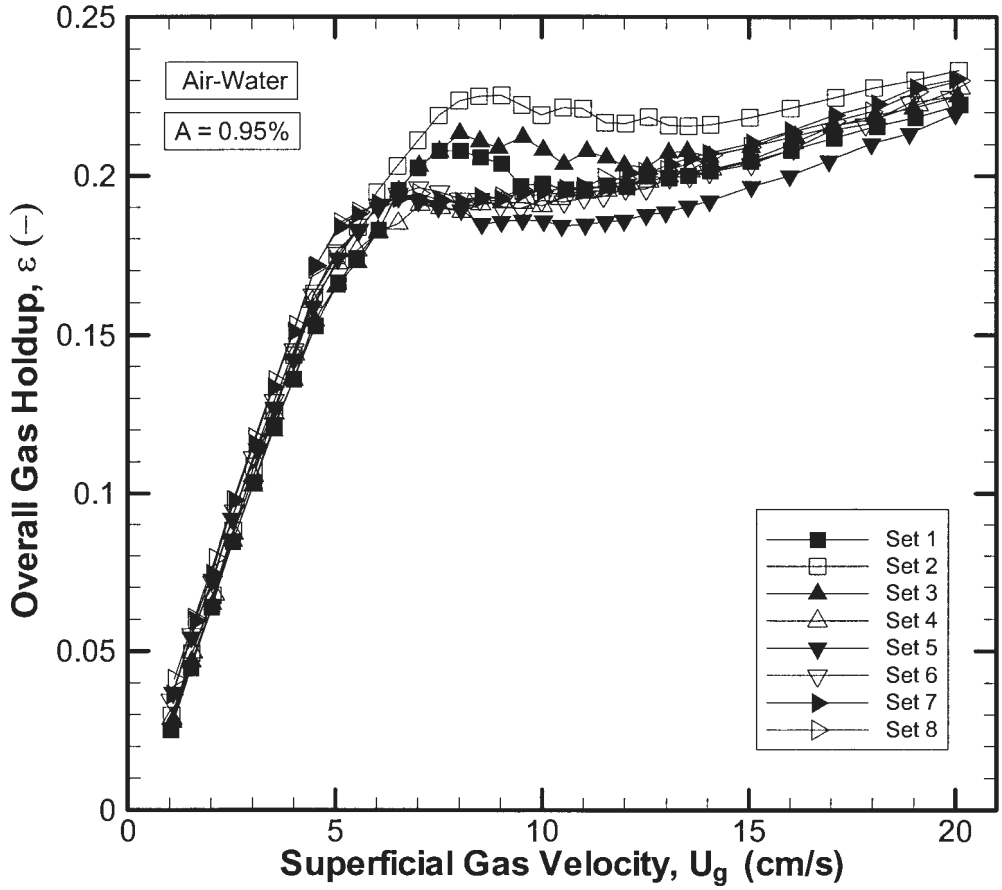

Figure L.1: Overall gas holdup for various air-water sets.